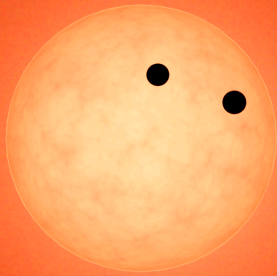




National Aeronautics and Space Administration



EXOPLANET EXPLORATION PROGRAM 2018 Technology Plan Appendix

Brendan Crill, Deputy Program Chief Technologist

Nick Siegler, Program Chief Technologist

JPL Document No: D-101271

Acknowledgments

Important contributions and reviews were made by Neil Zimmerman, Stefan Martin, Michael Bottom, Keith Patterson, Fang Shi, Patrick Morrissey, Paul Bierden, Anthony Harness, Michael Helmbrecht, Matthew Bolcar, David Redding, Evan Hilgemann, Bala Balasubramanian, Feng Zhao, Stuart Shaklan, Chas Shapiro, George Rieke, Mark Swain, Phil Stahl, John Callas, Tom Greene, Chas Beichmann, Eduardo Bendek, Olivier Guyon, Johannes Staghun, David Leisawitz, David Webb, and John Ziemer.

This document is cleared for public release (JPL CL # 18-0162).


Cover Art Credit: NASA/JPL-Caltech/ R. Hurt (IPAC), [artist rendition of the TRAPPIST-1 system](#).

This research was carried out at the Jet Propulsion Laboratory, California Institute of Technology, under a contract with the National Aeronautics and Space Administration. Reference herein to any specific commercial product, process, or service by trade name, trademark, manufacturer, or otherwise, does not constitute or imply its endorsement by the United States Government, or the Jet Propulsion Laboratory, California Institute of Technology.

© 2018 California Institute of Technology. Government Sponsorship acknowledged.


APPROVALS

Approved by:

 E-SIGNED by Gary Blackwood
on 2018-02-01 14:06:28 GMT

Dr. Gary Blackwood
Program Manager
Exoplanet Exploration Program
NASA / Jet Propulsion Laboratory
California Institute of Technology


Date

 E-SIGNED by Douglas Hudgins
on 2018-02-01 20:20:58 GMT

Dr. Douglas Hudgins
Program Scientist for Programs
Exoplanet Exploration Program
Science Mission Directorate
NASA Headquarters


Date

Concurred by:

 E-SIGNED by Karl Stapelfeldt
on 2018-02-01 05:15:36 GMT

Dr. Karl Stapelfeldt
Program Chief Scientist
Exoplanet Exploration Program
NASA / Jet Propulsion Laboratory
California Institute of Technology


Date

 E-SIGNED by Keith Warfield
on 2018-02-08 16:47:06 GMT

Keith Warfield
Program Chief Engineer
Exoplanet Exploration Program
NASA / Jet Propulsion Laboratory
California Institute of Technology


Date

Prepared by:

 E-SIGNED by Brendan Crill
on 2018-02-01 04:34:24 GMT

Dr. Brendan Crill
Deputy Program Chief Technologist
Exoplanet Exploration Program
NASA / Jet Propulsion Laboratory
California Institute of Technology

Date

 E-SIGNED by Nick Siegler
on 2018-02-01 17:38:44 GMT

Dr. Nicholas Siegler
Program Chief Technologist
Exoplanet Exploration Program
NASA / Jet Propulsion Laboratory
California Institute of Technology

Date

Table of Contents

| | | |
|----------|--|-----------|
| A | Introduction | 1 |
| A.1 | Program Goals | 2 |
| A.2 | Previously Funded Efforts | 4 |
| A.3 | Technology Selection and Prioritization Criteria | 6 |
| B | Visible/Near-Infrared Coronagraph/Telescope Technology Gaps | 16 |
| B.1 | Contrast | 18 |
| B.1.2 | CG-2: Coronagraph Demonstrations and Modeling | 21 |
| B.1.3 | CG-3: Deformable Mirrors | 25 |
| B.1.4 | CG-4: Data post-processing Algorithms and Techniques | 28 |
| B.2 | Contrast Stability | 29 |
| B.2.1 | CG-5: Wavefront sensing and control | 30 |
| B.2.2 | CG-6 Mirror Segment Phasing Sensing and Control | 33 |
| B.2.3 | CG-7: Telescope Vibration Sensing and Control or Reduction | 35 |
| B.3 | Angular Resolution | 36 |
| B.3.1 | CG-1: Large Aperture Mirrors | 37 |
| B.3.2 | Large Monolithic Mirrors | 38 |
| B.3.3 | Large Segmented Mirrors | 39 |
| B.4 | Detection Sensitivity | 41 |
| B.4.1 | CG-8: Ultra-low Noise Visible Band Detectors | 41 |
| B.4.2 | CG-9: Ultra-low Noise Near-Infrared Detectors | 43 |
| C | Starshade Technology Gaps | 46 |
| C.2 | Starlight Suppression | 49 |
| C.2.1 | S-1: Controlling Scattered Sunlight | 50 |
| C.2.2 | S-2: Starlight Suppression and Model Validation | 52 |
| C.3 | Formation Sensing and Control | 56 |
| C.3.1 | S-3: Lateral Formation Sensing | 56 |
| C.4 | Deployment Accuracy and Shape Stability | 58 |
| C.4.1 | S-4: Petal Shape and Stability | 59 |
| C.4.2 | S-5: Petal Positioning Accuracy and Opaque Structure | 60 |
| D | Mid-IR Coronagraph/Telescope Technology Gaps | 64 |
| D.1 | Contrast | 65 |
| D.1.1 | CG-15: Mid-infrared Coronagraph Optics and Architecture | 66 |
| D.1.2 | CG-16: Cryogenic Deformable Mirror | 67 |
| D.2 | Angular Resolution | 68 |
| D.2.1 | CG-14: Mid-IR Large Aperture Telescopes | 68 |
| D.3 | Detection Sensitivity | 69 |
| D.3.1 | CG-13: Low-noise Mid-IR detectors | 69 |
| E | Other Technology Gaps | 71 |
| E.1 | Contrast | 71 |
| E.1.1 | CG-10: UV/V/NIR mirror coatings | 71 |

| | | |
|------------|---|-----------|
| <i>E.2</i> | <i>Detection Sensitivity</i> | 73 |
| E.2.1 | CG-12: Ultra-low noise UV detectors | 73 |
| <i>E.3</i> | <i>Radial Stellar Motion Sensitivity (for planetary mass measurement)</i> | 74 |
| E.3.1 | M-2: Laser Frequency Combs for Space-based EPRV | 75 |
| E.3.2 | M-1: Extreme Precision Ground-based Radial Velocity | 76 |
| <i>E.4</i> | <i>Tangential Stellar Motion Sensitivity (for planetary mass measurement)</i> | 77 |
| E.4.1 | M-3: Astrometry | 77 |
| <i>E.5</i> | <i>Mid-IR Transit and Secondary Eclipse Spectroscopy</i> | 79 |
| E.5.1 | M-4: Ultra-Stable Mid-Infrared Detectors | 80 |
| F | Technology Watch List | 82 |
| F.1 | <i>Advanced Cryocoolers</i> | 82 |
| F.2 | <i>Sub-Kelvin Coolers</i> | 82 |
| G | Prioritization | 83 |
| H | Conclusion | 84 |
| I | Document Change Log | 85 |
| J | Acronyms | 86 |
| K | References | 88 |

| | | |
|-----------------|---|----|
| Table 1: | TDEM awards for calls from 2009, 2010, 2012, 2013, 2014, 2015, and 2016. Typically, technology work commences two years after the solicitation is released (column 1). | 4 |
| Table 2: | Technology gap prioritization criteria | 7 |
| Table 3: | The 2018 ExEP Technology List. | 8 |
| Table 4: | A reproduction of Table 1 of Nemati et al. (2017) showing the rms wavefront error that degrades the ATLAST APLC coronagraph contrast to 10^{-10} for a per-segment wavefront aberration (left) and global wavefront aberration (right)..... | 34 |
| Table 5: | ExEP Technology Watch List..... | 82 |

A INTRODUCTION

The purpose of this Technology Plan Appendix is to guide near-term (1–5 year) technology development for future space observatories and ground-based support instruments related to NASA's Exoplanet Exploration Program (ExEP or Program). The ExEP responds to and supports the 2014 NASA Strategic Plan,¹ the 2014 NASA Science Plan,² and the 2014 Update to the Astrophysics Implementation Plan.³

A long-term goal of the Program is to discover and characterize worlds that could harbor life. a New Worlds Mission, such as that envisaged by the 2010 Decadal Survey *New Worlds, New Horizons in Astronomy and Astrophysics* (NWNH)⁴—a mission capable of directly imaging terrestrial planets in the habitable zones of stars in the solar neighborhood, and measuring their spectra to search for signs of life. Such a mission will require extreme starlight suppression and other new technology developments. A possible path to developing the necessary technologies was presented in Crill and Siegler (2017).⁵

In the near term, the technology needs captured here should also enable other missions, such as Probe-class (life-cycle cost nominally less than \$1B) or Explorer-class missions (life-cycle cost less than \$250M), with compelling science as funded by NASA's Astrophysics Division.

This Appendix lists the enabling and enhancing technology needs of the ExEP that support the efforts of NASA's Astrophysics Division to respond to the 2010 Decadal Survey factoring in the Mid-Decadal (2016) recommendations.⁶ This response is captured in the Astrophysics Division Implementation Plan (last updated in 2016).⁷ The greatest emphasis is placed on technologies that enable the direct imaging and spectroscopic characterization of Earth-like planets in the habitable zone of Sun-like stars, though the program also tracks technologies that allow the study of broader classes of exoplanets and those that enable characterization such as mass.

The Technology Gap sections (sections B, C, and D) define the technology gaps and quantify, when possible, the difference between expected performance requirements and the current state-of-the-art. These sections also summarize recent key developments and communicate, when known, what is planned in the near future. Alternative technologies are also presented, as appropriate.

Note that, while the ExEP will track all the listed technology gaps, a number of them are cross-cutting and important to all three Astrophysics Division science themes (Cosmic Origins, Physics of the Cosmos, and the ExEP). Several of the ExEP technology needs may be funded by the other Programs.

This Appendix communicates overall technology needs to aid scientists, engineers, and technology managers in academia, industry, research labs, and NASA centers in deciding which technology areas they are best suited to develop. However, not all the technologies to fly a New Worlds mission listed here are currently solicited under the Research Opportunities in Space and Earth Sciences (ROSES) Strategic Astrophysics Technology (SAT) Program (ROSES 2016, Appendix D.8). The specific technologies that are solicited under the SAT Program are described in the call for proposals. In general, an effort is made to identify and solicit for the tallest technology tent poles within the limits of available funding, using the prioritization

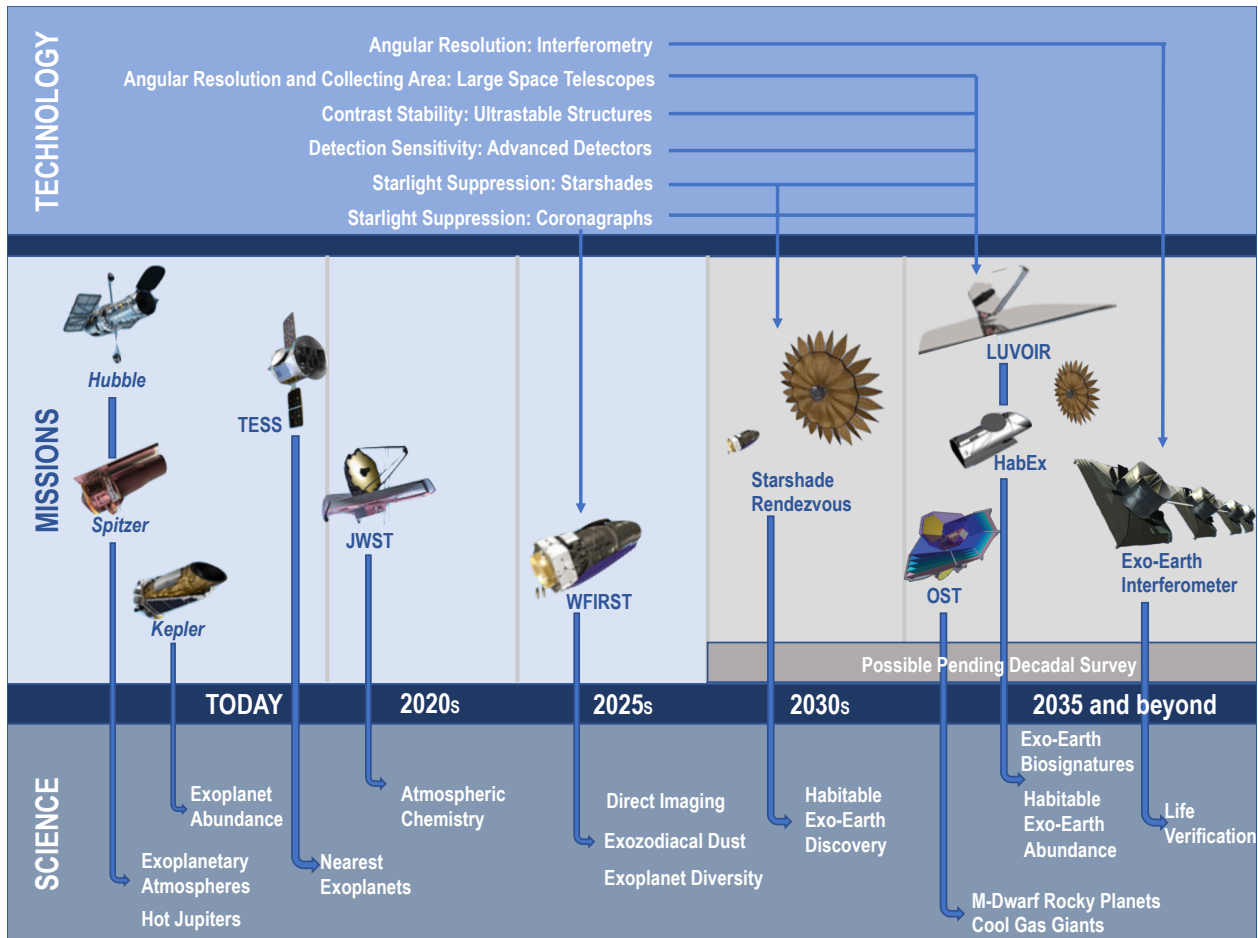


Figure 1: NASA's timeline of current, future, and possible Exoplanet missions.

process described in this Appendix. Please note that in the case of a discrepancy between the ROSES language and this Appendix, the ROSES language has precedent.

A.1 Program Goals

The 2010 Decadal Survey recommended the creation of a New Worlds Technology Development Program “to lay the technical and scientific foundation for a future mission to study nearby Earth-like planets” (pp. 215–217). The Technology Development for Exoplanet Missions (TDEM) element of the SAT Program was established to support the maturation of key technologies that will enable NASA to achieve that goal. Previous work under the auspices of the SAT/TDEM Program, as well as the results of the Exo-Coronagraph (Exo-C) and Exo-Starshade (Exo-S) probe studies,⁸ which concluded in 2015, demonstrate that both coronagraphs and external occulters (starshades) are scientifically meritorious and their technology needs feasible for a future New Worlds mission.

The NASA Astrophysics Division response to the Decadal Survey’s recommendations (2016 Astrophysics Implementation Plan Update) describes a path for implementing the Wide-Field Infrared Survey Telescope (WFIRST),⁹ the top large-scale mission recommendation and the next strategic mission after the James Webb Space Telescope (JWST). It also recommends concept development for future strategic missions for consideration by the 2020 Decadal Survey.

In 2016, NASA entered the formulation phase of the WFIRST mission, which makes use of a 2.4-m-diameter Astrophysics Focused Telescope Asset donated to NASA by another federal agency. A high-contrast coronagraph instrument with wavefront control has been baselined as a technology demonstration instrument within the planned WFIRST implementation. The WFIRST coronagraph will make important steps toward enabling starlight suppression necessary to directly image exo-Earths, but will not achieve the necessary contrast performance. Consequently, this Appendix describes the technologies devoted to instrument performance on post-WFIRST missions capable of directly imaging and characterizing Earth-like planets.

Many of the exoplanet detection and characterization technology needs described here are intended to support the exoplanet science objectives of the two NASA Astrophysics Division 2020 Decadal Survey large mission concept studies—the Large Ultra-Violet Optical InfraRed (LUVOR) Surveyor and the Habitable Exoplanet Imaging (HabEx) Mission (see Figure 2). Both telescope designs are expected to be driven by exo-Earth direct detection and characterization capabilities, and we assume that, unlike the case with WFIRST, the engineering requirements will drive the telescope requirements to meet the challenging contrast requirements when using a coronagraph. A third large mission concept, the Origins Space Telescope (OST), originally known as the Far-Infrared Surveyor, will include exoplanet transit spectroscopy as a central science theme, and may also include a mid-infrared coronagraph capable of directly imaging Jupiter and Saturn analogs orbiting nearby stars.

The mission concept studies commenced in 2016 for approximately three-year durations. The studies are led by Science and Technology Definition Teams (STDTs) and supported by NASA field centers for engineering and design work. Each mission concept STDT is expected to deliver an Interim Report in 2018 which will present a preliminary description of science goals, system architecture, and instrument suite. In advance of the Interim Reports (and the Final Reports expected in 2019), the teams have also submitted, in the summers of 2016 and 2017, lists of technology gaps to the two NASA Program Offices¹⁰ consisting of technology development needs for reaching the likely science objectives of each mission. Each of these STDT gap lists were reviewed as part of the annual ExEP technology selection and prioritization process, and the ExEP technology gap lists presented in this Appendix reflect our assessment of the STDTs's lists as of the end of 2017. As the work of the STDTs advances, the technology needs may change in future editions.

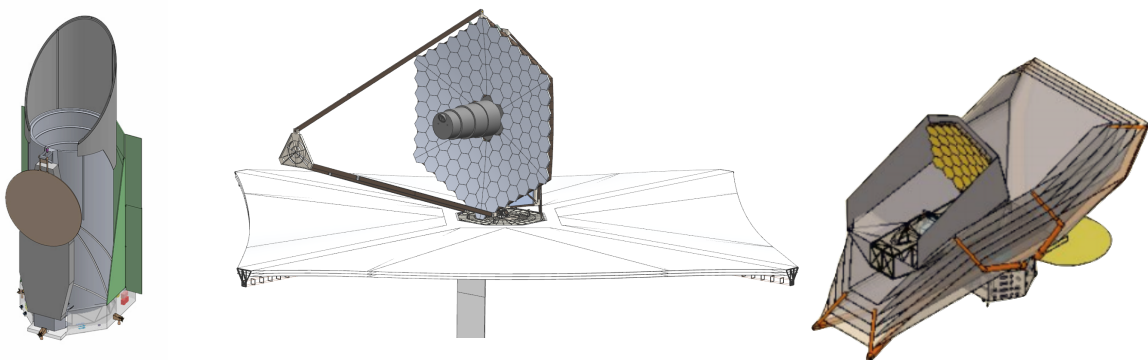


Figure 2: Renderings of the Decadal Survey large mission concepts HabEx (left), LUVOR (center), and OST (right). Each of these missions include exoplanet science as a driving science goal. HabEx and LUVOR aim to directly

image and characterize of rocky exoplanets orbiting nearby Sun-like stars in the visible and near-infrared bands. OST aims to characterize the atmospheres of rocky exoplanets orbiting M dwarfs using transit spectroscopy and to image directly cool gas giants in wide orbits. Primary telescope aperture size for the concepts rendered here are 4 m, 15m, and 9.1 m, respectively, for HabEx, LUVOIR, and OST. Images courtesy of Keith Warfield, Matt Bolcar, and OST team.

NASA's ExEP supports activities that contribute to the maturation of key technologies that will enable these exoplanet mission concepts. The Program funds and facilitates experiments and analyses selected by NASA HQ through yearly solicitations issued through the omnibus ROSES NASA Research Announcement (NRA). The Program also provides support in the form of infrastructure, modeling, expertise, and test facilities to selected Principal Investigators (PIs).

As a part of ROSES, NASA currently funds technology development through the Astrophysics Research and Analysis (APRA) solicitation and the SAT/TDEM solicitations. APRA covers low Technology Readiness Level (TRL) technology research (TRL 1-2) while SAT/TDEM covers maturation of mid-range TRL technologies (TRL 3-5). This two-stage approach is intended to support the advancement of technology envisaged by the 2010 Decadal Survey. All the previous tasks funded under the 2009, 2010, 2012, 2013, 2014, 2015, and 2016 SAT/TDEM solicitations are listed in **Table 1**; SAT/TDEM whitepapers and abstracts can be found online.¹¹ Abstracts of funded APRA awards can also be found online.¹²

A.2 Previously Funded Efforts

Table 1 lists the previously funded TDEM awards, grouped by research area. Final Milestone Reports for completed TDEMs as well as Milestone Whitepaper Reports for those still in process are posted on the ExEP Technology website.¹³

Table 1: TDEM awards for calls from 2009, 2010, 2012, 2013, 2014, 2015, and 2016. Typically, technology work commences two years after the solicitation is released (column 1).

| Year | PI | Institution | Proposal Title |
|---|---------------|----------------------------------|---|
| CORONAGRAPH STARLIGHT-SUPPRESSION DEMONSTRATIONS | | | |
| 2009 | Mark Clampin | NASA Goddard Space Flight Center | Visible Nulling Coronagraph Technology Maturation: High Contrast Imaging and Characterization of Exoplanets |
| 2009 | Olivier Guyon | Univ. of Arizona | Phase-Induced Amplitude Apodization Coronagraphy Development and Laboratory Validation |
| 2009 | John Trauger | JPL/Caltech | Advanced Hybrid Lyot Coronagraph Technology for Exoplanet Missions |
| 2010 | Olivier Guyon | Univ. of Arizona | Advances in Pupil Remapping (PIAA) Coronagraphy: improving Bandwidth, Throughput and Inner Working Angle |
| 2010 | Richard Lyon | NASA Goddard Space Flight Center | Compact Achromatic Visible Nulling Coronagraph Technology Maturation |
| 2010 | Jagmit Sandhu | JPL/Caltech | Visible Nulling Coronagraph (VNC) Technology Demonstration Program |

| Year | PI | Institution | Proposal Title |
|------|----------------|----------------------------------|---|
| 2010 | Eugene Serabyn | JPL/Caltech | Demonstrations of Deep Starlight Rejection with a Vortex Coronagraph |
| 2013 | Brian Hicks | NASA Goddard Space Flight Center | Segment Aperture Nulling Coronagraphy |
| 2014 | Matthew Bolcar | NASA Goddard Space Flight Center | Next Generation Visible Nulling Coronagraph |
| 2014 | Eugene Serabyn | JPL/Caltech | Broadband Light Rejection with the Optical Vortex Coronagraph |
| 2016 | John Trauger | JPL/Caltech | Super Lyot ExoEarth Coronagraph |
| 2016 | Ruslan Belikov | NASA/Ames | Laboratory Demonstration of High Contrast Using PIAACMC on a Segmented Aperture |
| 2016 | Ruslan Belikov | NASA/Ames | Development of a Method for Exoplanet Imaging in Multi-Star Systems* |

STARSHADE STARLIGHT-SUPPRESSION DEMONSTRATIONS

| | | | |
|------|------------------|------------------------------------|--|
| 2009 | N. Jeremy Kasdin | Princeton Univ. | Starshades for Exoplanet Imaging and Characterization: Key Technology Development |
| 2010 | N. Jeremy Kasdin | Princeton Univ. | Verifying Deployment Tolerances of an External Occulter for Starlight Suppression |
| 2012 | Suzanne Casement | Northrop Grumman Aerospace Systems | Starshade Stray Light Mitigation through Edge Scatter Modeling and Sharp-Edge Materials Development |
| 2012 | Tiffany Glassman | Northrop Grumman Aerospace Systems | Demonstration of Starshade Starlight-Suppression Performance in the Field |
| 2012 | N. Jeremy Kasdin | Princeton Univ. | Optical and Mechanical Verification of an External Occulter for Straight Suppression (<i>transferred to starshade technology activity</i>) |
| 2013 | Webster Cash | Univ. of Colorado | Development of Formation Flying Sensors |
| 2013 | N. Jeremy Kasdin | Princeton Univ. | Formation Flying for External Occulters (<i>transferred to starshade technology activity</i>) |
| 2014 | Mark Thomson | JPL/Caltech | Optical Shield for the Starshades Inner Disk Subsystem (<i>transferred to starshade technology activity</i>) |

WAVEFRONT SENSING AND CONTROL OF SCATTERED STARLIGHT

| | | | |
|------|--------------------|----------------|--|
| 2009 | John Krist | JPL/Caltech | Assessing the Performance Limits of Internal Coronagraphs Through End-to-End Modeling |
| 2009 | M. Charley Noecker | Ball Aerospace | Advanced Speckle Sensing for Internal Coronagraphs and Methods of Isolating Exoplanets from Speckles |

* Funded by directed work package from NASA APD (not SAT)

| Year | PI | Institution | Proposal Title |
|---------------------------|--------------------|-------------------------------|--|
| 2010 | Paul Bierden | Boston Micromachines | MEMS Deformable Mirror Technology Development for Space-Based Exoplanet Detection |
| 2010 | Michael Helmbrecht | Iris AO | Environmental Testing of MEMS Deformable Mirrors for Exoplanet Detection |
| 2010 | N. Jeremy Kasdin | Princeton Univ. | Integrated Coronagraph Design and Wavefront Control using Two Deformable Mirrors |
| OTHER TECHNOLOGIES | | | |
| 2009 | Donald Figer | Rochester Inst. of Technology | A Photon-Counting Detector for Exoplanet Missions |
| 2010 | Stuart Shaklan | JPL/Caltech | Coronagraph Starlight Suppression Model Validation: Coronagraph Milestone Report #3 |
| 2013 | Eduardo Bendek | NASA Ames Research Center | Enhanced Direct Imaging Exoplanet Detection with Astrometric Mass Determination |
| 2015 | Jim Breckinridge | University of Arizona | Threshold Raw Retrieved Contrast in Coronagraphs is Limited by Internal Polarization |

A.3 Technology Selection and Prioritization Criteria

The exoplanet science and technology community, including the large mission STDs, submitted proposed technologies during an annual solicitation period during the summer of 2017. Along with the Technology List from the 2017 edition of the Technology Development Plan Appendix, these were first judged against a selection criterion to determine the relevance to ExEP:

A technology considered for tracking by the ExEP works towards enabling or enhancing the direct imaging or characterization of exoplanets.

Technologies that address ExEP's technology gaps are the ones prioritized for development and considered for resource allocation. Some of these technologies may be funded outside of the ExEP. The remaining technologies considered to benefit exoplanet science are captured onto a Watch List of other technology opportunities that may benefit exoplanet science. These gaps are tracked and re-evaluated annually for potential prioritization.

The ExEP Technology List is listed in **Table 3**, in order of priority based on:

- Impact
- Urgency
- Trend

These selection and prioritization criteria were proposed by the ExEP Program Chief Technologist and ExEP Deputy Technology Development Manager, and presented to the Exoplanet Program Analysis Group (ExoPAG) and its Executive Committee for review and feedback. After this review, the criteria were presented to the ExoTAC for formal review. With

the addition of this review step, the language used to score the 2018 gap list differs slightly from 2017, reflecting the important feedback from the ExoTAC.

The higher the number within each criterion, the higher the contribution to the prioritization. Results of the prioritization effort can be found in Section G. These criteria are subjectively defined in **Table 2**. A total score for each technology gap is determined with a weighted sum: Impact and Urgency scores are each weighted by a factor 10 and Trend is weighted by a factor 5. The ExEP Program Chief Technologist and ExEP Deputy Program Chief Technologist proposed initial scores within each category based on the criteria language. These initial scores are Peer Reviewed by the ExEP Program Chief Scientist, the ExEP Deputy Program Chief Scientist, the ExEP Chief Engineer, any subject matter experts, and technologists from the Cosmic Origins and Physics of the Cosmos Astrophysics Division program offices. The ExoTAC formally reviewed the scores, providing suggestions which are reflected in the scoring and the resulting ranking shown here.

Table 2: Technology gap prioritization criteria

| | |
|--------------------------------|--|
| Impact: (weight: 10) | 4: Critical strategic technology for the New Worlds Technology Development Program envisioned in <i>New Worlds, New Horizons</i> (2010 Decadal Survey) and in the NASA Astrophysics Implementation Plan; without this technology, the mission would not launch |
| | 3: Highly desirable - not mission-critical, but provides major benefits in enhanced science capability, reduced critical resources need, and/or reduced mission risks; without it, missions may launch, but science or implementation would be compromised |
| | 2: Desirable - not required for mission success, but offers significant science or implementation benefits; if technology is available, would almost certainly be implemented in missions |
| | 1: Minor science impact or implementation improvements; if technology is available would be considered for implementation in missions |
| Urgency (weight: 10) | 4: Advances technology or reduces risk needed for missions currently in Pre-Formulation or formulation. |
| | 3: In time to inform the 2020 Decadal Survey; not necessarily at some TRL but reduced risk. |
| | 2: Earliest projected launch date < 15 yr (< 2033) |
| | 1: Earliest projected launch date > 15 yr (> 2033) |
| Trend (weight: 5) | 4: (a) no ongoing current efforts, or (b) little or no funding allocated |
| | 3: (a) others are working towards it but little results or their performance goals are very far from the need, (b) funding unclear, or (c) time frame not clear |
| | 2: (a) others are working towards it with encouraging results or their performance goals will fall short from the need, (b) funding may be unclear, or (c) time frame not clear |
| | 1: (a) others are actively working towards it with encouraging results or their performance goals are close to need, (b) it's sufficiently funded, and (c) time frame clear and on time |

Table 3: The 2018 ExEP Technology List.

| ID | Technology | Technology Gap | Technology Description | Current Performance | Needed Performance |
|------|---|------------------------------|--|--|--|
| CG-2 | Coronagraph Demo's and Modeling | Coronagraph Contrast | Coronagraph optics and architecture that suppress diffracted starlight by a factor of $< 10^{-10}$ at visible and infrared wavelengths | <p><u>Lab:</u> 6×10^{-10} raw contrast at 10% bandwidth across angles of 3-15 λ/D demonstrated with a linear mask and an <u>unobscured</u> pupil in a static vacuum lab environment (Hybrid Lyot)</p> <p>$< 1.6 \times 10^{-9}$ raw contrast at 10% bandwidth across angles of 3-9 λ/D demonstrated with a circularly-symmetric mask and <u>obscured</u> pupil in a static vacuum lab environment (WFIRST)</p> <p><u>Flight:</u> 10^{-4} raw contrast 540 nm at 10 λ/D (HST)</p> | Coronagraph masks and optics capable of creating circularly symmetric dark regions in the focal plane enabling raw contrasts $\leq 10^{-10}$, with minimal contribution from polarization aberration, IWA $\leq 3 \lambda/D$, throughput $\geq 10\%$, and bandwidth $\geq 10\%$ on obscured and segmented pupils in a simulated dynamic vacuum environment. |
| S-1 | Controlling Scattered Sunlight | Starlight Suppression | Limit edge-scattered sunlight and diffracted starlight with optical petal edges that also handle stowed bending strain. | Edges manufactured with machining and electrical discharge machining do not meet scatter requirements; etched amorphous metal edges meet scatter specs integrated in-plane shape tolerance is to be demonstrated. | Integrated petal optical edges maintaining precision in-plane shape requirements after deployment trials and limit solar glint contributing $< 10^{-10}$ contrast at petal edges. |
| S-2 | Starlight Suppression and Model Validation | Starlight Suppression | Experimentally validate at flight-like Fresnel numbers the equations that predict the contrasts achievable with a starshade. | Validated optical model with demonstrated 10^{-6} suppression at white light, 58 cm mask, and Fresnel number F (at the starshade tips) = 210; 6×10^{-6} suppression demonstrated at F = 15; 4.6×10^{-8} suppression demonstrated at F~27 | Experimentally validated models with total starlight suppression $\leq 10^{-8}$ in scaled flight-like geometry, with F between 5 and 40 across a broadband optical bandpass. Validated models are traceable to 10^{-10} contrast system performance in space. |
| S-3 | Lateral Formation Sensing | Starshade Contrast Stability | Demonstrate lateral formation flying sensing accuracy consistent with keeping telescope in starshade's dark shadow. | Sub-scale lab demonstration showing ability to center telescope within ± 1 m of the center of the starshade shadow. | Demonstrate sensing lateral errors ≤ 0.24 m 3σ accuracy at the flight signal-to-noise ratio at scaled flight separations. Demonstrate control algorithms with scaled lateral control error ≤ 1 m radius. |

| ID | Technology | Technology Gap | Technology Description | Current Performance | Needed Performance |
|------|--|---|--|--|--|
| S-5 | Petal Positioning Accuracy and Opaque Structure | Deployment Accuracy and Shape Stability | Demonstrate that a starshade can be autonomously deployed to within its budgeted tolerances after exposure to relevant environments. | Petal deployment tolerance (≤ 1 mm) verified with low fidelity 12 m prototype and no optical shield; no environmental testing (Exo-S design). | Deployment tolerances demonstrated to ≤ 1 mm (in-plane envelope) with flight-like, minimum half-scale structure, with petal optical edge interfaces, that is optically opaque when deployed, and includes interfaces to launch restraint. Verify the structure will meet shape stability (petal edge position) after exposure to relevant environments. |
| S-4 | Petal Shape and Stability | Deployment Accuracy and Shape Stability | Demonstrate a high-fidelity, flight-like starshade petal meets petal shape tolerances after exposure to relevant environments. | Manufacturing tolerance (≤ 100 μm) verified with low fidelity 6m prototype and no environmental tests. Petal deployment tests conducted but on prototype petals to demonstrate rib actuation; no shape measurements, no long-duration stowage tests. | Deployment tolerances demonstrated to ≤ 100 μm (in-plane tolerance profile for a 7 m petal on the 34m-diameter Exo-S design; tolerances scale roughly linearly with starshade diameter) with flight-like, minimum half-scale petal fabricated and maintains shape with exposure to relevant environments and is optically opaque. |
| CG-3 | Deformable Mirrors | Coronagraph Contrast | Flight-qualified large-format deformable mirrors and their electronics | <u>Lab:</u> Electrostrictive 64x64 actuator DMs have been demonstrated to meet $\leq 10^{-9}$ contrasts and $< 10^{-10}$ stability in a vacuum environment and 10% bandwidth; 48x48 actuator DM passed random vibrate testing <u>Flight:</u> No SOA | 4 m primary mirror: $\geq 96 \times 96$ actuators 10 m primary mirror: $\geq 128 \times 128$ actuators Enable raw contrasts of $\leq 10^{-9}$ at $\sim 20\%$ bandwidth and IWA $\leq 3 \lambda/D$ Flight-qualified device and drive electronics (radiation hardened, environmentally tested, life-cycled including connectors and cables) Mirror stability maintains 10^{-10} contrast for observation time scales |

| ID | Technology | Technology Gap | Technology Description | Current Performance | Needed Performance |
|------|---|--------------------------------|---|---|---|
| CG-1 | Large Aperture Primary Mirrors | UVOIR Angular Resolution | Large monolith and multi-segmented mirrors that meet tight surface figure error, coating uniformity, and thermal control requirements at visible wavelengths | <p><u>Flight Monolith:</u></p> <p>3.5-m sintered SiC with < 3 μm SFE (Herschel)</p> <p>2.4 m ULE with ~ 10 nm SFE (HST)</p> <p>Depth: Waterjet cutting is TRL 9 to 14", but TRL 3 to > 18". Fused core is TRL 3; slumped fused core is TRL 3 (AMTD).</p> <p>Segmented (no flight SOA): 6.5 m Be with 25 nm SFE (JWST)</p> <p>Non-NASA: 6 DOF, 1-m class SiC and ULE, < 20 nm SFE, and < 5 nm wavefront stability over 4 hr with thermal control</p> | <p>Aperture: 4–16 m; SFE < 10 nm rms (wavelength coverage 400–2500 nm)</p> <p>Wavefront stability better than 10 pm rms per wavefront control time step.</p> <p>Segmented apertures leverage 6 DOF or higher control authority meter-class segments for wavefront control.</p> <p>Environmentally tested</p> |
| CG-6 | Mirror Segment Phasing Sensing & Control | Coronagraph Contrast Stability | Segmented or monolith large aperture mirrors require segment phasing and rigid-body sensing and control of the segments or the surface figure to achieve tight static and dynamic wavefront errors. | <p>6 nm rms rigid body positioning error and 49 nm rms stability (JWST error budget)</p> <p>SIM and non-NASA: nm accuracy and stability using laser metrology</p> <p>Capacitive gap sensors demonstrated at 10 pm.</p> <p>No flight SOA; ground-based (Keck) achieved 6 nm positioning error in operations</p> | <p>Systems-level considerations to be evaluated but expect will require WFE stability less than 10 pm rms sensitivity and control over periods of tens of minutes</p> |

| ID | Technology | Technology Gap | Technology Description | Current Performance | Needed Performance |
|------|---|--------------------------------|--|---|--|
| CG-7 | Telescope Vibration Sense/Control or Reduction | Coronagraph Contrast Stability | Isolation, reduction, and/or damping of spacecraft and payload vibrational disturbances | <p>80 dB attenuation at frequencies > 40 Hz (JWST passive isolation)</p> <p>Disturbance-Free Payload demonstrated at TRL 5 for JWST with 70 dB attenuation at "high frequencies" with 6-DOF low-order active pointing.</p> <p>GAIA cold gas microthrusters or LISA pathfinder colloidal microthrusters for fine pointing can reduce disturbance environment.</p> | Vibration isolation or reduction of vibration disturbance sources to a level that enables < 1 nm wavefront error stability. |
| CG-9 | Ultra-Low Noise Near-Infrared Detectors | NIR Detection Sensitivity | Near-infrared wavelength (900 nm to 2.5 μm), extremely low noise detectors for exo-Earth spectral characterization with Integral Field Spectrographs | <p><u>Lab</u>: HgCdTe photodiode arrays have read noise $\lesssim 2$ e-rms with multiple nondestructive reads; 2k\times2k format; dark current < 0.001 e-/s/pix; very radiation tolerant (JWST)</p> <p>HgCdTe APDs have dark current $\sim 10\text{--}20$ e-/s/pix, RN $\ll 1$ e-rms, and < 1k\times1k format</p> <p>Sub-Kelvin photon-counting detectors (KID, TES): 0 read noise/dark current; radiation tolerance is unknown; <1k\times1k format</p> <p><u>Flight</u>: HST WFC3/IR HgCdTe dark current 0.05 e-/px/s, 12 e- read noise, 1k\times1k format</p> | <p>Read noise $\ll 1$ e-rms, dark current noise < 0.001 e-/pix/s, in a space radiation environment over mission lifetime</p> <p>$\geq 2\text{k}\times 2\text{k}$ format</p> |

| ID | Technology | Technology Gap | Technology Description | Current Performance | Needed Performance |
|------|--|------------------------------------|---|---|--|
| CG-5 | Wavefront Sensing and Control | Coronagraph Contrast Stability | Sensing and control of line-of-sight jitter and low-order wavefront drift | <p><u>Lab</u>: < 0.5 mas rms per axis LOS residual error demonstrated in lab with a fast-steering mirror attenuating a 14 mas LOS jitter and reaction wheel inputs; ~12 pm rms sensitivity of focus (WFIRST)</p> <p>Higher low-order modes sensed to 10–100 nm WFE rms on ground-based telescopes</p> <p><u>Flight</u>: No SOA</p> | Sufficient fast line-of-sight jitter (< 0.5 mas rms residual) and slow thermally-induced WFE sensing and control (≤ 10 pm rms sensitivity) to maintain closed-loop < 10^{-10} raw contrast with an obscured/segmented pupil and simulated dynamic environment |
| CG-8 | Ultra-Low Noise Visible Detectors | Vis Detection Sensitivity | Low-noise visible detectors for faint exoplanet characterization with an Integral Field Spectrograph | <p><u>Lab</u>: 1kx1k silicon EMCCD detectors provide dark current of 7×10^{-4} e⁻/px/sec; CIC of 0.01 e⁻/px/frame; zero effective read noise (in photon counting mode) after irradiation when cooled to 165.15K (WFIRST); 4kx4k EMCCD fabricated but still under development</p> <p><u>Flight</u>: HST WFC3/UVIS CCD 3.1 e⁻ read noise, dark current 2×10^{-3}, format 2kx2k</p> | Effective read noise < 0.1 e ⁻ rms; CIC < 3×10^{-3} e ⁻ /px/frame; dark current < 10^{-4} e ⁻ /px/sec tolerant to a space radiation environment over mission lifetime $\geq 2k \times 2k$ format |
| M-4 | Ultra-Stable Mid-IR Detectors | Transit Spectroscopy of Exo-Earths | Ultrastable detectors for the mid-infrared band (7 - 20 microns) enabling transit spectroscopy of rocky exoplanets in the Habitable Zone of M-dwarfs. | <p><u>Lab</u>: JWST/MIRI is expected to achieve 10-100 nm transit stability</p> <p><u>Flight</u>: Spitzer IRAC Si:As detector data have demonstrated about 60 ppm precision in transit observations of several hours</p> | < 5 ppm stability for 5 hours |
| M-3 | Astrometry | Tangential Stellar Motion | Measure the mass and orbital parameters of Earth-like planets by performing astrometry of FGK stars to the sub-micro-arcsecond level. | <u>Flight</u> : GAIA typical uncertainty in astrometry for DR1 catalog is 300 microarcseconds; goal for V band magnitude 7-12 stars is 10 microarcseconds. | 0.1 microarcsecond uncertainty enables survey of nearby FGK stars. Astrophysical limits (such as variable stellar surface structure) need to be well-understood. Telescope wavefront error stability and detector thermal and mechanical stability must enable sub-microarcsecond astrometry measurements. |

| ID | Technology | Technology Gap | Technology Description | Current Performance | Needed Performance |
|-------|---|------------------------------|--|--|--|
| CG-4 | Data Post-Processing Algorithms and Techniques | Coronagraph Contrast | Data post-processing techniques to uncover faint exoplanet signals from residual speckle noise at the focal-plane detector | Few 100 × speckle suppression has been achieved by HST and by ground-based AO telescopes in the NIR and in contrast regimes of 10^{-4} to 10^{-5} , dominated by phase errors. | A 10-fold contrast improvement in the visible from 10^{-9} raw contrast where amplitude errors are expected to be important (or a demonstration of the fundamental limits of post-processing) |
| CG-10 | Mirror Coatings for UV/NIR/Vis | Coronagraph Contrast | Mirror coatings that enable high reflectivity to wavelengths as short as 90 nm | Al coating with combination of MgF_2 , LiF, and/or AlF_3 overcoat: 90-120 nm: < 50% reflectivity 120-300 nm: 85% reflectivity 300 nm-2 μ m: > 90% reflectivity Polarization differences between orthogonal polarization states, uniformity, and durability of coatings on large optics is unknown. <u>Flight:</u> HST uses MgF_2 ; 85% reflectivity $\lambda > 120$ nm; 20% reflectivity $\lambda < 120$ nm | A mirror coating that that achieves 90-120 nm: > 70% reflectivity 120-300 nm: > 90% reflectivity 300 nm-2 μ m: > 90% reflectivity Polarization phase and amplitude difference < 1% between orthogonal polarization states. |
| M-2 | Laser Frequency Combs | Radial Stellar Motion | Laser Frequency Combs (LFCs) are precise calibration sources for extreme-precision radial velocity measurement. | <u>Lab:</u> Electro-optic-modulation frequency combs demonstrated on ground-based observatories with needed mode spacing, need miniaturization and power reduction. Non-NASA work is advancing miniaturization. <u>Flight:</u> Fiber laser-based optical frequency combs demonstrated on sounding rocket (TEXUS 51 4/15 and TEXUS 53 1/16) w/ ~ few hundred MHz mode spacing. System mass is > 10 kg. | Space-based Laser Frequency Combs to calibrate high resolution, fiber-fed spectrographs for radial velocity precision better than 10 cm/s. Desired parameters are: • mode spacing of 5-10 GHz • bandwidth span 380 nm to 2400 nm • Allen deviation < 10^{-10} • Low SWaP |
| CG-13 | Ultra Low Noise Mid-IR detectors | Mid-IR detection sensitivity | Low noise and detectors for the mid-infrared band (7 - 20 microns) enabling exoplanet direct imaging. | <u>Flight:</u> JWST/MIRI | < 5 ppm stability for 5 hr; noise requirements TBD, likely to be 10 x better than JWST/MIRI |

| ID | Technology | Technology Gap | Technology Description | Current Performance | Needed Performance |
|-------|---|-----------------------------|---|---|---|
| M-1 | Extreme Precision Ground-based Radial Velocity | Radial Stellar Motion | Ground-based radial velocity instrumentation capable of measuring the mass of candidate exo-Earths in the habitable zone and to maximize efficiency of space telescope surveys. | Single measurement precision: 80 cm/s HARPS instrument; NN-EXPLORE's NEID (WYNN observatory) in development: goal 27 cm/s | Signal from exo-Earths is 10 cm/s; Need to reduce systematic errors to 1 cm/s on multi-year timescales; statistical uncertainties of 1 cm/s on monthly timescales for late F, G, and early K stars |
| CG-14 | Mid-IR Large Aperture Telescopes | Mid-IR Angular Resolution | Cryogenic (4K), large-aperture (> 9m) telescopes to achieve high angular resolution needed to direct-image cool exoplanets in wide orbits (> 5 AU) | JWST Be mirror segments may meet requirements now, so TRL 5 with an extremely expensive technology; TRL 3 exists for other materials like SiC. Cryogenic low-dissipation actuators exist at TRL 3-5. | Develop a feasible and affordable approach to producing a 10-m-class telescope with sufficiently high specific stiffness, strength, and low areal density to be launched; while maintaining compatibility with cryogenic cooling and FIR surface quality/figure of $\sim 1\mu\text{m}$ rms. Material property measurements at cryogenic temperatures for structures and optics such as damping, emissivity, thermal conductivity, etc. |
| CG-15 | Mid-IR Coronagraph Optics and Architecture | Mid-IR Coronagraph Contrast | Coronagraph optics and architecture that suppress diffracted starlight by a factor of $< 10^{-6}$ over a broad mid-IR band (7-30 microns) | The current state of the art for mid-infrared coronagraphs are the three four-quadrant phase masks of JWST-MIRI. These provide narrow-band imaging with contrasts up to 10^{-4} in three narrow bands from 10.65-15.5 micron with inner working angles of 0.33-0.49". The MIRI coronagraphs do not offer spectral dispersion. | A spectro-imaging instrument with an inner working angle of 0.1" at $10\mu\text{m}$. This is likely less than $2\lambda/D$ for the available aperture. The best IWA is needed to detect a 300 K Neptune-sized planet at 10 pc at a 1-2 AU separation, and the contrast should be 10^{-6} to detect Saturn at 10 pc (~ 1 microJy @ 24 micron, $3\lambda/D$ for 16 m aperture) with $R \sim 10$. The maximum spectral dispersion should be sufficient to resolve the 15 micron CO_2 band ($R \sim 500$). |
| CG-16 | Cryogenic Deformable Mirrors | Mid-IR Coronagraph Contrast | Flight-qualified deformable mirrors operable at cryogenic temperatures, and their drive electronics. | <u>Lab</u> : 19-actuator DMs at 40 K to < 1 micron rms (Trines et al 2016) | Requirements on actuator stroke, stroke resolution, heat dissipation, and actuator count are TBD but must be operable at cryogenic temperatures. |

| ID | Technology | Technology Gap | Technology Description | Current Performance | Needed Performance |
|-------|-------------------------------------|--------------------------|--|---|---|
| CG-12 | Ultra-Low Noise UV Detectors | UV Detection Sensitivity | Low-noise ultraviolet (200-400 nm) detectors to characterize exoplanets with an integral field spectrograph. | <p><u>Lab</u>: Micro-channel Plates (MCP): 0 read noise, $\lambda \sim 90 - 300$ nm, spurious count rate 0.05 - 0.5 counts/cm²/s; QE 20-45%; resolution element size 20 mm. EMCCD: 0 read noise, dark current > 0.005 e-/res/hr; QE 30-50%; resol. el. size 20 μm</p> <p><u>Flight</u>: HST HRC: In relevant UV band (250 nm): QE 33%, read noise 4.7 e-, dark current 5.8×10^{-3}, 1024x1024</p> | <p>Read Noise: 0 e-/resolution/s</p> <p>Dark Current: 0 e-/resolution/s</p> <p>Spurious Count Rate: < 0.05 counts/cm²/s</p> <p>QE: 75%</p> <p>Resolution size $\leq 10 \mu$m</p> <p>Tolerant to space radiation environment over mission lifetime.</p> |

B VISIBLE/NEAR-INFRARED CORONAGRAPH/TELESCOPE TECHNOLOGY GAPS

Exo-Earth direct imaging and spectral characterization will require starlight suppression that exceeds the current best ground-based performances by several orders of magnitude. Coronagraphs come in numerous architectures, each with its own strengths and weaknesses with respect to telescope aperture (monolithic, segmented), obscuration (unobscured, obscured by secondary mirror and its support struts), and wavefront error sensitivity (e.g. line-of-sight jitter, telescope vibration, polarization).

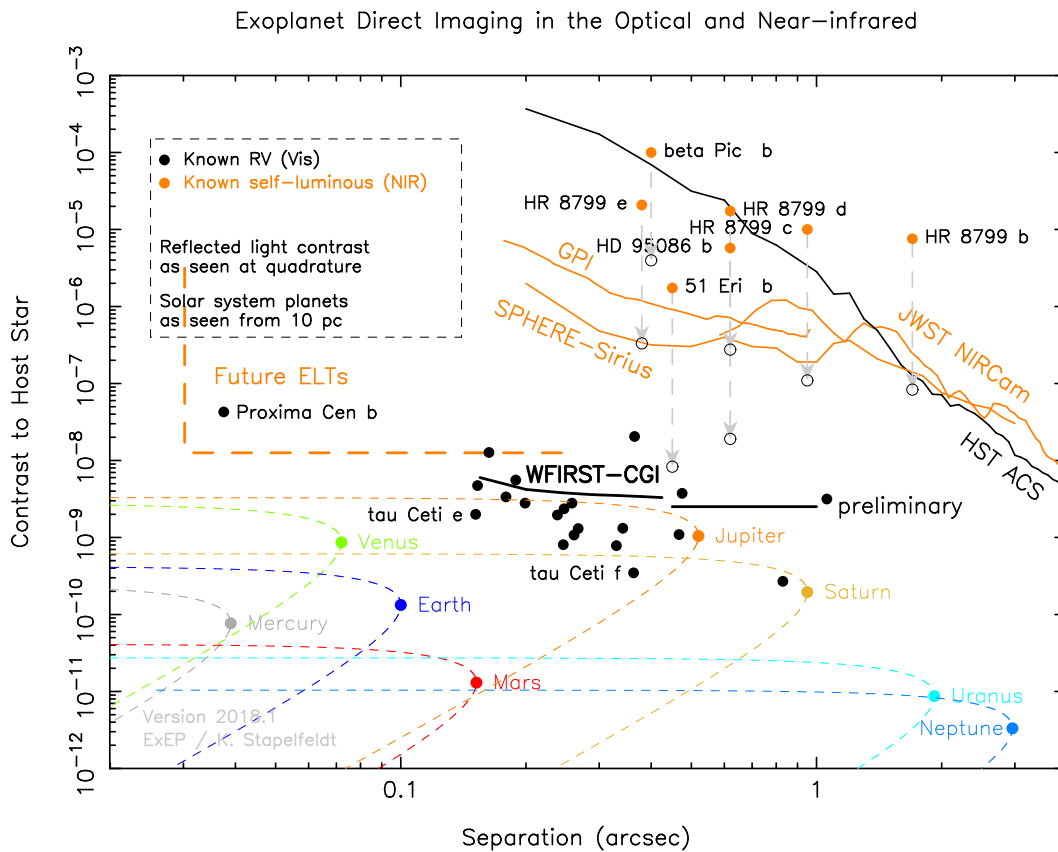


Figure 3: Contrast (ratio of planet brightness to host star brightness) versus apparent angular separation. The filled orange circles indicate the direct imaging of young, self-illuminous planets imaged in the near-infrared by ground-based telescopes. Contrasts for the planets of the Solar System are for analogous planets placed 10 pc away. The solid black dots are contrast estimates of measured radial velocity planets, including Proxima Cen b. The orange curves show measured performance of ground-based coronagraphs. The GPI curve shows typical performance, while the SPHERE curve shows the best achieved performance to-date on Sirius. Achieved performance with HST/ACS coronagraphic masks, and the predicted performance of JWST/NIRCams masks are also shown. The current best estimate performance at 565 nm for the WFIRST coronagraph instrument (CGI) is shown as the solid black curve. The curve extending from 0.13" to 0.5" is based on performance achieved in a testbed. From 0.5" to 1", performance is based on a notional coronagraph mask designed to maximize outer working angle. For consistency, the planets discovered in the near-infrared are shown with vertical arrows pointing to the predicted contrast ratios at visible wavelengths (WFIRST-CGI is expected to conduct science between 442 and 980 nm).

The removal of diffraction is only part of the coronagraph’s design goals. It must also remove the scattered light observed in the focal plane, appearing as speckles, due to imperfections in the optics. This is done through the control of deformable mirrors (Section B.1.3). As a final

step, post-processing of the data images (Section B.1.4) can further improve the effective contrast.

The most important ongoing development in coronagraph technology is the baselining of a coronagraph instrument on the WFIRST space mission as it will be the first coronagraph with wavefront control to fly in space, advancing both space and ground state-of-the-art starlight suppression. While both the Hubble Space Telescope (HST) and the JWST have onboard coronagraphs, neither have the corresponding wavefront sensing and control required to achieve better than 10^{-8} contrast sensitivity and close inner working angles (IWA) ($< 3 \lambda/D$). WFIRST will also have the first ultra-low noise visible detector and deformable mirrors to reach low-Earth orbit or beyond. **Figure 3** shows the predicted performance of WFIRST-CGI in contrast vs. angular separation.

The obscured pupil of the WFIRST telescope (due to its on-axis secondary mirror and support struts) introduces complex diffraction features that are absent in designs with unobscured pupils. Consequently, the WFIRST coronagraph architectures and optics have started the era of high-contrast/obscured pupil coronagraph design and demonstration that will serve on-axis and segmented telescope aperture designs of the future.

The ExEP Technology List (**Table 3**) targets the next generation coronagraphs beyond WFIRST which will be capable of directly imaging exo-Earths around Sun-like stars in the solar neighborhood. As mentioned earlier, the list of coronagraph technologies have been broadened to include more of the telescope system since all contributing noise sources must be accounted for if contrasts of 10^{-10} are to be reached at 10^{-11} stability levels.

The coronagraph technologies listed in **Table 3** address four technology gaps shown in Figure 4:

1. **Contrast (Section B.1)** – the ability to block the on-axis light from a target star creating a dark region in the science focal plane where the faint off-axis reflected light of a planet could be detected. Technologies listed by ExEP to close this gap are Coronagraph Demonstrations and Modeling (CG-2; Section B.1.2), Deformable Mirrors (CG-3; Section B.1.3), and Data Post-processing Algorithms and Techniques (CG-4; Section B.1.4).
2. **Contrast Stability (Section B.2)** – the ability to sense and control the incoming starlight maintaining the desired contrast long enough for full science integration. The technologies listed by ExEP that address this gap are Mirror Segment Phasing Sensing and Control (CG-6; Section B.2.2), Telescope Vibration Sense/Control or Reduction (CG-7; Section B.2.3), and Wavefront Sense/Control (CG-5; Section B.2.1).
3. **Detection Sensitivity (Section B.4)** – the ability to detect extraordinarily few photons dispersed across many pixels of a spectrograph and not be lost in the detector’s read-out noise. The technologies on ExEP’s list that address this missing capability are Ultra Low-Noise Visible-band Detectors (CG-9; Section B.4.1) and Ultra Low-Noise Near-Infrared Detectors (CG-8; Section B.4.2).
4. **Angular Resolution (Section B.3)** – the ability to probe terrestrial regions around stars (e.g., the habitable zone) requires a minimum aperture size. The more distant the star, the larger the telescope aperture needed to probe these regions. Large apertures provide not just improved angular resolution but also improved sensitivity to faint objects (sharper point spread functions), higher throughput, lower integration times,

and the capability to probe habitable zones of stars further away. The technology listed by ExEP to close this gap is Large Aperture Primary Mirrors (CG-1; Section B.3.1).

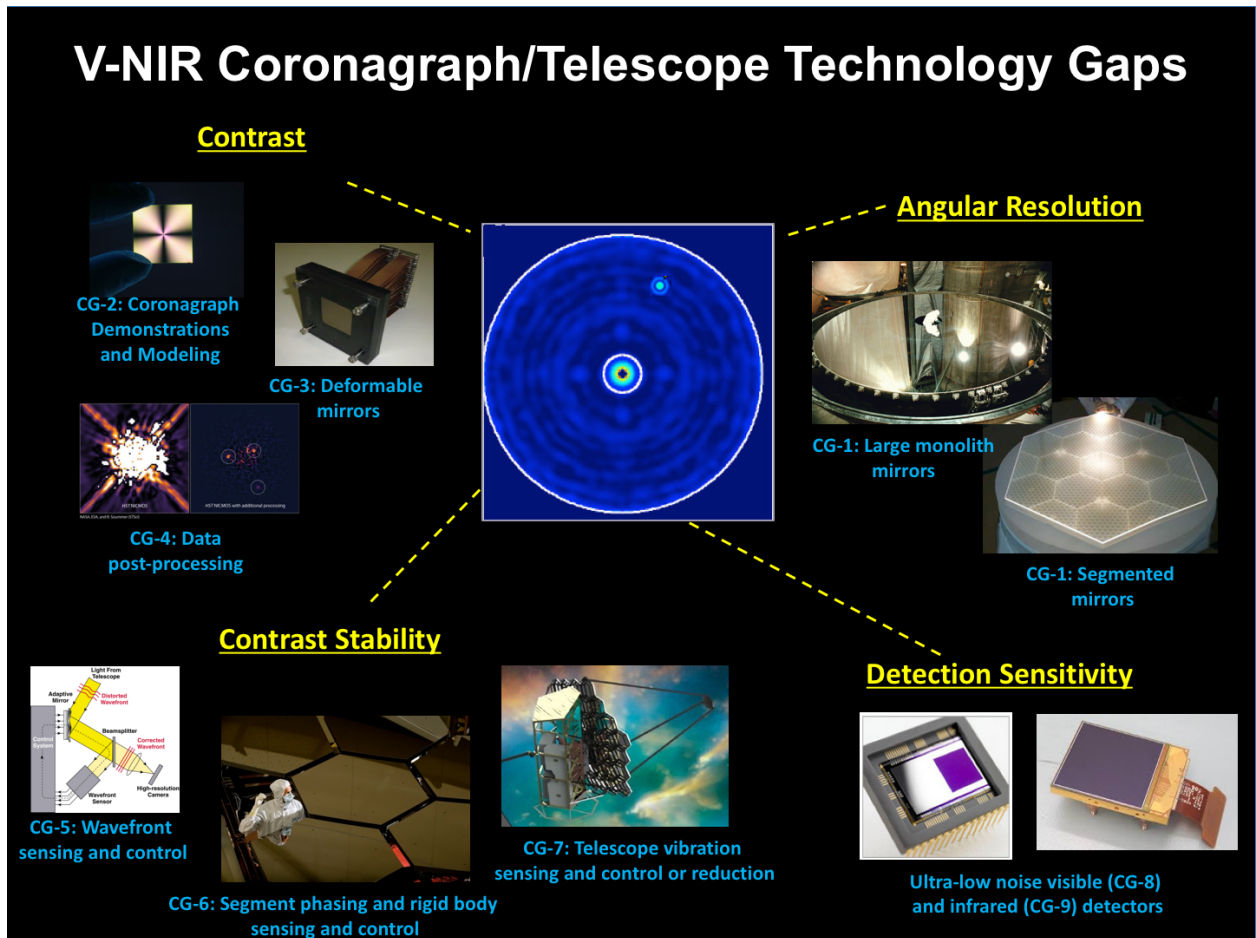


Figure 4: The four Visible-band and Near-Infrared Coronagraph Technology Gaps (in yellow font) to directly image and characterize exo-Earths around Sun-like stars and the candidate technologies for closing the gaps.

B.1 Contrast

Specialized coronagraph optics suppress on-axis starlight and allow the off-axis planet light to transmit through the instrument achieving the high contrast detection of the planet with respect to its host star. A continuing program to advance the performance of masks, apodizers, and beam-shaping optics, as well as to actively control wavefront error, to better than WFIRST coronagraph performance requirements ($< 10^{-8}$, $3 \lambda/D$, 10% bandwidth) is needed. This should include designs to improve inner working angles ($< 3 \lambda/D$), contrast performance ($< 10^{-9}$), bandwidth ($\geq 10\%$), and core PSF throughput ($\geq 10\%$), in dynamic vacuum environments on both obscured and segmented apertures.

Coronagraphs using a variety of architectures have achieved contrasts in laboratory tests that begin to approach these requirements.¹⁴ Demonstrated state-of-art results with unobscured pupils at 10% bandwidths are shown in **Figure 5**; **Figure 6** shows contrast demonstrations at a variety of bandwidths. The deepest narrowband (2% bandwidth) simulated starlight

suppression achieved is 1.2×10^{-10} raw contrast at 800 nm across angles of $3-16 \lambda/D$. It was demonstrated in the HCIT with a Hybrid Lyot Coronagraph (HLC) linear mask on an unobscured pupil in a static vacuum lab environment.^{15,16,17}

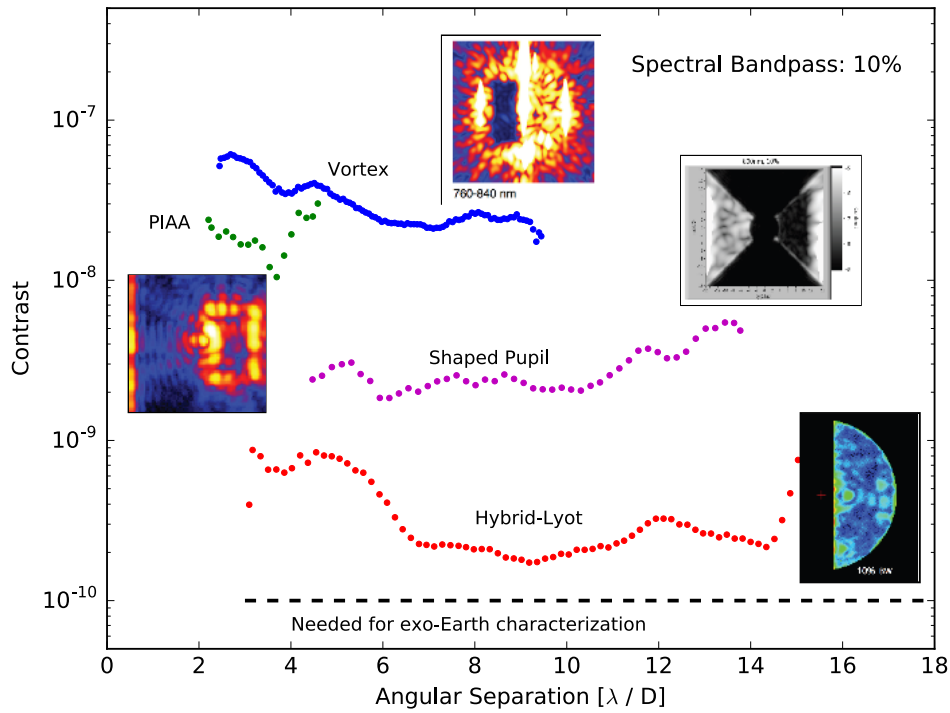


Figure 5: Coronagraph laboratory demonstrations using 10% bandwidth visible light. Adapted from Lawson et al (2013)

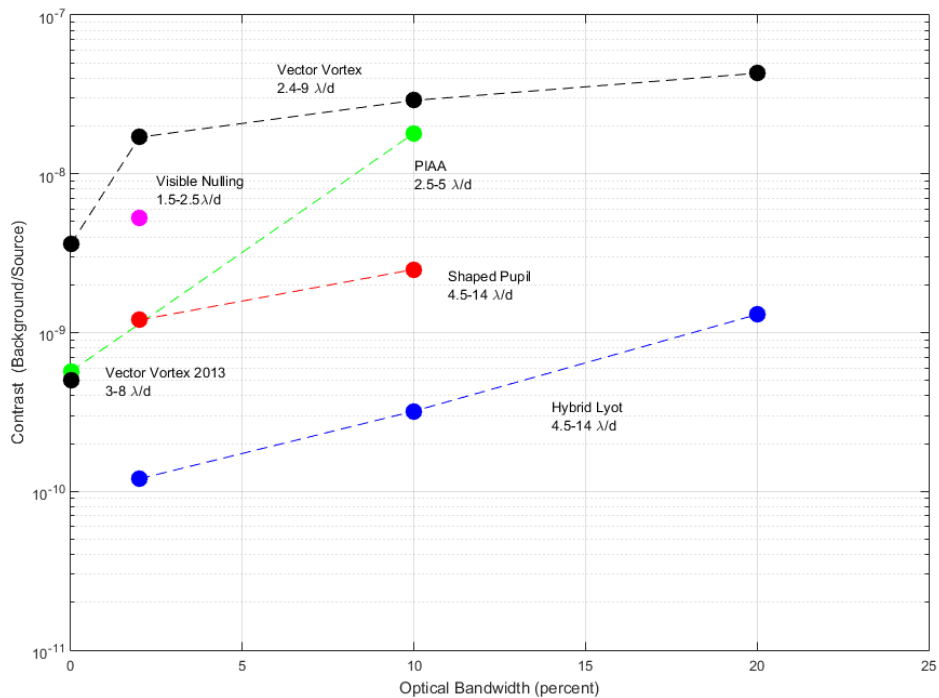


Figure 6: Demonstrated coronagraph contrast as a function of bandwidth. All experiments were conducted with unobscured pupils and demonstrated in vacuum chambers under static environment conditions at 800 nm to near-infrared light.

B.1.1.1 Decadal Survey Testbed

In anticipation of coronagraph demonstrations to support large monolithic and segmented telescopes reaching the 10^{-10} contrast requirement, the ExEP is upgrading one of the High Contrast Imaging Testbeds (HCIT) and vacuum chambers at JPL, building a new testbed to further reduce the noise floor that limits 10^{-10} contrast levels. The new testbed, the Decadal Survey Testbed, passed optical design peer reviews, and began parts procurements in the summer of 2017. The testbed has been designed from the ground up to minimize testbed jitter, improve thermal stability, and minimize stray light. A Hybrid Lyot coronagraph has been chosen to initially work with an unobscured pupil, as this architecture is the laboratory state-of-the-art at 10% bandwidth. The Hybrid Lyot is baselined on WFIRST and was also the selected primary coronagraph from the Exo-C study¹⁸ for off-axis monolith mirror space telescopes.

Achievement of the 10^{-10} raw contrast milestone is planned for the fall of 2018 at which point another coronagraph architecture could be selected in support of an off-axis monolith mission concept such as the HabEx mission concept, or a static segmented pupil mask could be inserted to demonstrate performance with a simulated on-axis segmented telescope such as HabEx's architecture B or LUVOIR's architecture A. The subsequent step planned for 2020 could be the addition of a simulated telescope and disturbance source for either coronagraph architecture to produce a "dynamic" demonstration. "Static" demonstration here and throughout implies no intentionally introduced line of sight errors or other wavefront disturbances, while "dynamic" refers to the experiments where at least some of these disturbances are deliberately introduced into the testbed and the coronagraph is required to sense and compensate for them.

The ExEP will work and consult with other coronagraph testbeds operating in ambient conditions in potentially advancing coronagraph performance from mid-contrast to high-contrast demonstrations. Examples are the HiCat facility at the Space Telescope Science Institute (PI Remi Soummer), the High Contrast High-Resolution Spectroscopy for Segmented Telescopes Testbed at Caltech's Exoplanet Technology Lab (PI Mawet), the Ames Coronagraph Experiment testbed at NASA ARC (PI Belikov), and the University of Arizona (PI Guyon).

B.1.2 CG-2: Coronagraph Demonstrations and Modeling

CG-2: V/NIR Coronagraph Demonstrations and Modeling

Description: The ExEP seeks demonstrations of coronagraph architectures that achieve the necessary contrast, inner working angle, throughput, and bandwidth to directly image and spectrally characterize rocky exoplanets orbiting in the habitable zone of Sun-like stars.

SOA (Lab): 6×10^{-10} raw contrast at 10% bandwidth across angles of 3-15 λ/D demonstrated with a linear mask and an unobscured pupil in a static vacuum lab environment (Hybrid Lyot)

$< 1.6 \times 10^{-9}$ raw contrast at 10% bandwidth across angles of 3-9 λ/D demonstrated with a circularly-symmetric mask and obscured pupil in a static vacuum lab environment (WFIRST)

SOA (Flight): 10^{-4} raw contrast 540 nm at 10 λ/D (HST)

Needed capability: Coronagraph masks and optics capable of creating circularly symmetric dark regions in the focal plane enabling raw contrasts $\leq 10^{-10}$, with minimal contribution from polarization aberration, IWA $\leq 3 \lambda/D$, throughput $\geq 10\%$, and bandwidth $\geq 10\%$ on obscured and segmented pupils in a simulated dynamic vacuum environment.

Supported Missions or Mission Concepts: WFIRST, LUVOIR, HabEx

Current State-of-the-Art:

Demonstrated coronagraph contrast results with unobscured apertures as a function of optical bandwidth are shown in **Figure 6**. Pupil obscurations in on-axis designs (stemming from the secondary mirror and its structural supports) and mirror segmentation further diffract light making deep contrasts more challenging. Resolved angular star sizes due to the larger telescope diameters under consideration provide another level of difficulty for coronagraphs. The WFIRST-CGI has already demonstrated 1.6×10^{-9} raw contrast at 10% bandwidth across angles of 3-9 λ/D demonstrated with a circularly-symmetric mask on their highly obscured pupil, in a static vacuum lab environment. Deep-contrast coronagraphs for systems with pupil obscurations and segmentation can be designed in general, but at the expense of throughput and hence typically results in a degraded signal-to-noise ratio in the image plane.

Progress Over the Last Year:

WFIRST:

The WFIRST-CGI continued to advance its dual Hybrid Lyot and Shaped Pupil¹⁹ coronagraphs. The Hybrid Lyot coronagraph repeatedly demonstrated in vacuum to obtain 5×10^{-9} mean contrast with 10% bandwidth centered at 550 nm in a fully annular dark hole spanning 3-9 λ/D , using the low-order wavefront sensing and control (LOWFS/C; See Section B.2.1 for more details) to correct dynamic wavefront disturbances expected on the WFIRST observatory.²⁰ The GSFC Prototype Imaging Spectrograph for Coronagraphic Exoplanet Studies (PISCES) integral field spectrometer, integrated into the Shaped-Pupil testbed in the HCIT, achieved contrast of 1.09×10^{-8} over an 18% bandwidth.²¹ This work achieves an important step towards the goal of using a coronagraph to search for spectral features of biosignatures in the atmospheres of exoplanets.

At the time of this writing the CGI team was re-establishing its expected performance requirements after the WIETR (WFIRST Independent External Technical/Management/Cost Review) report. Responding to the report, NASA clarified the CGI's status as a technology

development instrument. Baseline technology rather than science requirements will be presented at the Project Systems Requirements Review in the spring of 2018.

Segmented Coronagraph Design and Analysis

To meet the challenge of segmented and obscured aperture coronagraphy, the ExEP's Segmented Coronagraph Design and Analysis (SCDA) study continued funding several groups to design and model different coronagraph architectures that enable 10^{-10} contrast sensitivities with optimal throughput and robustness to many wavefront errors. In addition to the baseline 12 m SCDA set of segmented and obscured apertures,²² the SCDA teams are working with the LUVVOIR design study team to include their 15 m aperture. Robustness calculations will determine the sensitivities of these coronagraph designs to the effects of optical misalignments, and help to establish error budgets. How these error budgets translate to sensing and control of the wavefront errors through mechanical movements will be a critical question for the future of these architectures.

The Apodized Pupil Lyot Coronagraph (APLC) approach has achieved the most success to-date. As of this writing, it is the only coronagraph design meeting 10^{-10} contrast requirements with reasonable throughput and sensitivities; response to segment-to-segment phasing errors is under study. The ExEP's SCDA study is planned to continue advancing design for coronagraphs that work with segmented apertures through at least September of 2018.

Large Mission Concept Studies

The LUVVOIR and HabEx concept studies developed baseline coronagraph designs in preparation for delivering interim reports in 2018. The coronagraph instrument for LUVVOIR's architecture A (a telescope with a 15 m primary mirror), ECLIPS, includes a baseline APPLC appropriate for the telescope's segmented 15 m primary mirror and obscuration by the secondary mirror and supports. ECLIPS includes near-UV, visible band, and near-IR channels with integral field spectrograph modes.

The HabEx mission's initial telescope architecture includes an off-axis 4 m telescope (and thus a clear pupil), supporting a coronagraph with a charge-6 vortex mask, providing robustness to low-order wavefront error modes.

The Origins Space Telescope concept study includes a high contrast coronagraph designed for direct imaging of Saturn and Jupiter analogs at mid-infrared wavelengths. These technologies require specific optimization for longer wavelengths (such as cryogenic operability) but the development of UV/O/IR coronagraph technology may be useful at longer wavelengths as well (See Sect. D) for more detail about mid-IR coronagraph technology).

TDEMs

Jim Breckinridge and Russell Chipman’s TDEM-15²³ work is investigating the role of polarization in coronagraphy, calculating the polarization-related degradation of performance for WFIRST, HabEx, and LUVOIR coronagraphs. While polarization effects have not been a limiting factor in laboratory demonstrations approaching 10^{-10} contrast ratio sensitivities, when coupled with telescopes, polarization-induced wavefront aberrations may potentially limit a coronagraph’s starlight suppression performance^{24,25}. This TDEM team launched an effort to model the WFIRST, HabEx, and LUVOIR fore-optics. Using their customized vector ray trace code POLARISM, the investigators so far are seeing close agreement with the standard modeling tools. The Serabyn TDEM-14 charge-4 vortex coronagraph demonstration achieved first light in the HCIT in November 2017, reaching 5.1×10^{-8} contrast at 2% bandwidth centered at 550 nm in a dark hole spanning $3-9 \lambda/D$ on the first day, dominated by a light leak incoherent with the simulated star. A future iteration, after removing the leak source, the testbed will aim towards a milestone goal of contrast better than 10^{-9} . Future demonstrations will also include higher charge vortex masks to improve contrast performance.

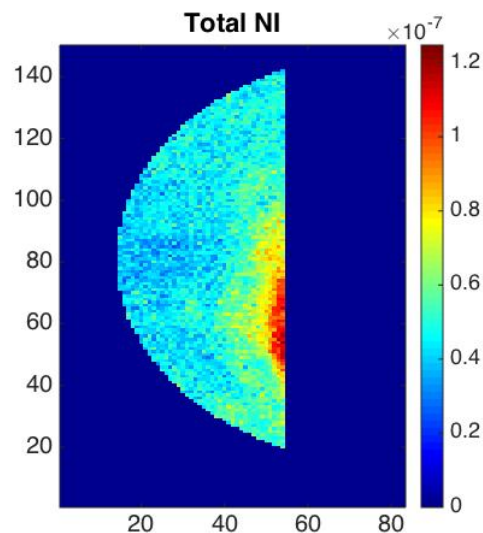


Figure 7: First light results from PI Gene Serabyn’s Vector Vortex demonstration in the HCIT using a Charge 4 mask. Dark hole contrast reached in a $3-9 \lambda/D$ annular region for 2% band at 550 nm was 5.07×10^{-8} . Work is ongoing to reduce the unmodulated diffraction sources to achieve the TDEM milestone of 10^{-9} contrast.

Next Steps:

A gap remains between present capabilities and the needed demonstration of a 10^{-10} contrast ratio visible band coronagraph at $3 \lambda/D$ inner working angle and 10% bandwidth. A number of activities in modeling, mission concept studies, and laboratory demonstrations continue to work towards this goal and to the eventual maturing of coronagraph technology for infusion into a flight mission.

Prior to delivering their final reports in 2019, the HabEx and LUVOIR mission concept studies will continue to further refine their science case and perform preliminary trades at the system

level that will help to better define the coronagraph mask and optical layout needs for future exo-Earth-finding missions.

Advances in coronagraph modeling will continue in order to help understand laboratory demonstrations and to perform design work. The SCDA study will continue through 2018. Work will focus on error budgeting of the leading designs for the initial set of SCDA apertures and coordination with the LUVOR team's selection of large segmented mirror apertures. The TDEM-15 Breckinridge polarization modeling will also continue to assess polarization effects and recommend mitigation strategies for HabEx and LUVOR or other potential exo-Earth missions.

Lab demonstrations in the HiCAT testbed at STScI will demonstrate (in air) APLC coronagraph designs for LUVOR based on an extension of the work done in the SCDA study. A highly complicated gray-scale mask for the APLC will be designed at the STScI and fabricated at JPL's MicroDevices Laboratory as well as at an outside vendor. This coronagraph design will also include a segmented mirror to correct actively segment-to-segment relative tip/tilt/piston errors.

The HCIT will continue to advance the state-of-the-art in laboratory demonstrations. The Serabyn TDEM-14 effort will continue vacuum tests in HCIT in 2018, first aiming towards 10^{-9} contrast with the charge-4 mask and later including a charge-6 vortex mask similar to the mask baselined by HabEx. In 2018, the ExEP will commission the Decadal Survey Testbed in HCIT with a demonstration of a 10^{-10} contrast using a Hybrid Lyot. Upon commissioning, this testbed will become available for all TDEM PIs.

Two new TDEM efforts were awarded in 2017 to continue to advance the state-of-the-art for coronagraph contrast demonstrations. A TDEM-16 (PI Belikov, NASA/Ames) was awarded to advance PIAACMC architecture, and another TDEM-16 (PI Trauger JPL/Caltech) was awarded to advance a next-generation Lyot coronagraph. Each of the new TDEMs will first undertake design optimization within the particular coronagraph architecture, followed by demonstrations on a clear pupil using ExEP's HCIT. Both coronagraph architectures aim for demonstrations achieving high contrast with segmented and obscured pupils.

Prioritization:

This technology received Impact, Urgency, and Trend scores of 4, 4, and 2, respectively. Coronagraph optics and laboratory demonstrations constitute a key aspect to maturing starlight suppression technology that enables future exo-Earth-finding missions, giving it the highest Impact score. This technology is potentially applicable to the WFIRST mission, which has less stringent requirements than a future exo-Earth mission, but can still benefit from advances in coronagraph mask technology. Hence, the Urgency is also at the highest level. The Trend score is 2 because the WFIRST project, ground-based investigations, and a number of active TDEM awards are already making progress towards the final starlight suppression needs.

B.1.3 CG-3: Deformable Mirrors**CG-3: Deformable Mirrors**

Description: Flight-qualified large-format deformable mirrors and their electronics capable of achieving and maintaining 10^{-10} contrast performance.

SOA (Lab): Electrostrictive 64×64 actuator DMs have been demonstrated to meet $\leq 10^{-9}$ contrasts and $< 10^{-10}$ stability in a vacuum environment and 10% bandwidth; 48×48 actuator DM passed random vibrate testing

SOA (Flight): None

Needed capability: 4 m primary mirror: $\geq 96 \times 96$ actuators; 10 m primary mirror: $\geq 128 \times 128$ actuators. Enable raw contrasts of $\leq 10^{-9}$ at $\sim 20\%$ bandwidth and IWA $\leq 3 \lambda/D$. Flight-qualified device and drive electronics (radiation hardened, environmentally tested, life-cycled including connectors and cables). Mirror stability maintains 10^{-10} contrast for observation time scales.

Supported Missions or Mission Concepts: WFIRST, LUVOIR, HabEx

High-contrast coronagraphs depend on deformable mirrors (DMs) to (1) create dark regions by compensating for surface and coating irregularities on the telescope primary mirror, and (2) maintain the dark region (stability). DMs maintain speckle stability in the dark region by correcting for the relatively slow thermal drifts the observatory will experience in its orbit during science observations. Additionally, in some cases, the DMs can be pre-shaped to work in concert with the coronagraph masks to mitigate the diffraction effects of obscured apertures.^{26,27}

Current State-of-the-Art:

The WFIRST coronagraph will use two 48×48 element electrostrictive lead magnesium niobate (PMN) DMs made by Adaptive Optics Associates Xinetics in Devens, MA, a subsidiary of Northrop Grumman. These mirrors have been routinely used in the HCIT vacuum testbeds since 2003. With a 500 μm actuator stroke and 1 mm pitch sizes, they have participated in all the HCIT demonstrations better than 10^{-9} with unobscured pupils. These DMs are built up from electro-ceramic blocks with actuators separated by 1 mm (see **Figure 8**). These blocks are assembled into modules covered by a single-mirror facesheet and driven by a Gen 5 voltage supply (not multiplexed) with 100 V range and 16-bit resolution. One Xinetics DM has already successfully undergone a 3-axis random vibration test to 10.8 g rms.

Alternative DMs include MEMS devices, such as those fabricated by Boston Micromachines Corp (BMC). These DMs are made of a polysilicon membranes coated with one or more layers for the reflective surface and are actuated by 32×32 or 64×64 electrostatic actuators on the backside. BMC offers both continuous face-sheet and segmented mirrors. Pitch sizes come less than 0.5 mm and maximum stroke is about 5 μm for 250 V drive voltage. These mirrors are currently considered as a backup for the WFIRST coronagraph.

Iris AO DMs are MEMS devices with three electrostatic actuators underneath a segmented mirror surface. The three actuators provide piston, tip, and tilt to a segment. The hexagonal segments are 700 microns wide, vertex to vertex. The actuators are long stroke (8 μm or 5 μm , depending on the model) over 200 V. The small step precision is limited by electronics digital/analog bit depth. The current Iris AO built electronics are 14 bits, but 20-bit super-

resolution electronics are in development. An Iris AO MEMS DM has demonstrated a monochromatic raw contrast of 5×10^{-9} over angular separations of $1.5\text{--}2.5 \lambda/D$ using a Visible Nuller Coronagraph at GSFC.²⁸

Progress Over the Last Year:

The pre-environmental characterization of BMC MEMS deformable mirrors was carried out in the Vacuum Surface Gauge testbed at JPL in 2017. The mirrors were shown to hold a flat surface to better than 1 nanometer rms over several days. A 50×50 MEMS wafer was developed under SBIR.

For wavefront control at the sub-nanometer level improvements in electronics are needed, not only for miniaturization but also in driving mirror actuators at high resolution. Development and testing of higher-bit-count DAC electronics for DM operations was carried out under SBIR funding. Iris AO demonstrated electronics with 19.6 bits of super-resolution and 30-minute stability.

Development of a new MEMS DM began as an APRA-funded collaboration between Microscale, Inc and JPL. The Microscale DM is directly mounted on an ASIC in order to enable multiplexing of the large number of interconnects, potentially a useful way to achieve miniaturization.

Next Steps:

Future DM needs for larger space telescopes such as HabEx or LUVOIR will include larger format sizes and improved stability with interest in longer stroke and tighter pitch sizes. Larger format DMs allow for larger outer working angles for debris disk science as well as probing the closest exoplanetary systems. Format needs for 4 m-class telescopes may be 96×96 actuators and 10 m-class telescopes may even request 128×128 actuators or larger. Larger Xinetics DMs have been built through mosaicking smaller units. A 64×64 actuator device has operated successfully in the HCIT for over a decade. This larger format was achieved by mosaicking four 32×32 ceramic blocks. A 66×66 unit has also been mosaicked from 11×11 units for the Palm 3000 adaptive optics system at the Palomar Observatory. It is expected that the same technique could be used to meet future large format DM needs although no investments have been made.

While increasing the actuator count of DMs is straightforward, with mosaicking in the case of electrostrictive DMs and with scaling of the wafer design for MEMS, handling the enormous number of interconnects and the drive electronics channels remains a challenge. Increasing the actuator count of MEMS DMs creates the additional challenge of close-packing large numbers of wirebonds, a subject of APRA- and SBIR-funded investigations that will continue in 2018.

WFIRST will also help advance the DM state-of-the-art over the next few years. Expected activities include:

- Stability measurements of DMs
- Flight qualifying the drive electronics
- Redesigning the electronic interconnects to the actuators

- Miniaturizing the drive electronics
- Improving the facesheet surface figure error so as to gain more stroke
- Life test the DM actuators
- Complete environment testing including thermal, dynamic, and radiation testing

In the near term, the WFIRST project plans in 2018 to complete the development of an engineering model of the electrostrictive DMs and complete full environmental tests (random vibrate, thermal cycling, and thermal vacuum tests).

There is interest in smaller pitch sizes (< 1 mm) for future large aperture telescopes to reduce the size of the optical beam and hence, the optics and in larger stroke (> 500 nm) devices.

Improved gain calibration for the actuators may be needed for future missions; the 8% gain

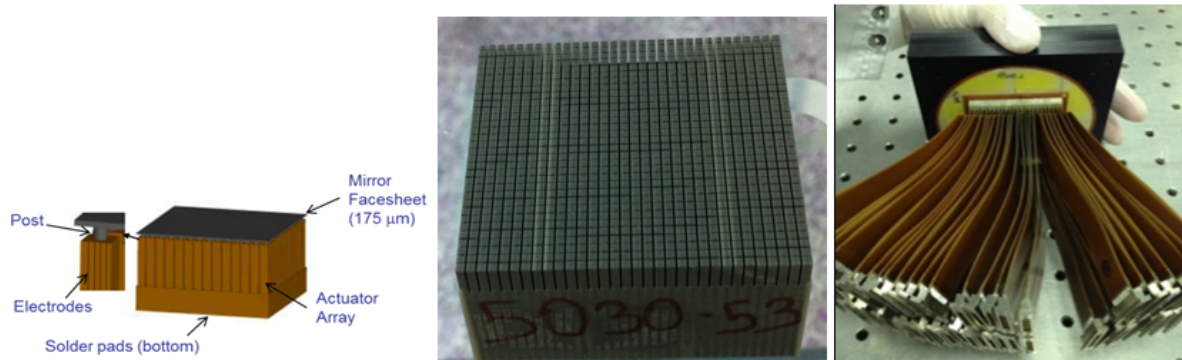


Figure 8: (Left) Schematic of the bulk ceramic block with cut actuators mounted to a facesheet. (Center) Bulk block with 1 mm cut posting actuators. (Right) Connector cables extending from the back of the DM.

DMs will be tested in the stratosphere in science operation conditions. Two balloon-borne projects, PICTURE-C²⁹ and HiCIBaS³⁰, are expected to deploy and launch in 2018 and will demonstrate autonomous operations of DMs in a high contrast imaging application. DEMI, a MIT-led cubesat project that will achieve on-orbit demonstration of active wavefront control with a BMC MEMS DM, passed Preliminary Design Review (PDR) in 2017 and aims for a launch in the next several years.³¹ None of these smaller telescopes will achieve the performance needed to directly image an exo-Earth, but will gain valuable experience with operations and in advancing DM technology.

Prioritization:

This technology received Impact, Urgency, and Trend scores of 4, 4, and 2, respectively. As an essential optical element that enables coronagraphs to achieve high contrast through dynamic control of residual wavefront error and its drift, ExEP considers this technology to have the highest impact score. The urgency is high as well, as the WFIRST-CGI instrument can benefit from advances in DM technology in the near term. Current investments from CGI, the TDEM, APRA, and SBIR programs are expected to make advances in the near-term, resulting in a lower trend score.

B.1.4 CG-4: Data post-processing Algorithms and Techniques

CG-4: Data Post-Processing Algorithms and Techniques

Description: Data post-processing techniques to remove residual speckle noise at the focal-plane detector further improving contrast sensitivity.

SOA: Few 100× speckle suppression has been achieved by HST and by ground-based AO telescopes in the NIR and in contrast regimes of 10^{-4} to 10^{-5} , dominated by phase errors.

Needed capability: A 10-fold contrast improvement in the visible from 10^{-9} raw contrast where amplitude errors are expected to be important (or a demonstration of the fundamental limits of post-processing)

Supported Missions or Mission Concepts: WFIRST, LUVVOIR, HabEx

The removal of quasi-static speckle noise from imagery data using post-processing techniques can further improve the final contrast and inner working angle capabilities achieved by coronagraphs. Counting on an order of magnitude improvement in the final contrast may loosen both wavefront control and telescope stability requirements needed for raw contrast. Some post-processing techniques require angular diversity by rolling the instrument (and spacecraft) azimuthally with respect to the star, or rely on observing a reference star. The specifics of the post-processing technique, however, levy operational requirements and calibration requirements on the spacecraft system and need to be understood from the system level early in the design process.

Current State-of-the-Art:

Remi Soummer et al.³² applied ground-based techniques to HST NICMOS data and achieved signal-to-noise (SNR) improvements of 100 times for data with an initial contrast of 10^{-5} in the near-infrared. The use of similar techniques to improve contrast in the visible is under study via simulations in the WFIRST CGI technology development program. Initial results are promising with expected contrast improvement of 5 to $10^{33, 34}$ for initial contrasts of around 10^{-9} to 10^{-8} , depending on angular separation and the actual post-processing method. However, it is important to note that such post-processing improvements are only obtained in the speckle noise-limited regime, i.e. when shot noise is negligible compared to speckle noise.

Applying state-of-art post-processing techniques onto image data at 10^{-9} -level contrasts in the visible are unprecedented. This is a regime where amplitude wavefront errors may become as important as phase errors. Most of the high contrast coronagraphic imaging post-processing algorithms and applications have been conducted only in the near-infrared so far.

Progress Over the Last Year:

Zimmerman, Pueyo, and Soummer (2017) demonstrated a principal component separation-based algorithm using WFIRST CGI lab data to remove speckles by reference differential imaging. The algorithm consistently performed a factor of 3-5 better than simple PSF subtraction. Importantly, they showed that frame-to-frame speckle stability does not by itself determine the post-processing gain; the diversity of a reference library captured over a long time baseline can amplify the gain.

Next Steps:

New WFIRST CGI lab data sets will be acquired with a lower flux light source consistent with a typical target star in order to test the interaction of post-processing algorithms with Poisson noise. Post-processing tests will also continue on numerically simulated WFIRST CGI data sets. The new simulated data will make use of revised coronagraph mask designs, and for the first time will include the effects of pointing jitter, wavefront jitter, and pupil shear errors. Together these efforts will lead to more realistic predictions of contrast gain as the coronagraph instrument is assembled and closer to its final flight design conditions (spectral bandwidth, dynamical perturbations, etc.).

Beyond WFIRST, at the 10^{-10} contrast levels required for exo-Earth detection, it remains to be seen whether speckle noise will be detected at high enough signal-to-noise relative to statistical photon and detector noise, for post-processing algorithms to be able to remove it with enough precision to make significant contrast gains.

Prioritization:

This technology received Impact, Urgency, and Trend scores of 4, 2, and 2, respectively. This technology is considered to be enabling for an exo-Earth mission, as it potentially can achieve gains in contrast by distinguishing planets from residual diffraction speckles. The Urgency is relatively low, as it applies to missions beyond WFIRST. Additionally, as a ground data processing algorithmic technology, it can be matured relatively late in the life of a mission as compared to hardware. The trend score is 2, because the ongoing work by WFIRST-CGI and ground-based instrument are investigating algorithmic concepts that may apply to exo-Earth missions.

B.2 Contrast Stability

A coronagraph must maintain its contrast performance long enough to directly image or spectrally characterize a planet. For a system required to achieve contrast sensitivities of 10^{-10} , this places challenging requirements on the telescope system's overall wavefront error stability in the presence of thermal and mechanical disturbances: depending on the system architecture, this can be on order of 10 to 100 pm wavefront error stability over a control loop step (typically 10 minutes). This ambitious stability requirement can be met by designing a telescope and coronagraph with three goals in mind: robustness to disturbance, passive stability, and active control where needed. The technologies listed by the ExEP that address this gap are Mirror Segment Phasing Sensing and Control (CG-6; Section B.2.2), Telescope Vibration Sense/Control or Reduction (CG-7; Section B.2.3), and Wavefront Sensing and Control (CG-5; Section B.2.1).

While the individual components are needed, subsystem performances are inter-dependent and can be traded between each other. Therefore, a systems-level view is particularly interesting; "Wavefront Stability Demonstrations and Assessments" are included in the TDEM

component of the 2017 SAT. Component-level investigations are also of interest if they can be shown to have wavefront and structural stability applications across multiple telescope/coronagraph architectures.

Saif et al. are funded under the COR component of SAT to develop the capability for pm-scale metrology, using stability on fast time scales. In 2017, 25 pm control of an actuator was demonstrated in air, and in CY 2018 the team plans to set up an ultra-stable vacuum test chamber. This is an essential capability for validating a mirror system for an exo-Earth-finding mission.

Because their primary science goals include direct imaging and characterization of exo-Earths, both the LUVOIR and HabEx mission concepts are focusing their system architecture studies on the ability of the overall system to achieve pm-class wavefront error stability. These architectures are advancing rapidly and use multiple levels of disturbance reduction, passive isolation and active control.^{35,36,37,38}

In addition to systems level demonstrations and assessments, ExEP is interested in the maturation of specific subsystem and component technologies that contribute to the required overall system stability, as long as they can be shown to be applicable to a wide range of architectures.

The NASA Astrophysics Division is, in addition, soliciting proposals in 2018 for an industry one-year studies on a system-level design and modeling studies and associated testbed demonstrations.³⁹

B.2.1 CG-5: Wavefront sensing and control

CG-5: Wavefront Sensing and Control

Description: Sensing and controlling line-of-sight jitter and low-order wavefront drift

SOA (Lab): < 0.5 mas rms per axis LOS residual error demonstrated in lab with a fast-steering mirror attenuating a 14 mas LOS jitter and reaction wheel inputs; ~12 pm rms sensitivity to focus (WFIRST)

SOA (Ground): Higher low-order modes sensed to 10–100 nm WFE rms on ground-based telescopes

SOA (Flight): None

Needed capability: Sufficient fast line-of-sight jitter (< 0.5 mas rms residual) and slow thermally-induced WFE sensing and control (≤ 10 pm rms sensitivity) to maintain closed-loop < 10^{-10} raw contrast with an obscured/segmented pupil and simulated dynamic environment.

Supported Missions or Mission Concepts: WFIRST, LUVOIR, HabEx

A coronagraph removes starlight diffraction (e.g. Airy rings) and can remove any other stellar leak that is static and known a priori. However, random diffraction speckles (static, quasi-static, and dynamic) remain, and may limit contrast levels to 10^{-6} to 10^{-4} , depending on the optical component quality. An adaptive optics (AO) system is necessary for reaching and maintaining the contrast levels needed for exo-Earth imaging. Unlike conventional ground-based AO, high contrast AO for space missions is typically accomplished by using a focal-plane based Wavefront Control (WFC) system in order to avoid non-common path errors. A DM is used to provide the necessary measurement diversity in focal-plane images as well as to subsequently remove the

speckles. Faster wavefront control of tip/tilt aberrations due to telescope jitter can be achieved with a fast steering mirror.

An additional need is the ability to suppress starlight from a close companion star. This light will be incoherent with light from the target star and thus not suppressible with standard wavefront control algorithms. Many non-M-dwarf stars are in multiple-star systems, thus this capability enlarges the number of stellar systems available for direct imaging observations. Another particularly important binary system is Alpha Centauri, which is 2.4 times closer than any other Sun-like star.

Current State-of-the-Art:

The WFIRST coronagraph's Low-order Wavefront Sensing and Control (LOWFS/C) system represents the state-of-the-art for both ground and space systems. It was designed to suppress expected dynamic wavefront error drifts due to thermal and mechanical disturbances, such as vibrations from spacecraft reaction wheels. The WFIRST LOWFS/C consists of a Zernike wavefront sensor which samples on-axis light rejected by the coronagraphic masks. The sensor reads out at high speeds (~ 500 Hz) and a control system then feeds back to a deformable mirror and to a fast steering mirror. WFIRST demonstrated in early 2017⁴⁰ a coronagraph contrast better than 10^{-8} at working angles from $3 - 9 \lambda/D$ using the LOWFS/C system in the presence of a WFIRST-telescope-like thermal and mechanical disturbances. The demonstration achieved focus control to 12 pm rms and line-of-sight jitter of 14 mas rms was suppressed to 0.5 mas rms.

To handle binary (or multiple) star systems, a technique called "multi-star wavefront control" has been demonstrated.⁴¹ This technique does not in principle need any changes in hardware of existing space mission designs like WFIRST, LUVOIR, and HabEx (although it could benefit from a mild "print-through" pattern commonly found on many DMs, or another mild grating in the system).

Progress Over the Last Year:

As part of their coronagraph and telescope system designs, the LUVOIR and HabEx mission concepts are investigating the necessary spatial and temporal needs for wavefront stability. These requirements entered into their baseline coronagraph designs which will be shown as their preliminary reports are released in 2018.

In order to further develop the Multi-star Wavefront Control technique, in 2017, a NASA directed work package was awarded to Belikov (NASA/Ames). The team plans to collaborate with the WFIRST, HabEx, and LUVOIR teams in order to develop control algorithms specific to the particular mission or mission concept and to eventually demonstrate them in a high contrast environment.

Next Steps:

A remaining challenge is the achievement of fast wavefront control in the presence of realistically low light levels, and also control of higher order Zernike modes, directions to be investigated by the WFIRST-CGI project. Existing systems are believed to still be orders of magnitude away from fundamental limits of algorithm efficiency and can thus be significantly

improved in terms of speed. Additionally, the polarization aberrations induced by the relatively fast primary and secondary mirror optics will be simulated in future CGI demonstrations. Other areas of improvement include achieving control in a wider wavelength band, in combining off-axis wavefront control with on-axis wavefront control to improve the coronagraph sensitivity to line-of-sight jitter, at even deeper contrasts, and in multiple polarization channels. While the WFIRST LOWFS/C system has achieved pm-class measurement sensitivity to low order wavefront errors, systems level assessments by HabEx and LUVOIR are investigating the higher-order sensing and control needs of the telescope and how these could be coupled in a feed-forward sense to active controls in the opto-mechanical system.

For example, the performance of a coronagraph behind LUVOIR's segmented primary mirror is most sensitive to the relative piston and tip/tilt of the individual segments (see section B.2.2 below) which are not well-described by low-order Zernike modes. An out-of-band wavefront sensor (OBWS; operating in the UV while science observations occur in the visible) could use a dichroic to feed a Zernike wavefront sensor, avoiding the spatial filtering of the occulting spot reflection, and thus measure the wavefront errors over a much wider range spatial frequencies. The exact sensitivity to temporal and spatial modes depends on the brightness of the guide star, which could potentially be an artificial one created by a cubesat-sized companion spacecraft,⁴² and the use of an OBWS in the overall control system must be looked at in concert with other components of the opto-mechanical system.

These assessments could change the requirements on the wavefront sense and control system of a future exo-Earth imaging mission. The demonstrated WFIRST CGI LOWFS sensitivity to line-of-sight jitter translates into 0.03 milliarcseconds for LUVOIR and 0.1 milliarcseconds for HabEx, which will be evaluated.

Prioritization:

This technology received Impact, Urgency, and Trend scores of 4, 3, and 2, respectively. Wavefront sense and control is essential for handling thermal and mechanical disturbances during a deep observation, and is thus an enabling technology for an exo-Earth mission (Impact = 4). The Urgency is relatively high as progress towards the must be shown by the time of the 2020 Decadal Survey. The WFIRST mission is maturing this technology, as is ExEP's Decadal Survey Testbed. In addition, the HabEx and LUVOIR mission concept studies are better determining the requirements on a LOWFS/C system for exo-Earth detection, and thus the trend score is 2.

B.2.2 CG-6 Mirror Segment Phasing Sensing and Control

CG-6: Mirror Segment Phasing Sensing and Control

Description: Segmented mirrors require segment phasing and rigid-body sensing and control of the segments and the surface figure to achieve tight static and dynamic wavefront errors.

SOA (Lab): 6 nm rms rigid body positioning error and 49 nm rms stability (JWST error budget); SIM and non-NASA: nm accuracy and stability using laser metrology; capacitive gap sensors demonstrated at 10 pm

SOA (Ground-based): Keck has achieved 6 nm positioning error rms

SOA (Flight): None

Needed capability: Systems-level considerations to be evaluated but expect will require WFE stability less than 10 pm rms sensitivity and control over periods of tens of minutes with obscured/segmented pupil and simulated dynamic environment

Supported Missions or Mission Concepts: LUV0IR, HabEx

Unlike a traditional monolithic telescope mirror, a multi-segment large-aperture mirror will require phasing and rigid-body sensing and control of the segments to achieve tight static and dynamic wavefront errors at visible and near-infrared wavelengths. Wavefront errors caused by segment rigid body positioning errors, dynamic vibrations, and slow thermal drifts can significantly impact coronagraph coherent imaging and hence contrast. For example, a coronagraph working with a segmented mirror, to avoid speckle noise brighter than typical exoplanets, requires a segment-to-segment dynamic co-phasing error to change less than 10 pm rms between WFSC updates (from a few minutes to many tens of minutes depending on the host star's brightness).⁴³

Current State-of-the-Art:

The Keck ground-based telescope and JWST sense and control the rigid-body positions of their segments by utilizing wavefront sensing and control, such as phase retrieval, Shack-Hartman sensing, and dispersed fringe sensing.⁴⁴ Keck also uses capacitive edge sensors. JWST's optical error budget includes 6 nm rms for rigid body positioning and 49 nm rms stability. While these methods are proven for phasing diffraction-limited segmented optical systems such as JWST, it remains to be seen if they can achieve the tens of picometer-level stability required for exoplanet imaging at visible wavelengths.

Picometer-accuracy laser metrology was demonstrated by the Space Interferometry Mission with large beam launchers. More compact beam launchers, lightweight enough to mount to the edges of segments, have been developed over the last few years for non-NASA customers but were designed to operate at the nanometer-precision level. Additional development in laser metrology is needed if a laser metrology truss is to be used for sensing segment positioning.

Progress Over the Last Year:

The LUV0IR mission concept study is developing an architecture that combines the use of a laser metrology truss to measure positional changes of the large optics to the expected pm-level stability requirements, complemented by high bandwidth edge sensors. Feinberg et al (2017)⁴⁵ set for the 15 m LUV0IR telescope a required update rate for mirror segments on the order 2 minutes if wavefront errors are measured with a magnitude 10 star, and showed Ball

Aerospace’s demonstration of a capacitive distance measurement to < 10 pm for a Fabry-Perot etalon application, which is a key first step towards a picometer-level segment edge sensor. Using the ATLAST concept as a reference, Nemati et al. (2017) considered the effects on coronagraph contrast in the presence of segment-to-segment and global errors in a large segmented telescope.⁴⁶ The results are reproduced in Table 4. The segment piston and tilt errors represent the relative positioning of the mirror segments and agree with previous estimates that set a roughly 10 pm rms phasing error. The exact details depend on the reference mission and the coronagraph under consideration.

| Segment Errors | | Global Errors | |
|---------------------|-----|---------------------|------|
| Mode | pm | Mode | pm |
| Segment Piston | 7 | Global Bend about Y | 209 |
| Segment Tilt | 13 | Global Bend about X | 224 |
| Segment Power | 23 | Global Spherical | 624 |
| Segment Astigmatism | 32 | Global Hexafoil | 778 |
| Segment Trefoil | 87 | Global Zernike Coma | 1049 |
| Segment Hexafoil | 314 | Global Trefoil | 2322 |
| | | Global Seidel Coma | 2872 |
| | | Global Power | 5798 |

Table 4: A reproduction of Table 1 of Nemati et al. (2017) showing the rms wavefront error that degrades the ATLAST APLC coronagraph contrast to 10^{-10} for a per-segment wavefront aberration (left) and global wavefront aberration (right).

Nissen et al (2017)⁴⁷ investigated the applicability of laser metrology to correction of wavefront error drift for coronagraph instruments on several telescopes. For the baseline 15 m LUVOIR, the conclusion is that current capabilities of laser metrology systems allow control at the 40 pm rms level, as long as the beam launchers, corner cubes, and interfaces can be thermally controlled at the milliKelvin level. The authors also determined that laser metrology to sense and control the relative positions of the primary and secondary mirrors is also applicable to the HabEx concept.

Next Steps:

More work is needed to study the wavefront stability problem at a systems level, of which segment phasing is a component. Work defining requirements and architectures will continue to advance within the HabEx and LUVOIR mission concept studies. LUVOIR will consider a second 9 m architecture, and HabEx is considering a second 6.5 m segmented architecture as an alternative to their initial 4 m monolith study.

The picometer-level capacitive sensor, if it is needed as a part of the systems-level solution, should be matured by demonstration in an edge-sensor-like configuration.

Studies should additionally determine whether higher order active wavefront control (beyond piston, tip/tilt) is needed at the segment level, potentially adding further actuation.

Prioritization:

This technology received Impact, Urgency, and Trend scores of 4, 3, and 3, respectively. For an exo-Earth mission using a coronagraph instrument on a segmented telescope, this is an enabling technology, and thus receives an Impact score of 4. The Urgency is also high as progress in this technology, even at a design level, could have an impact on the recommendations of the 2020 Decadal Survey. The trend score is relatively high as a plan for demonstrating the needed performance is not yet in place, though the call for industry studies (see Sect. B.2) provides an avenue for performing assessments in this area.

B.2.3 CG-7: Telescope Vibration Sensing and Control or Reduction

CG-7: Telescope Vibration Sensing and Control or Reduction

Description: Isolation, reduction, and/or damping of spacecraft and payload vibrational disturbances

SOA (Lab): 80 dB attenuation at frequencies > 40 Hz (JWST passive isolation); Disturbance-Free Payload demonstrated at TRL 5 for JWST with 70 dB attenuation at high frequencies with 6-DOF low-order active pointing. GAIA cold gas microthrusters or LISA pathfinder colloidal microthrusters for fine pointing can reduce disturbance environment.

SOA (Flight): none

Needed capability: Vibration Isolation or reduction of vibration disturbance sources to a level that enables < 1nm wavefront error rms stability.

Supported Missions or Mission Concepts: LUV01R, HabEx

Isolation and damping of spacecraft and payload vibrational disturbances, or reducing these disturbances to acceptable levels, is critical in enabling a coronagraph to reach 10^{-10} contrast sensitivities at IWAs less than $3 \lambda/D$. Leakage of starlight due to pointing instability or jitter and vibration in the telescope that exceed the control range of the coronagraph's LOWFS/C will potentially scatter light onto the imaging detector and degrade the detection contrast within the dark hole. Precision pointing stability needed by the telescope during integration to keep the star inside the correction capabilities of the coronagraph may need to be better than a few mas⁴⁸ (depending on LOWFS/C capability; see Section B.2.1).

The effects of mechanical disturbances on the stability of the telescope can be handled in a number of ways including reduction of the disturbances through design, or by dynamic isolation. For isolation of a telescope system with reaction wheels, typical expected attenuations > 100 dB end-to-end are needed.^{49,50} "End-to-end" implies isolation between disturbance source and the optical telescope element and coronagraph instrument. The isolation requirements also critically depend on the mirror stiffness and mass; stiffer mirrors have a lower wavefront error for a constant vibration levels, as do more massive mirrors.

Micropropulsion thrusters for fine pointing, used exclusively or in a hybrid fashion with reaction wheels, is another option to reduce the disturbance levels. Hybridizing the LOWFS/C fast steering mirror system with the fine guidance system is also an approach that could be considered, though there are costs in coronagraph throughput and does not allow control of wavefront errors other than tip/tilt.⁵¹

Current State-of-the-Art:

Several aerospace companies have demonstrated systems that allow for active dynamic isolation candidates. A non-contact isolation system by Lockheed Martin known as the Disturbance-Free Payload⁵² demonstrated 68 dB of broadband isolation in a JWST testbed and is self-assessed at TRL 5 for large observatories. The payload and spacecraft bus are separate bodies that fly in close-proximity, allowing precision payload control and simultaneous isolation from spacecraft disturbances.

The use of cold gas microthrusters to achieve extreme spin-rate stability has been demonstrated on-orbit by GAIA. Colloidal microthrusters were used in LISA Pathfinder, which has demonstrated micro-Newton thrust control on orbit.

Progress Over the Last Year:

HabEx and LUVOIR studies are developing architectures which will set the necessary stability requirements. The Lockheed Martin non-contact isolation has been preliminarily shown by the LUVOIR design team to provide the needed isolation for LUVOIR's 15 m telescope.⁵³ Both teams have looked at reducing traditional jitter injected by reaction wheels through the assessment of microthrusters.

Next Steps:

Telescope stability, like wavefront stability in general, is a systems-level challenge and is most efficiently addressed by a reference design that includes selected coronagraph and telescope architectures. Work in defining requirements has begun within both the LUVOIR and HabEx mission concept studies and will extend through the concept studies as a key aspect. In addition, characterizing WFIRST's transmitted spacecraft disturbances to the coronagraph instrument will be valuable for understanding the threshold disturbance the coronagraph LOWFS/C can attenuate.

Prioritization:

This technology received Impact, Urgency, and Trend scores of 4, 3, and 3, respectively. For an exo-Earth mission using a coronagraph instrument on a segmented telescope, this is an enabling technology, and thus receives an Impact score of 4. The Urgency is also high as progress in this technology, even at a design level, could have an impact on the recommendations of the 2020 Decadal Survey. The trend score is relatively high as a plan for demonstrating the needed performance is not yet in place, though both the work of the HabEx and LUVOIR design teams are studying this technology. Additionally, the call for industry studies (see Sect. B.2) can allow additional assessments in this area.

B.3 Angular Resolution

The habitable zone of an exo-Earth at 10 pc has an angular extent of 100 mas at planet quadrature (see **Figure 3**). To just detect such a planet at 400 nm, a telescope requires an angular resolution of 25 mas if we conservatively assume a $3\lambda/D$ coronagraph, and thus this

telescope would have a 3.3 m diameter primary mirror aperture. However, detecting the many spectral biosignatures at longer wavelengths would require even larger apertures. Imposing the same parameters for detecting the planet at 760 nm (oxygen line), a 6.3-m telescope is required; detecting the planet in a water line at 940 nm requires a telescope aperture approaching 8 m. Improvements in a coronagraph's inner working angle can help drive the necessary aperture size down, as would investigations of our solar neighborhood limited to within 10 pc.

Aside from angular resolution, large primary mirrors enhance planet sensitivity due to reduction in science integration time with greater collecting areas and throughput enabling probing of a larger number of more distant stars' habitable zones and improved spectral resolution. The telescope's primary mirror size and architecture (monolithic or segmented, obscured versus unobscured) is among the most important decisions a space telescope team will have to make, especially when considering optimizing the performance of a coronagraph.

In addition, the biggest unknown needed to select the telescope size is the fraction of Sun-like stars with Earth-size planets in their habitable zones, also known as η_{Earth} . As η_{Earth} increases, sufficient statistics about the habitability of exoplanets can be built with fewer observations of planetary systems. If η_{Earth} is near 0.1, then a 10-m-class telescope is required to detect and characterize approximately 30 candidate habitable zones for exo-Earths⁵⁴. If η_{Earth} is above 0.8 then only a 4 m-class telescope would be required to detect and characterize the same number of candidate habitable zones. η_{Earth} is expected to be better constrained in the near future, based on additional analysis of the Kepler data.

B.3.1 CG-1: Large Aperture Mirrors

CG-1: Large Aperture Mirrors

Description: Large monolith and multi-segmented mirrors for space that meet tight surface figure error, coating uniformity, and thermal control requirements at visible wavelengths

SOA (Monolith): 3.5-m sintered SiC with < 3 μm SFE (Herschel); 2.4-m ULE with ~10 nm SFE (HST); Depth: Waterjet cutting is TRL 9 to 14", but TRL 3 to >18". Fused core is TRL 3; slumped fused core is TRL 3 (AMTD).

SOA (Segmented): (no flight SOA): 6.5 m Be with 25 nm SFE (JWST); Non-NASA: 6 DOF, 1-m class SiC and ULE, < 20 nm SFE, and < 5 nm wavefront stability over 4 hr with thermal control

Needed capability: Aperture: 4–16 m; SFE < 10 nm rms (wavelength coverage 400–2500 nm); Wavefront stability better than 10 pm rms per wavefront control time step; Segmented apertures leverage 6 DOF or higher control authority meter-class segments for wavefront control. Environmentally tested

Supported Missions or Mission Concepts: LUVVOIR, HabEx

Here we consider large telescope mirror technology with better than 10 nm rms surface figure error and compatible with the 10 pm wavefront error stability needed for exo-Earth coronagraphy. The large primary mirror can be either segmented or a monolith. The exact requirements on the telescope are system-dependent and trades can be made with other subsystems. In this particular technology area, we consider the manufacturability of the mirror, the backing structure, and the thermal control that meets the stability requirements (because thermal control is so integrated in the choice of mirror material and the mounting of the mirror). Mirror coating technology is considered separately (see Section E.1.1). Additionally,

the technology for maintaining segment phasing, low order wavefront sense and control, and vibrational isolation and disturbance reduction are considered as separate, though closely related, technologies for closing the Contrast Stability technology gap (Section B.2).

However, here we do include the technology for thermal control of telescopes. Historically, space telescopes use passive thermal control. For example JWST's telescope is in a Sun-shade shadow and HST's telescope is in a heated tube. And again, while not designed to meet the requirements of a UVOIR exoplanet science mission, JWST is predicted to have a 31 nm rms WFE response to a worst-case thermal slew of 0.22 K and take 14 days to passively achieve < 10 pm per 10 min stability. This is too long for a coronagraphic exoplanet mission. HST is a cold-biased telescope heated to an ambient temperature. However, it is not a controlled thermal environment. Thus, HST's wavefront error changes by 10–25 nm every 90 min (1–3 nm per 10 min) as it moves in and out of the Earth's shadow.

When considered for use with a starshade (see Sect. C) instead of a coronagraph instrument, the wavefront error stability requirements of a large aperture telescope are greatly relaxed, and diffraction due to obscurations and segmentation become less of an issue.

B.3.2 Large Monolithic Mirrors

Monolith primary mirrors in an off-axis telescope provide an ideal unobscured pupil for a coronagraph, but are more limited in size than a deployable segmented mirror. The maximum size monolithic mirror has been limited to approximately 4-6 m by currently available 5-m-class launch vehicle fairings. For example, the largest monolithic space telescope ever flown is the Herschel Telescope and its primary mirror is 3.5 m. Fortunately, with the advent of NASA's Space Launch System (SLS) and its planned 8.4- and 10-m fairings, it is possible to consider monolithic 4- to 8-m-class mirrors. Alternative rectangular monolith telescope architectures with high aspect ratios could use existing fairings to stow a primary mirror with even greater angular resolution in one direction, though with a non-circular point spread function. This telescope technology is compatible with coronagraphy.⁵⁵

Mirror mass and diameter traditionally have been key telescope design parameters, especially with respect to cost. This has led to light-weighting technologies that continue to be developed. But the SLS's larger fairings and greater mass capacity allow designers to reconsider the benefits of more mass in the overall system (greater stiffness, lower resonance frequencies, greater thermal inertia, etc.).

HabEx is baselining an off-axis telescope with a 4 m monolith.^{56,57} Analysis indicates that exoplanet science requires a primary mirror that has a total wavefront error that is stable on the order of 10 pm per wavefront control step.⁵⁸ Thermal stability and control is another key challenge for they will have to address in their design. While any future large space mission will probably be in the thermally stable Earth-Sun L2 Lagrange orbit, there will still be thermal load variations as a function of pointing angle relative to the Sun (as shown on JWST).

Current State-of-the-Art:

The largest monolith mirror optimized for performance in the visible-band is HST, made of ultra-low expansion (ULE) glass with 10 nm surface figure error. WFIRST will be the same size. A 3.5 m monolith primary mirror (made of SiC) flew as part of the Herschel observatory, though it

was optimized for mid and far-infrared wavelengths, and had a surface figure error of 3 μm . Glass mirrors in the 8 m or larger class achieving 7-8 nm surface figure error have been manufactured for use in ground-based observatories (Subaru, VLT) though space missions usually need lower density per area, and a higher resonant frequency (stiffness).

Progress Over the Last Year:

The HabEx design study team has developed a point design with United Technologies Aerospace Systems (UTAS) for their 4 m primary mirror telescope.⁵⁹ It includes a 35 cm-thick open-back Zerodur mirror by Schott with milling (340 mm pockets/4 mm ribs), giving a 93 Hz first mode (unmounted); 120 Hz first mode mounted design. Four meter Zerodur blanks have already been manufactured by Schott. Thermal surface figure distortions, including CTE nonuniformity, have been shown by analysis to create ~ 100 pm of wavefront error on time scales of minutes. According to UTAS heritage, gravity sag corrections to < 1 nm precision can be done. Because the lower first mode increases wavefront error, a lower disturbance environment is required to drive it back down. The HabEx design team has decided to adopt microthrusters in their design, rather than reaction wheels, for pointing the observatory in an effort to provide a more benign disturbance environment (see Sect. B.2.3).

A SAT/TCOR was awarded in 2017 (PI Phil Stahl/NASA Marshall Space Flight Center) to demonstrate predictive thermal control for large glass space mirrors, specifically in the context of enabling pm wavefront error stability for high contrast imaging.⁶⁰ This effort will develop and validate structural-thermal-optical-performance (STOP) models of glass mirrors by measurement of as-built CTE non-uniformity. The predictive thermal control concept uses the STOP models to enhance the speed and convergence of a thermal control loop.

Next Steps:

The HabEx mission concept study team is exploring the scientific benefits and technology needs of large monolith primary mirrors. Its interim report is expected in March 2018 and will include a detailed description of the technology needs for their primary mirror.

B.3.3 Large Segmented Mirrors

The development of large segmented mirrors and their supporting structures will enable astronomy to build ever-increasing large telescopes advancing both exoplanet and general astrophysics science, beginning with JWST. However, segmented mirrors have their own challenges to reach 10^{-10} contrast ratio levels at small IWAs. These challenges include diffraction from the segmentation pattern and segment-to-segment rigid body motion (i.e., tip/tilt and piston). See Sect. B.1.2 for descriptions of coronagraph designs that are compatible with this type of pupil, and Sec. B.2 for a discussion of technologies needed to maintain stability of a segmented system. Large apertures often have large corresponding on-axis secondary mirrors which, along with their support structures, provide additional diffraction challenges for a coronagraph instrument.

The experience of controlling 6 degree of freedom segments on JWST can be built upon to gain a higher precision, more stable, segmented aperture for exoplanet imaging. The surface figure error is required to be less than 10 nm rms and drift less than 10 pm due to thermal and

dynamic instability during a wavefront control cycle. Previously studied design architectures include the ATLAST (Advanced Technology Large Aperture Space Telescope) design⁶¹ and the High Definition Space Telescope (HDST) concept.⁶²

The LUVOIR design study team is baselining a deployable 15 m segmented primary mirror as their initial telescope architecture – sized to fit the largest faring expected to be available in the 2030's.

Current State-of-the-Art:

JWST is a segmented aperture telescope scheduled for launch in 2018. Its primary aperture is 6.5 m in diameter composed of 18 gold-coated beryllium segments, each 1.32 m tip-to-tip. Working in the near- to mid-infrared, the telescope operates at a temperature below 50 K. By operating at a warmer temperature, due to its visible to near-infrared observational spectrum, a potential exoplanet imaging mission can use other materials for its optical components and structure. These include ULE glass, and Silicon Carbide with a nanolaminate, which have demonstrated better than 5 nm rms SFE on 1 meter-class segments.

Progress Over the Last Year:

The LUVOIR design study team is exploring the scientific benefits and technology needs of large segmented primary mirrors. As part of the study, they have created a point design for its initial architecture A which uses 120 ULE glass segments. The segments rely on technology demonstrated by the Advanced Mirror Segment Demonstrator project.⁶³ Each segment will be connected to a composite backplane structure, whose thermal control system (similar to that considered for ATLAST⁶⁴) is compatible with 1 mK control.

Next Steps:

LUVOIR will study whether segment-level surface figure actuation is needed for pm-level wavefront error stability. A silicon-carbide substrate with many surface figure actuators, clad with Si and polished, may be a candidate technology that achieves better than 10 nm static wavefront error and the necessary control authority. The LUVOIR interim report is expected in March 2018 and will include a detailed description of the technology needs for their primary mirror.

Throughout the remaining study period, the HabEx and LUVOIR STDTs will continue their investigations into candidate telescope architectures, including a smaller B architecture for LUVOIR. HabEx may explore a segmented alternative.

Ultimately, maturing this technology at the level required for exo-Earth direct imaging will require building and testing multiple segments together. This will demonstrate relative phasing, integrated thermal control, and surface figure actuation as needed.

Prioritization:

This technology received Impact, Urgency, and Trend scores of 4, 3, and 3, respectively. Large telescopes enable the search for exo-Earths by providing the needed collecting area to detect

the faint objects and the angular resolution needed to probe habitable zones of nearby stars, and hence the Impact score is 4. The Urgency is also relatively high, some progress is needed prior to the 2020 Decadal Survey in order for the panel to judge the maturity of mirror technology for exo-Earth detection. The Trend score is also high as more investments are needed to mature the technology beyond the level of concept studies and sub-scale demonstrations.

B.4 Detection Sensitivity

The collected photon flux rate from exo-Earths, depending on the telescope size and the system throughput, is expected to be about one per several minutes. Consequently, the imaging detectors for both the detection and spectrometer channels of a coronagraph instrument must be highly sensitive, have ultra-low noise, and must be radiation hardened. In addition, the need for low spectral-crosstalk spectroscopy and large outer working angles to carry out disk science and imaging of the nearest exoplanets lead to the requirement for large format focal plane array—2k×2k pixels or larger.

Ongoing WFIRST investments are funding electron multiplying charge coupled device (EMCCD) development, though improvements for post-WFIRST missions are needed. These include better QE between 0.85 and 1 μm to help detect important water spectral lines, and longer lifetime in the space radiation environment.

B.4.1 CG-8: Ultra-low Noise Visible Band Detectors

CG-8: Ultra-Low Noise Visible Band Detectors

Description: Low-noise visible detectors for faint exoplanet characterization with an Integral Field Spectrograph

SOA (Lab): 1k×1k silicon EMCCD detectors provide dark current of 7×10^{-4} e-/px/sec; CIC of 0.01 e-/px/frame; zero effective read noise (in photon counting mode) after irradiation when cooled to 165.15 K (WFIRST); 4k×4k EMCCD fabricated but still under development

SOA (Flight): HST WFC3/UVIS CCD 3.1 e- read noise, dark current 2×10^{-3} , format 2k×2k

Needed capability: Effective read noise < 0.1 e- rms; CIC < 3×10^{-3} e-/px/frame; dark current < 10^{-4} e-/px/sec tolerant to a space radiation environment over mission lifetime. $\geq 2\text{k} \times 2\text{k}$ format

Supported Missions or Mission Concepts: LUVOIR, HabEx

Current State-of-the-Art:

The leading candidate detector technology in the visible is the silicon EMCCD detector, which can provide dark current noise of order 5×10^{-4} e-/px/sec while operating at 165 K, and clock induced charge (CIC) of order 0.01 e-/pix/frame, after (WFIRST) lifetime irradiation. The effective read out noise can be $\ll 1$ e- rms using electron-multiplying (EM) gain; depending on the device gain of the output amplifier that is being used. In addition, improved quantum efficiency at the long wavelength end of the visible band (closer to 1 micron where silicon becomes transparent) is desirable for biomarker detection, if it can be achieved without a major increase in dark current.

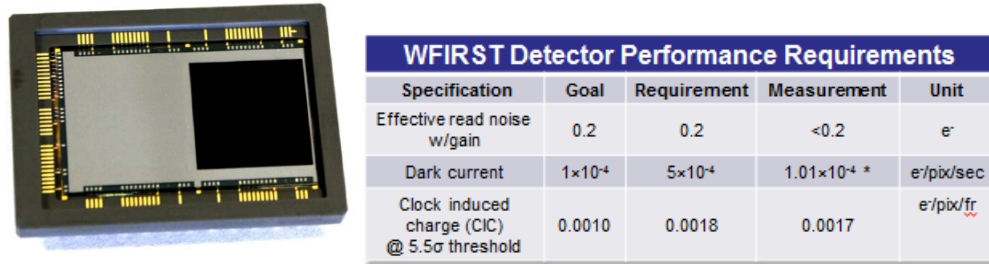


Figure 9: e2V CCD201-20 (1k×1k) detector and its characterization results conducted at the JPL CCD Detector Lab in 2015; data is beginning of life.

Microwave Kinetic Inductance Detectors (MKID) and Transition Edge Superconducting (TES) arrays are cryogenic alternatives capable of performing at visible wavelengths with essentially no read noise or dark current. Both require operations at cryogenic temperatures, and are less mature than EMCCDs (more about these technologies in Section B.4.2).

Multi-channel plate (MCP) amplifiers can enable photon-counting detectors in the visible band. Commercially available GaAs photocathodes are sensitive to wavelengths 350-850 nm and achieve very low dark current of order 0.2 counts/px/hr with modest cooling to -30 °C. Similar designs are currently operating in space (UVOT on SWIFT, S20 cathode).⁶⁵

P-channel skipper CCD amplifiers, optimized for very low light particle physics experiments, have sub-electron read noise and potentially improved radiation hardness compared to traditional CCDs.⁶⁶ These amplifiers have flexibility for tuning the readout scheme of portions of the array. The current designs have very long readout times (hours) in photon-counting mode that would need to be improved for a space flight application, as well as testing for suitability in low-light astronomical applications.

Low-noise CMOS sensors, such as the photon-counting quanta image sensor,⁶⁷ should in principle be less sensitive to the effects of radiation damage as compared to conventional or electron-multiplied CCDs, due to individual pixel readout, but are a relatively recent technological development.

Progress Over the Last Year:

The WFIRST coronagraph instrument has baselined the e2v CCD201-20 detector (1024×1024; 13×13 μm pixel pitch) for both of the coronagraph science cameras (imaging and IFS) and for the LOWFS camera. The project has carried out full characterization and displacement damage dose radiation testing and while the end-of-life performance has been shown to be adequate, the WFIRST project has worked with Teledyne-e2v to design and implement several changes to the detector that should improve the performance margin. This involves following procedures similar to those implemented on HST/WFC3 CCD detectors,⁶⁸ narrowing the path that small charge packets follow reducing the effects of the charge traps created by radiation damage.

Next Steps:

During 2018, the WFIRST-CGI plans to take delivery of the radiation-hardened EMCCD detectors for further testing. Other candidate technologies, both photoconducting and superconducting, will be further explored. For example, NASA's PICTURE-C balloon experiment is baselined to include a 10–20 kpix MKIDs device in 2019. NASA-GSFC is considering maturing TES devices for future exoplanet imaging missions.⁶⁹

Prioritization:

This technology received Impact, Urgency, and Trend scores of 4, 3, and 2, respectively. WFIRST's work in flight-qualifying EMCCD detectors for the CGI instrument may achieve performance that is already adequate for a future exo-Earth imaging mission. However, it is important to mature multiple classes of detectors towards the needs of exo-Earth imaging and spectroscopy.

B.4.2 CG-9: Ultra-low Noise Near-Infrared Detectors

CG-9: Ultra-Low Noise Near-Infrared Detectors

Description: Near-infrared wavelength (900 nm to 2.5 μm), extremely low noise detectors for exo-Earth spectral characterization with Integral Field Spectrographs

SOA (Lab): HgCdTe photodiode arrays have read noise $\lesssim 2$ e- rms with multiple nondestructive reads; 2k \times 2k format; dark current < 0.001 e-/s/pix; very radiation tolerant (JWST)

HgCdTe APDs have dark current $\sim 10\text{--}20$ e-/s/pix, RN $\ll 1$ e- rms, and < 1k \times 1k format

Sub-Kelvin photon-counting detectors (KID, TES): 0 read noise/dark current; radiation tolerance is unknown; <1k \times 1k format

SOA (Flight): HST WFC3/IR HgCdTe dark current 0.05 e-/px/s, 12 e- read noise, 1k \times 1k format

Needed capability: Read noise $\ll 1$ e- rms, dark current noise < 0.001 e-/pix/s, in a space radiation environment over mission lifetime; $\geq 2\text{k}\times 2\text{k}$ format

Supported Missions or Mission Concepts: LUVUOIR, HabEx

Near infrared detectors with high sensitivity in the spectral region of 900 nm to 2.5 μm (and maybe greater) are critical for the spectral characterization of exoplanets and identification of possible biosignatures. Future exo-Earth missions (HabEx, LUVUOIR) will consider infrared spectroscopy capabilities to detect hydrocarbons such as methane (1.00 μm , 1.69 μm , and 2.32 μm). The presence of methane in an oxygen-rich atmosphere like Earth's is one of the few known spectral combinations that point to a likely biotic origin. Spectral characterization of exo-Earths in the infrared requires sub-electron read noise and the dark current noise < 0.001 e-/pix/s, in a space radiation environment over mission lifetime. These properties in a larger array, such as 2k \times 2k or 4k \times 4k, are desirable.

Current State-of-the-Art:

HgCdTe photodiode arrays hybridized to astronomy readout integrated circuits are the state of the art with a read noise < ~ 2 e- rms with multiple non-destructive reads, dark current of < 0.001 e-/s/pix. These detectors have flown in Earth orbit and have proven to be very radiation tolerant. Two large format 4k \times 4k pixel arrays offered by Teledyne Imaging Sensors, with 10 and 15 μm pixel pitch are at TRL 4 (H4RG-10™ and H4RG-15™).

Other candidate detector technologies are currently less mature but are promising. With appropriately optimized process, the HgCdTe avalanche photodiode (APD) array offers the possibility of the high gain and low effective read noise of EMCCDs while being capable of the same QE performance as the JWST arrays. Because gain is built into each pixel—unlike the EMCCD—they promise photon counting if the dark current is sufficiently suppressed.⁷⁰ The state-of-the-art Selex/Leonardo SAPHIRA arrays have reported $\sim 10\text{--}20\text{ e}^-/\text{pix}/\text{s}$ dark current⁷¹. More work is needed to determine the actual noise floor and understanding the noise contributions from the HgCdTe photodiode versus the integrated readout circuit. This technology has been advanced with NASA APRA funding.

Cryogenic (superconducting) detectors such as MKIDS have no read noise or dark current, solving the spurious count rate problem associated with the non-cryogenic devices.⁷² These devices are scalable to large arrays. Transition edge sensor microcalorimeter arrays are another candidate cryogenic detectors with built-in energy resolution like the MKIDs. Nanowire single photon detection arrays can operate at higher temperatures and are multiplexed similarly to MKIDs.⁷³ Cryogenic detectors will require solutions for dynamic isolation, particularly from their cooler vibrations, and resolution (pixel count). The immediate challenge will be providing zero-vibration cooling. While cooling is not a detector technology, future telescope architectures must minimize vibrations sources to enable the coronagraph performance to reach the dual driving instrument goals of 10^{-10} contrast ratios at $<3\lambda/D$. Also, their radiation tolerance is unknown. Bernard Rauscher et al.⁷⁴ present a summary on the state-of-art and potential detector candidates for low-flux environments.

Progress Over the Last Year:

APRA-funded work on APD HgCdTe by Hall et al. has investigated ways to suppress the high dark current, suspected to be ROIC glow. Results have not yet been published but are expected in 2018.

Next Steps:

Reducing the spurious count rate should be the top priority of non-cryogenic photon-counting detectors followed by radiation hardening tests. Although conventional HgCdTe photodiode arrays may never function as photon-counting detectors due to leakage current at non-cryogenic temperatures, it is possible that today's H2RG and H4RG detectors are not yet approaching the fundamental physical noise limits of the photodiodes themselves.⁷⁵ Work distinguishing the contributions from the photodiode, interconnects, field-effect transistor, etc. would be valuable.

NASA's PICTURE-C balloon experiment is baselined to include a 10–20 kpix MKIDs device in 2019. NASA-GSFC is considering maturing TES devices for future exoplanet imaging missions.⁷⁶ The built-in energy resolution capabilities of the MKIDs and the TES devices are currently $R \leq 20$, short of the $R \geq 70$ desired by future biosignature-seeking spectrographs. Of course, these detectors could be operated in conjunction with a spectrally dispersing optical element.

Prioritization:

This technology received Impact, Urgency, and Trend scores of 4, 3, and 3, respectively. The capability to detect extremely dim exo-Earths requires photon-counting detectors and thus this is enabling technology for an exo-Earth mission with Impact score of 4. The Urgency is 3 because progress in this area could influence the recommendations of the 2020 Decadal Survey. The trend is set at 3, because while there are multiple detector options on the table that could achieve the needed performance, the time table for at least one detector reaching that point is unclear.

C STARSHADE TECHNOLOGY GAPS

External occulters, or starshades, suppress on-axis starlight so that the reflected starlight from the off-axis planets can be imaged. This is done by blocking most of the on-axis starlight and redirecting the diffraction pattern so that it interferes destructively at the entrance pupil of a telescope creating a shadow. Depending on the size of the telescope and wavelength range, this typically requires the starshade to be tens of meters in diameter and located tens of thousands of kilometers from the telescope (**Figure 10**). The starshade must position itself to maintain the shadow on the telescope, and its petals must maintain a very precise shape to produce the desired reduction in starlight relative to the light reflected by the planet. It must also be opaque and limit the amount of sunlight scattered from the petal edges into the telescope.

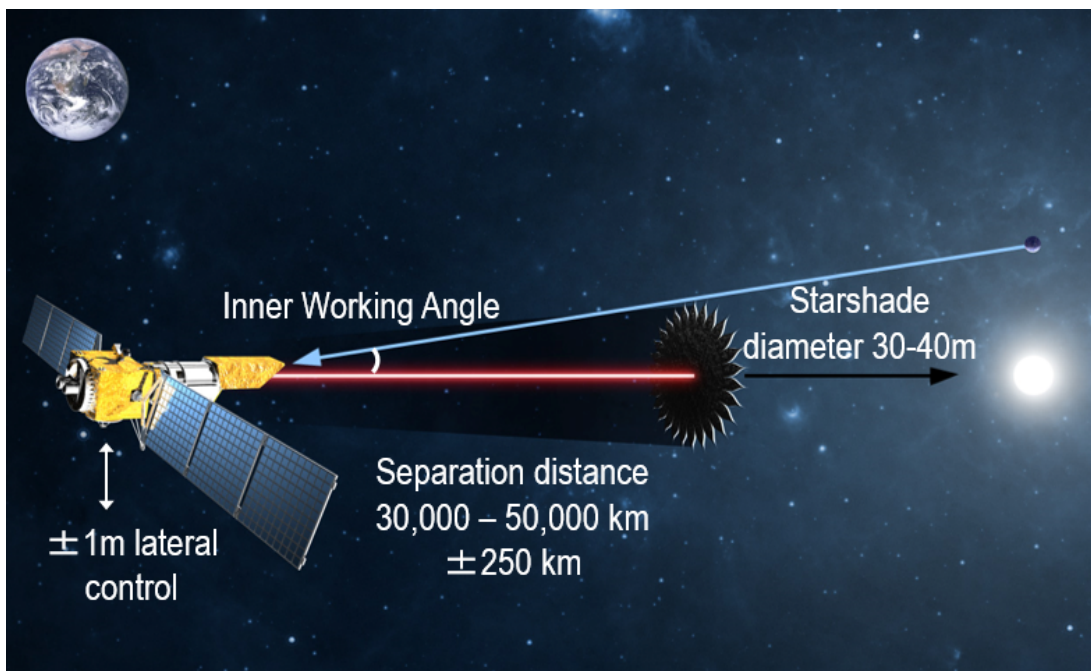


Figure 10: A typical starshade/telescope configuration. The starshade blocks starlight from reaching the telescope pupil, but allows light from the exoplanet.

If a circular occulter were used rather than one with numerous shaped petals, a Poisson spot, a circular bright region at the center of the image plane due to constructive interference of diffracted light, would ruin the ability to image faint exoplanets. Independent optical modeling predictions have shown excellent agreement concerning the contrast sensitivity to petal shape errors,⁷⁷ and detailed preliminary error budgets have been proposed.⁷⁸

The five starshade technologies tracked by the ExEP are in **Table 1**. They target starshades capable of rendezvous with the WFIRST telescope at the Sun-Earth L2 orbit as well as for a possible larger mission such as described by the HabEx mission concept. The technology needs are largely based on a WFIRST Rendezvous reference mission as detailed in the architecture of the NASA Exo-S probe study.⁷⁹ This study, sponsored by NASA's Astrophysics Division in 2014, demonstrated the valuable science return of a starshade mission with both a 1.1 m telescope,

and alternatively, the 2.4 m WFIRST telescope. This mission concept's starshade had a diameter of 20 - 40 meters. A new NASA-chartered probe concept study led by Sara Seager is currently updating the science case for a WFIRST-starshade rendezvous, with a report due at the end of 2018. The HabEx mission concept is currently baselining a 70 m-class starshade to accompany its space telescope.⁸⁰ While some of the technology needs for the smaller WFIRST rendezvous concept are directly applicable to a larger starshade, some may require different solutions. Currently the LUVVOIR mission does not include a starshade in its baseline architecture, instead, a coronagraph meets its starlight suppression needs. The requirements may change in the coming years as the HabEx and LUVVOIR STDs further advance their mission concepts.

The starshade technologies in **Table 3** address three starshade technology gaps (shown in **Figure 11**):

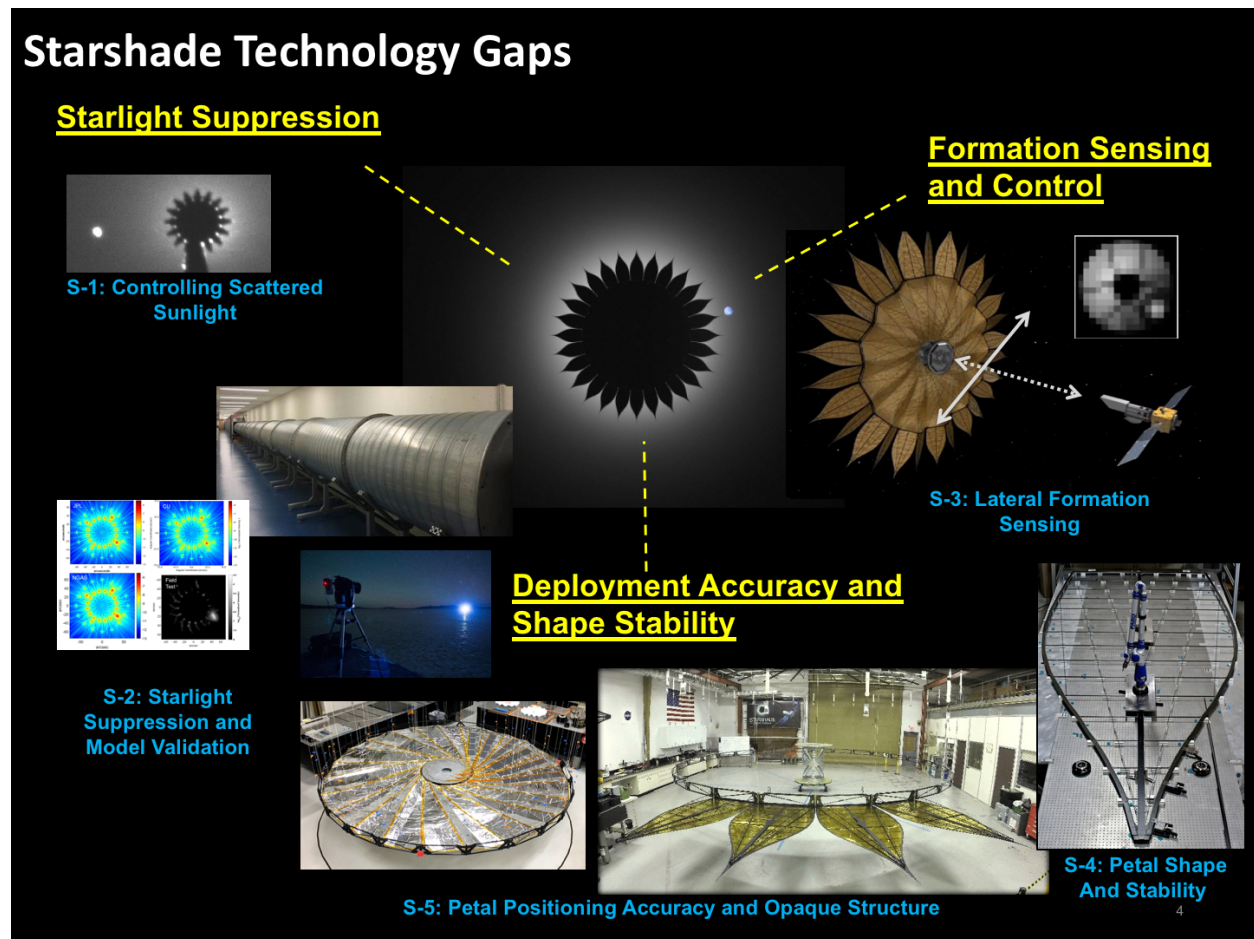


Figure 11: The three categories of starshade technology needs (in yellow font) to directly image and characterize exo-Earths around Sun-like stars.

1. **Starlight Suppression** – the starshade must produce the desired shape to within tolerances specified by an error budget to create contrast levels (local ratio of reflected exoplanet light to starlight in the same bandwidth) to better than 10^{-10} at the image plane. The precise positioning and manufacture of the starshade edges that meet design requirements will minimize the diffraction from on-axis starlight and scatter/diffraction

from off-axis Sunlight detected at the science focal plane. The starlight suppression capabilities of the starshade must be demonstrated on the ground to validate optical models and the error budget, which are used to predict performance in a space environment.

2. **Deployment Accuracy and Shape Stability** – the ability to stow, survive launch, and deploy the petals and inner disk to within the deployment tolerances budgeted to meet the shape, and ultimately, the contrast requirements. The final shape must be stable throughout operational environments within an allocated error budget. The optical shields within both the petals and the inner disk must fully deploy as an opaque structure.
3. **Formation Sensing and Control** – the ability to sense and control the lateral offset between the starshade and the telescope maintaining the desired contrast long enough for full science integration.

The criteria and rationale of the prioritization of the technologies can be found in Section A.3; the results of the prioritization can be found in Section G.

The published literature on starshades is inconsistent in defining starlight suppression, contrast, Fresnel number, and even the radius of the starshade (which can be defined in various ways due to the apodization function). We use the following definitions here, and suggest they be adopted as standards:

Contrast ratio is the ratio of starlight irradiance in an arbitrary resolution element of the focal plane to the irradiance that would be seen in that same resolution element were the star to be centered there.

Suppression is the ratio of the total starlight that enters the telescope with the starshade in place to that without the starshade. It is measured in the pupil plane.

Contrast ratio is defined at a resolution element in the focal plane. It has meaning for both coronagraphs and starshades. It varies over the focal plane and is only meaningful when a location is specified. In practice, an average value over an annulus between an inner working angle and an outer working angle is sometimes given. Since a “resolution element” depends on the properties of the optical system, including the telescope, the contrast ratio is affected by the performance of the entire system, not just the starshade.

Suppression, on the other hand, depends only weakly on the telescope, and therefore is determined essentially by the starshade alone. Since it involves quantities integrated over the pupil plane, it is always a single number.

Because the telescope focuses the residual starlight onto the image plane, forming an image of the starshade, light leaking around starshade petals becomes concentrated into certain areas of the image plane, so that the contrast ratio (e.g., 10^{-10}) in most elements is always ‘deeper’ than the suppression (e.g., 10^{-9}). The relationship between them depends on the position of interest in the image plane, the telescope resolution and the number of pixels across which the starshade is imaged.

The SAT/TDEM program in the past has succeeded in receiving proposals and funding all of the three key areas of starshade technology gaps shown in **Figure 11**, though now this technology

has been advanced through the Starshade Technology Development Activity (below). The Deployment Accuracy and Shape Stability technology gap (Section C.4) has also been the focus of several Small Business Innovation Research (SBIR) awards.

C.1.1.1 Starshade Technology Development Activity

After five years of funding starshade through the competed SAT/TDEM program, in March of 2016 the NASA APD Director chartered the formation of a focused starshade technology development activity. This approval allowed technology development for the starshade to transition from a competed, PI-led, SAT-funded effort to a directed, Program-managed and funded activity. The activity's purpose is to mature the technologies that close the three gaps to TRL 5 for future starshade mission concepts that include WFIRST Rendezvous and HabEx starshades. It is managed using NASA Procedural Requirements (NPR) 7120.8 as a management guideline. The authorization extends only through a first phase, akin to a planning or formulation phase. A formal review will be held before the activity can enter an implementation phase. Consequently, the SAT/TDEM program will no longer accept starshade proposals.

The key goals of the initial planning phase of the activity include:

1. Defining an initial reference design
2. Evaluating alternative approaches and completing the key trade studies
3. Defining a Starshade TRL 5 Development Plan with key performance parameters and milestones
4. Planning the execution stage

C.2 Starlight Suppression

Starshades must demonstrate experimentally at a subscale level that they can reach $\leq 10^{-10}$ contrast in a scaled flight-like geometry with Fresnel numbers 8-20 across a broadband optical bandpass. The challenge in this Fresnel number range is that the large starshade-telescope separation distances required for a small inner working angle prohibit ground-based optical performance verifications of large starshades. Instead performance will need to be verified in a two-part process. One, subscale tests will demonstrate contrast performance consistent with imaging an exo-Earth and validate the optical models, upon which full-scale shape tolerances are based. The scaling approach is to match the flight design in terms of the number of Fresnel zones across the starshade such that the diffraction equations defining the dark shadow are identical. Sub-scale tests will also be used to validate an error budget, using intentionally deformed starshades to verify predicts from optical models. Two, the deployment accuracy and shape tolerances will be verified on a full-scale petal and deployment mechanism. Key capabilities have already been demonstrated via early prototypes, however, only a limited number of tests have been conducted at a flight-like Fresnel number using flight-like materials and manufacturing. Section C.2.2 describes the demonstrations and model validation.

The primary goal of the starshade optical edges is to provide the correct apodization function to suppress starlight to sufficient levels for exoplanet direct imaging. However, in order to do so light emanating from sources other than the target star must also be taken into consideration as this has the potential to significantly degrade the image contrast. Of greatest importance is the issue of light from our Sun reflecting off the optical edges and entering the telescope. This solar glint appears primarily as two large lobes, created by the telescope point spread function, originating from a few petals oriented with edges broadside to the Sun. Methods to effectively eliminate this phenomenon such as spinning the starshade have been established. The overall intensity of scattered light must be limited to levels below that from the exozodiacal background so that measurement integration times are not significantly impacted. Section C.2.1 describes the petal edge technology required to meet the scattering requirements.

C.2.1 S-1: Controlling Scattered Sunlight

S-1: Controlling Scattered Sunlight

Description: Limit edge-scattered sunlight and diffracted starlight with optical petal edges that also handle any stowed bending strain.

SOA: Edges manufactured with machining and electrical discharge machining do not meet scatter requirements; etched amorphous metal edges meet scatter specs integrated in-plane shape tolerance is to be demonstrated.

Needed capability: Integrated petal optical edges maintaining precision in-plane shape requirements after deployment trials and limit solar glint contributing $< 10^{-10}$ contrast at petal edges.

Supported Missions or Mission Concepts: Starshade Probe for WFIRST, HabEx

The starshade requires an optical edge that can (1) be integrated to the petal's structural edge, (2) meet and maintain precision in-plane shape requirements after deployment and over a broad thermal environment, and (3) limit the intensity of solar glint such that a 10^{-10} contrast sensitivity can be achieved. Based on analyses for an Exo-S petal architecture⁸¹ it was determined that the optical edges should have a sharp beveled edge and/or low reflectivity to meet the requirement on solar glint. A guideline resulting from the Exo-S study is that the product of edge radius and reflectivity should be equal to or less than $12 \mu\text{m}\%$, while at the same time maintaining a stable in-plane shape, limiting thermal deformation of the petal and accommodating any stowed bending strain (some mechanical deployment architectures may not have bending strain issues).

Current State-of-the-Art:

Suitable edge materials have been demonstrated in several configurations, including very sharp ($< 1 \mu\text{m}$ radius of curvature) edges and blunt edges with low reflectivity. A thorough investigation into the viability of various coatings on blunt-edged metal was performed in a 2015 TDEM⁸² (PI Tiffany Glassman/Northrop Grumman) which included adhesion tests, thermal cycling, and humidity exposure.

Another approach uses amorphous metals that are able to be fabricated with very sharp and stable ($< 0.5 \mu\text{m}$ radius of curvature) edges. Chemical etching techniques were used to manufacture the edges as it provides a means to produce the necessary beveled edge and can be implemented at the meter-scale with micron-level in-plane tolerances. The solar glint performance of these coupons was also established using a custom scattered-light testbed and

measurements indicate that the scattered flux is predominantly dimmer than the predicted intensity of the background zodiacal light over a broad range of sun angles.⁸³

While suitable performance specifications on solar glint have been demonstrated at the coupon level for these amorphous metal edges, in-plane shape requirements have not yet been met on meter scale prototypes. Meter-scale optical edges is what may be needed to be bonded and assembled on starshade petals.

Progress Over the Last Year:

In the past year, the Starshade technology development activity achieved two milestones towards developing this technology. First, a model of edge scattering has been developed and validated for solar angles expected during a starshade mission using scatterometer measurements (see Figure 12).

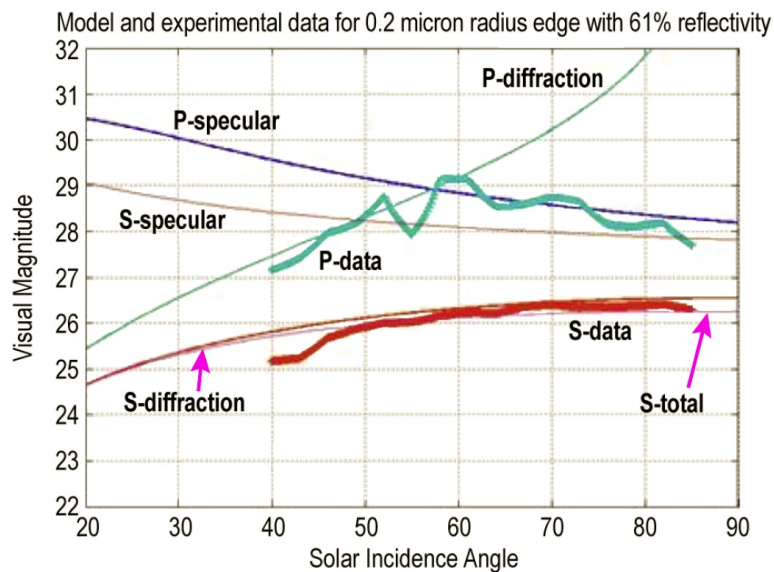


Figure 12: Scatterometer data vs. edge scatter model obtained by the starshade technology activity.

Secondly, a trade study of candidate optical edge solutions was undertaken and completed. Candidate materials were considered that could 1) meet scattering requirements 2) be shown to meet the mechanical shape stability, 3) have a path to integration with the structural edge of the starshade, and 4) be scaled to a full-scale petal optical edge. Various optically dark coatings were also tested. The study found that only the etched amorphous metal edge without a coating (Figure 13) met the scattering requirements over the full range of sun angles.

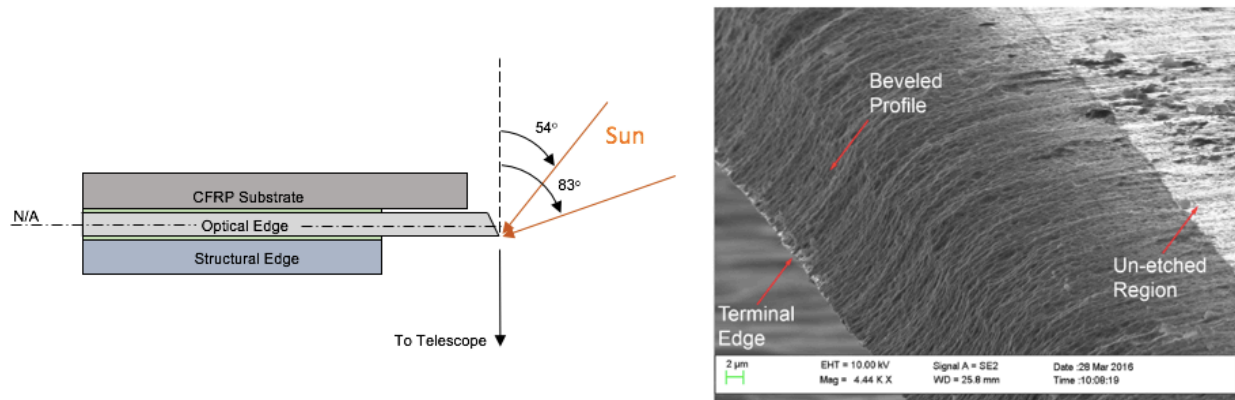


Figure 13 : Baseline optical edge. Left: configuration of a mounted optical edge; Right: a scanning electron microscope image of an etched amorphous metal edge.

Next Steps:

During 2018, the etched amorphous metal option will be further matured. Subscale edge segments at a scale of tens of centimeters and a subscale optical petal tip will be built, measured for scattering properties, and tested in relevant environments. The sensitivity of the optical edge scatter performance to edge defects and/or dust that can be attracted to statically charged optical edges will also be studied. An Phase I SBIR award to Photonic Cleaning Technologies will investigate a cleaning and protection method for the starshade edges using a polymer coating. Finally, these efforts feed into the larger TRL 5 plan which will result in construction and demonstration of 1-meter optical edge segments and tips by mid-2019.

Prioritization:

All of the starshade technologies tracked by ExEP received Impact, Urgency, and Trend scores of 4, 4, and 2, respectively. The highest Impact score is assigned since as a whole, starshade technology enables the reflected-light direct imaging and spectroscopy of Earth-sized planets in the habitable zone of Sun-like stars. The technologies also receive the highest Urgency score, as WFIRST, a mission currently in formulation, could benefit, should a starshade rendezvous mission be selected by NASA. The Trend score is 2, reflecting the focused technology funding that ExEP's Technology Development Activity is already providing.

C.2.2 S-2: Starlight Suppression and Model Validation

S-2: Starlight Suppression and Model Validation

Description: Experimentally validate at flight-like Fresnel numbers the equations that predict the contrasts achievable with a starshade.

SOA: Validated optical model with demonstrated 10^{-6} suppression at white light, 58 cm mask, and F (at the starshade tips) = 210; 6×10^{-6} suppression demonstrated at F=15; 4.6×10^{-8} suppression demonstrated at F ~ 27

Needed capability: Experimentally validated models with total starlight suppression $\leq 10^{-8}$ in scaled flight-like geometry, with F between 5 and 40 across a broadband optical bandpass. Validated models are traceable to 10^{-10} contrast system performance in space.

Supported Missions or Mission Concepts: Starshade Probe for WFIRST, HabEx

Because full-scale demonstrations of starlight suppression are not feasible on the ground (the telescope-starshade separation is several Earth radii), the validation of the optical properties of a starshade relies heavily on optical modeling and sub-scale validation. In order to accurately compute 10^{-10} contrast, these models must be validated against ground tests, especially in the same diffraction regime (same Fresnel number) as in-flight observations.

Current State-of-the-Art:

Several experiments over the last decade demonstrate the viability of creating a dark shadow with a starshade to contrasts better than 10^{-10} just outside the petal edge. They include lab demonstrations at the University of Colorado,^{84,85} Northrop-Grumman,^{86,87} Princeton University,^{88,89} larger scale tests in a dry lakebed by Northrop Grumman as part of their TDEM-12,⁹⁰ and larger scale demonstrations using the McMath Pierce solar observatory on astronomical objects. Each of these experiments has been limited in contrast performance to some extent by a subset of the following test environment issues:

- Wavefront errors due to collimating optics
- Dust in open air testing
- Diffraction effects due to the finite extent of the optical enclosure
- Diffraction off starshade support struts
- Imperfections in the subscale starshade due to challenges in fabricating at small dimensions.

Figure 14 summarizes the starlight suppression achieved with subscale starshades to-date, plotted against the Fresnel number of the test.

A 77 m-long starshade optical testbed at Princeton University was initiated as a TDEM (PI is Jeremy Kasdin/Princeton University, TDEM-12) and later reprogrammed to the Starshade Technology Development Activity. This testbed was designed to operate at flight-like Fresnel numbers, and recently has demonstrated suppression that approaches the requirement.^{91,92}

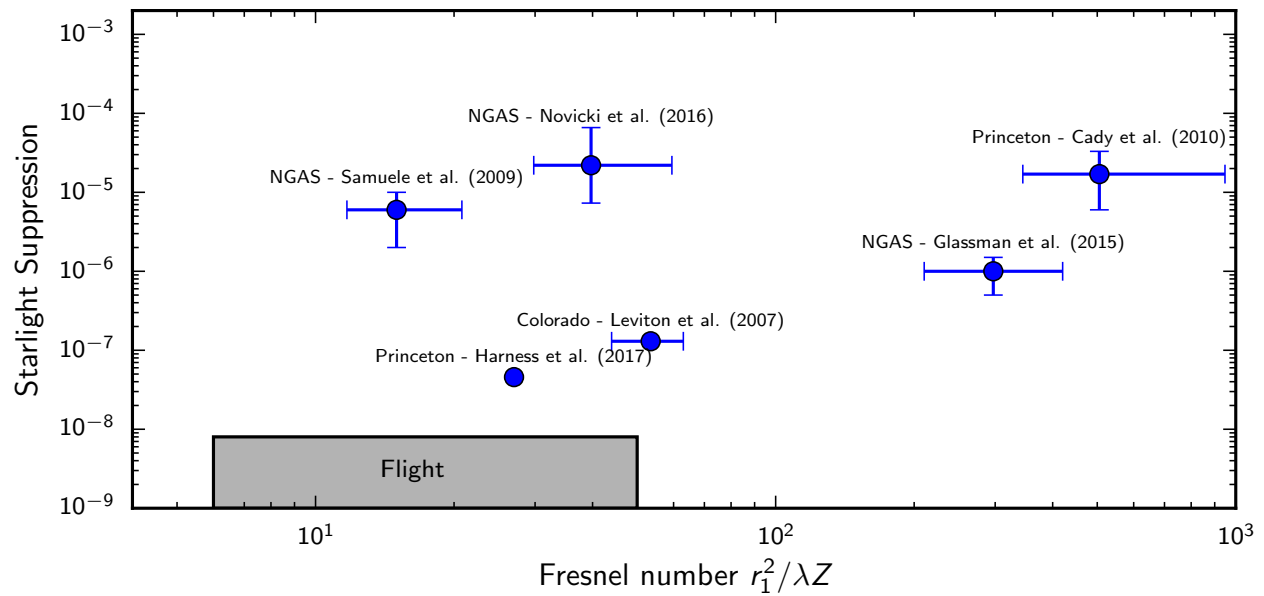


Figure 14: Light suppression versus Fresnel number for published starshade experiments. The Fresnel number is calculated with the starshade radius at the petal tips (r_1). Leviton et al., Proc. SPIE 6687 (2007); Sirbu, Kasdin, and Vanderbei, SPIE 9143 (2014) Samuele et al., SPIE 7731 (2010); Cady et al., Proc. SPIE 7731 (2010); Glassman et al., 2012 TDEM Report, NG Document #1469885 (2015); Novicki et al., SPIE 9904 (2016); Harness et al., Proc SPIE 10400 (2017). Error bars in suppression on the Leviton et al., and Kim et al. points are smaller than the plot marker. The grey box indicates the suppression needed for exo-Earth detection and Fresnel numbers expected for a range of flight starshade/telescope configurations. While 10^{-9} suppression is needed for exo-Earth detection, a small telescope may be limited by exo-zodiacal dust, and an accompanying starshade might have less stringent contrast needs.

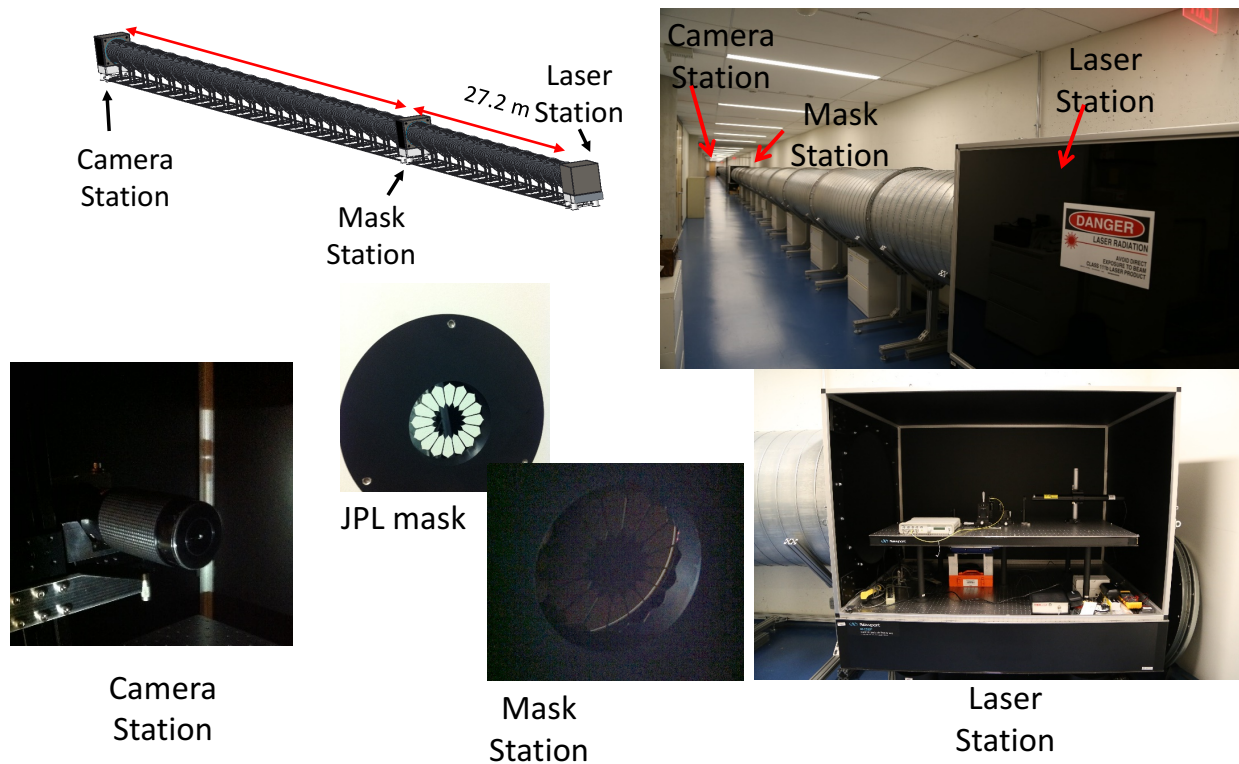


Figure 15: Schematic diagrams and pictures of the Princeton University starshade performance testbed (TDEM-12; PI Kasdin). Tubes are each 2 m in length and 1 m in diameter. They are painted with low reflectivity black paint and will include baffles to suppress stray light. (Figure credit: Anthony Harness)

Progress Over the Last Year:

The Princeton testbed shown in **Figure 15** operates a subscale starshade at a Fresnel number of 27. In the past year, improvements in the thermal stability of the testbed and in the manufacture of the subscale starshade had led to an average suppression of 4.8×10^{-8} .⁹³ The suppression is currently limited by defects in the subscale starshade at the micron scale. A good sign is the optical diffraction model has reproduced the experimental results when the as-built defects were included.⁹⁴ Improved manufacturing of the starshade masks are expected to reach flight-like contrast levels in 2018. At near flight-like contrast, atmospheric turbulence, even in the stable environment, may prove to be a factor in achieving agreement between models and measurements.

Next Steps:

The tests in the Princeton tube will continue with a further improved subscale starshades until flight-like contrast or a limiting factor is reached. Additionally, the models must reproduce the measured signal at the 10% at the flight Fresnel number and at flight-like contrast levels for the models to be validated.

To further test the robustness of the optical diffraction model, engineers are considering operating the Princeton testbed at longer wavelengths (NIR), also enabling larger starshades. The X-ray calibration facility (XRCF) facility at Marshall Space Flight Center has a 500 m long, 1.2 m diameter tube, and models have indicated that a subscale starshade test in this facility would be able to achieve flight-levels of suppression and contrast at flight-like Fresnel numbers. It will be considered as a candidate for future subscale starshades in order to validate further the robustness of the optical models at a different region of parameter space.

Prioritization:

All of the starshade technologies tracked by ExEP received Impact, Urgency, and Trend scores of 4, 4, and 2, respectively. The highest Impact score is assigned since as a whole, starshade technology enables the reflected-light direct imaging and spectroscopy of Earth-sized planets in the habitable zone of Sun-like stars. The technologies also receive the highest Urgency score, as WFIRST, a mission currently in formulation, could benefit, should a starshade rendezvous mission be selected by NASA. The Trend score is 2, reflecting the focused technology funding that ExEP's Technology Development Activity is already providing.

C.3 Formation Sensing and Control

The starshade and telescope must maintain a formation such that the darkest part of the shadow, which may only be slightly bigger than the telescope itself, overlaps with the telescope entrance. While many formation flying technologies and algorithms have already been developed under different programs, the key remaining technology for starshades is related to the lateral sensing necessary for controlling the starshades position.

C.3.1 S-3: Lateral Formation Sensing

S-3: Lateral Formation Sensing

Description: Demonstrate lateral formation flying sensing accuracy consistent with keeping telescope in starshade's dark shadow.

SOA: Sub-scale lab demonstration showing ability to center telescope within ± 1 m of starshade shadow.

Needed capability: Demonstrate sensing lateral errors ≤ 0.24 m 3σ accuracy at the flight signal-to-noise ratio at scaled flight separations. Demonstrate control algorithms with scaled lateral control error ≤ 1 m radius.

Supported Missions or Mission Concepts: WFIRST, Starshade Probe for WFIRST, HabEx

Maintaining precise alignment of the telescope, starshade, and target star is imperative to achieving the science goals of an exo-Earth-finding mission. The rapid degradation of starlight suppression as a starshade and space telescope moves radially out of alignment places a tight constraint on the lateral position of the starshade relative to the telescope-star line of sight. According to mission studies for Exo-S,⁹⁵ New Worlds Observer,⁹⁶ and THEIA,⁹⁷ a starshade spacecraft must control its lateral position to within about ± 1 m of the telescope boresight to keep the telescope within the darkest shadow. The benign disturbance environment at either Earth-Sun L2 or an Earth Drift-Away orbit makes controlling to the meter level straightforward with conventional chemical thrusters: better than 10 cm-level-control is regularly achieved in low Earth orbit for rendezvous and docking.⁹⁸ The challenge, however, is to sense the lateral

position error to within ± 30 cm. Comparatively, the axial separation distance, or range, between the starshade and telescope is loosely controlled to only within ± 250 km,⁹⁹ with sensing knowledge to within ± 1 km. The range is measured by a proximity radio with two-way ranging. These requirements are well within the state-of-the-art.

Current State-of-the-Art:

The starshade compatibility study of WFIRST has developed a sensing concept that uses a pupil plane sensor in the telescope for fine formation sensing using light from outside the science bandwidth. In the case of WFIRST, this sensor is the CGI's LOWFS camera. The concept exploits the fact that starshade only achieves extreme suppression within a particular band. Out-of-band, the spot of Arago (see Figure 16) appears at a much brighter level than in-band, and thus the pupil plane signal can be used to sense the misalignment of the starshade and telescope to the centimeter scale. Simulations and scaled benchtop laboratory demonstrations have shown that this is a feasible approach.¹⁰⁰ While the work so far has focused on a potential WFIRST/starshade rendezvous mission, this procedure should be straightforward to scale to larger starshades and space telescopes with different science bands.

Progress Over the Last Year:

Bottom et al (2017)¹⁰¹ presented a model of formation sensing with a WFIRST-like system, using the pupil-plane camera of the LOWFS, with a bandpass different from the starshade science observations. The approach shows that a library of pre-computed pupil-plane simulations can be fitted to the sensed image with the misalignment as a free parameter, achieving centimeter-level sensitivity to the misalignment. The authors, in addition, used a laboratory testbed at flight Fresnel number to begin validating the model.

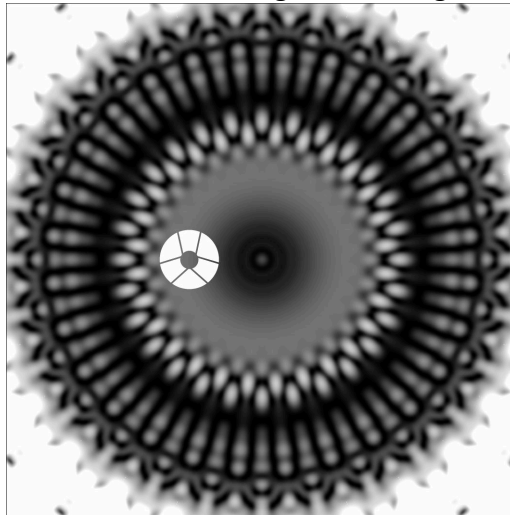


Figure 16: An out-of-band simulated starshade shadow with the WFIRST pupil superposed. The spot of Arago is visible at the center of the shadow. Reproduced from Bottom et al. (2017).

Next Steps:

The starshade technology development activity plans to address this technology in depth in 2018. The Starshade Lateral Alignment Testbed Experiment (SLATE) at JPL consists of a collimated source, a 6 mm-diameter starshade, a WFIRST pupil simulator and a pupil plane sensor placed at a scaled distance of about 2 m from the starshade, preserving the Fresnel number of the flight configuration. The model used to generate the pupil-plane image library will be validated against testbed measurements.

Finally, a model of the lateral sensing accuracy achieved on the scaled demonstration will be interfaced with a simulation of the spacecraft control loop in order to demonstrate that the sense and control concept achieves the required precision.

Prioritization:

All of the starshade technologies tracked by ExEP received Impact, Urgency, and Trend scores of 4, 4, and 2, respectively. The highest Impact score is assigned since as a whole, starshade technology enables the reflected-light direct imaging and spectroscopy of Earth-sized planets in the habitable zone of Sun-like stars. The technologies also receive the highest Urgency score, as WFIRST, a mission currently in formulation, could benefit, should a starshade rendezvous mission be selected by NASA. The Trend score is 2, reflecting the focused technology funding that ExEP's Technology Development Activity is already providing.

C.4 Deployment Accuracy and Shape Stability

To function as an occulter, casting a dark shadow on the formation-flying telescope, the starshade must accurately deploy to, and maintain the correct shape. There are two technologies that must be matured in order to close this gap. First, the petals must meet the in-plane shape and maintain that shape stably over the full range of operational environments (see Sect. C.4.1). Second, Petal Positioning and Opaque Structure (Sect. C.4.2) is the technology needed to deploy petals from their stowed launch configuration to within the required tolerances and maintain that position with an opaque barrier to starlight. For some deployment architectures, these two technologies may be addressed together.

Two distinct implementations are being considered for the packaging and deployment of a starshade; these are called the “folded” and “wrapped” architectures, referring to the means of stowing the petals (**Figure 17**).

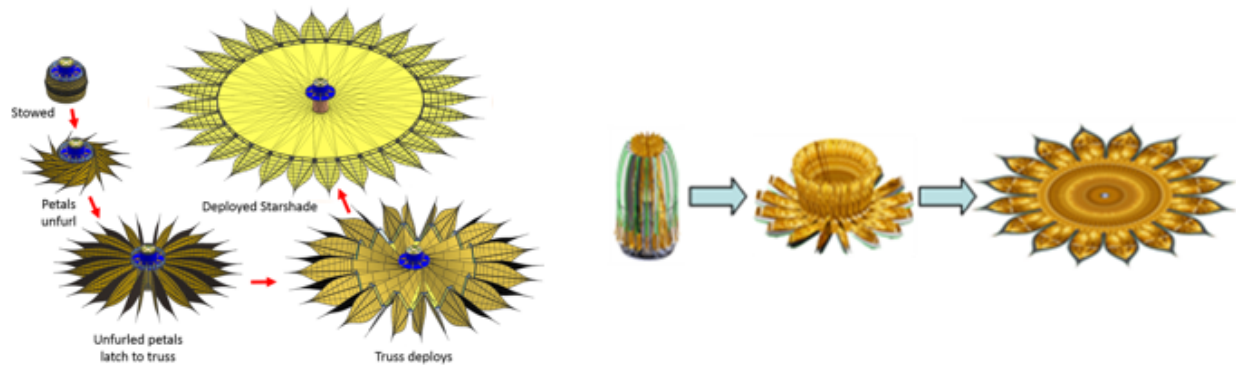


Figure 17: Illustration of the two candidate stowing and deployment architectures under consideration: (Left) the “wrapped” architecture¹⁰²; (right) the “folded” architecture¹⁰³.

The folded deployment architecture uses telescopic booms that radially expand to deploy the starshade’s inner disk and petals (**Figure 17**, right). This architecture leverages technology for the JWST sunshield deployment (designed and built by Northrup Grumman) as well as non-NASA activities. The wrapped approach uses a radially deployable perimeter truss, from which attached concentrically-wrapped petals would unfurl (**Figure 17**, left). The architecture leverages the Northrup Grumman Astro Aerospace AstroMesh communications antenna, most recently successfully flown with NASA’s Soil Moisture Active Passive mission (Astro Aerospace is a subsidiary of Northrup Grumman). This is the architecture adopted by the NASA Exo-S mission concept study for 30–40 m-class starshades.

C.4.1 S-4: Petal Shape and Stability

S-4: Petal Shape and Stability

Description: Demonstrate a high-fidelity, flight-like starshade petal meets petal shape tolerances after exposure to relevant environments.

SOA: Manufacturing tolerance ($\leq 100 \mu\text{m}$) verified with low fidelity 6 m prototype and no environmental tests. Petal deployment tests conducted but on prototype petals to demonstrate rib actuation; no shape measurements, no long-duration stowage tests.

Needed capability: Tolerances demonstrated to $\leq 100 \mu\text{m}$ (in-plane tolerance profile for a 7 m petal on the 34 m-diameter Exo-S design; tolerances scale roughly linearly with starshade diameter) with flight-like, minimum half-scale petal fabricated and maintains shape with exposure to relevant environments and is optically opaque.

Supported Missions or Mission Concepts: Starshade Probe for WFIRST, HabEx

Current State-of-the-Art:

The TDEM-09 activity led by PI Jeremy Kasdin of Princeton established the state-of-the-art, using the mathematically optimized shape approach, and successfully demonstrated the allocated manufacturing tolerance ($\leq 100 \mu\text{m}$) of an early 6 m petal prototype. The low fidelity prototype did not include an optical shield that makes the petal opaque, optical edges that effectively minimize the effect of scattered and diffracted sunlight, or undergo environmental testing.

Progress Over the Last Year:

A starshade shape tolerancing analysis by Shaklan et al (2017)¹⁰⁴ investigated a set of starshade/telescope combinations, including a hypothetical 26 m starshade paired with WFIRST and a 72 m starshade paired with a 4 m HabEx. A key finding was that physical requirements on the petal shape scale roughly linearly with starshade size.

Next Steps:

One of the key next steps before the petal technology advances further is the conducting of a mechanical deployment trade study. See the next section for more details on this important trade. After the trade is completed, petal components and sub-scale petals will be manufactured and tested in expected environments for shape and stability.

Prioritization:

All of the starshade technologies tracked by ExEP received Impact, Urgency, and Trend scores of 4, 4, and 2, respectively. The highest Impact score is assigned since as a whole, starshade technology enables the reflected-light direct imaging and spectroscopy of Earth-sized planets in the habitable zone of Sun-like stars. The technologies also receive the highest Urgency score, as WFIRST, a mission currently in formulation, could benefit, should a starshade rendezvous mission be selected by NASA. The Trend score is 2, reflecting the focused technology funding that ExEP's Technology Development Activity is already providing.

C.4.2 S-5: Petal Positioning Accuracy and Opaque Structure

S-5: Petal Positioning Accuracy and Opaque Structure

Description: Demonstrate that a starshade can be autonomously deployed to within its budgeted tolerances after exposure to relevant environments.

SOA: Petal deployment tolerance (≤ 1 mm) verified with low fidelity 12 m prototype and no optical shield; no environmental testing (Exo-S design).

Needed capability: Deployment tolerances demonstrated to ≤ 1 mm (in-plane envelope) with flight-like, minimum half-scale structure, with petal optical edge interfaces, that is optically opaque when deployed, and includes interfaces to launch restraint. Verify the structure will meet shape stability (petal edge position) after exposure to relevant environments.

Supported Missions or Mission Concepts: Starshade Probe for WFIRST, HabEx

Current State-of-the-Art:

Petal deployment has been demonstrated to meet tolerances at the 12 m scale using an off-the-shelf retrofitted 12 m diameter Astromesh Antenna and four representative petals. As a more flight-like proof of concept, a 10 m diameter inner disk subsystem was built deploying the inner disk from a stowed configuration (see **Figure 18**). To demonstrate the deployment of an opaque optical shield, a 5 m prototype was developed and partially integrated with its inner disk (see **Figure 19**). The optical shield builds on an origami fold pattern that allows for proper interfaces to the central spacecraft and perimeter truss disk.



Figure 18: A 10 m inner disk subsystem prototype demonstrates deployment from a stowed configuration and final positioning of the starshade petals. The testbed also allows for studying the petal-inner disk interface. The entire testbed has its weight offloaded by a gravity compensation system. (Image: JPL/Caltech)

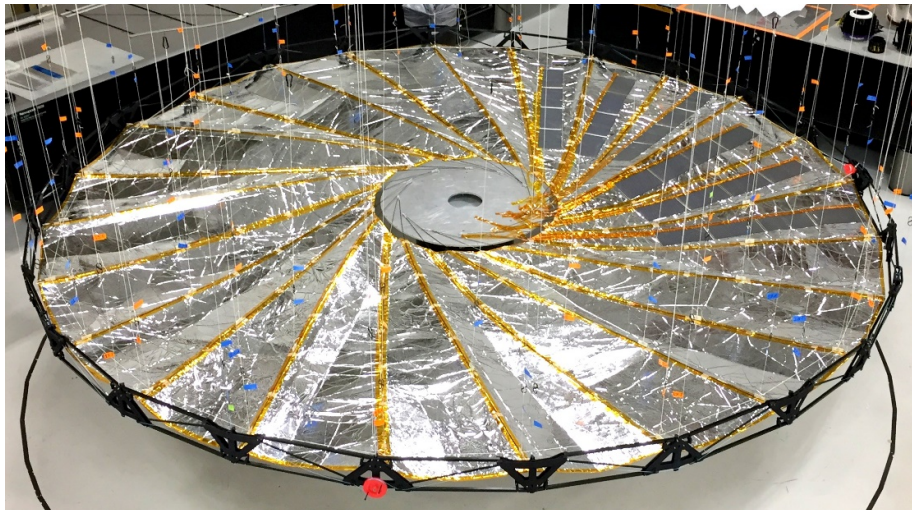


Figure 19: A 5 m prototype starshade inner disk mechanical structure along with its opaque optical shield. The optical shield is constructed of two layers of Mylar separated by a low-density polyurethane foam. Vertical strings are part of the gravity-offloading ground support equipment, designed through an SBIR with Rocco, LLC. (Image: JPL/Caltech)

Progress Over the Last Year:

Building on the successful demonstration of a low-fidelity 5 m opaque origami inner disk in 2016, steps were taken in 2017 towards a higher fidelity demonstration (**Figure 19**) partially integrated into the mechanical inner disk. To offload the effects of gravity, an SBIR-funded gravity offloading system was delivered by Rocco in 2017, as well as a design for a 10 m disk. The Petal Launch Restraint and Unfurler Subsystem (PLUS) design was delivered to JPL by SBIR partner Tendeg in 2017 for the wrapped architecture and to be demonstrated with a full set of 24 petals that are representative of the strain energy of flight petals. The launch restraint

system unfurls the petals using a carousel set of rollers for quasi-static unfurling of the petals. The unfurling mechanism is jettisoned after launch.

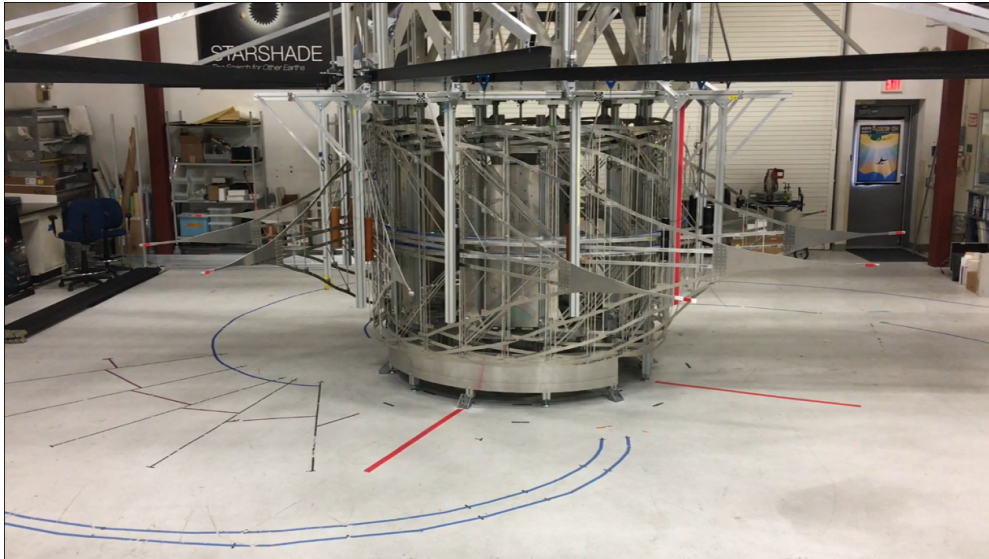


Figure 20: The Petal Launch Restraint and Unfurler Subsystem testbed at JPL. It was designed through an SBIR led by Tendeg, LLC. The prototype serves as a proof of concept for the unfurling of the starshade petals from a fully wrapped and stowed launch configuration. The vertical bars serve to restrain the petals from unfurling further and inadvertently making contact with each other. (Image: JPL/Caltech)

A study of a 70 m-class starshade suitable for HabEx¹⁰⁵ showed that the wrapped petal architecture is compatible with a 5 m-diameter launch fairing, though further analysis is required to show the feasibility of this stowing architecture for this larger class of starshade.

Next Steps:

Building on the 5 m inner disk demonstration with its optical shield from 2016, the wrapped architecture will demonstrate the deployment of a 10 m prototype positioning its petals to within required tolerances. Also, a thermal analysis is needed to show that the petals can maintain their positions after thermal cycling during operations, expected due to the wide range of sun angles that the starshade experiences. This includes coefficient of thermal expansion measurements of the materials that will be used in the starshade in order to confirm the design.

The starshade deployment architecture is undergoing a trade study between wrapped and folded architectures, with results expected in 2018. This will enable the Starshade Technology Development Activity to focus resources on a single reference design. The trade study team is made up of a multi-institutional team of engineers from inside and outside of NASA. The HabEx study will perform further analyses of the 70 m-class starshade, including thermo-mechanical, deployment accuracy, and launch load analyses.

Prioritization:

All of the starshade technologies tracked by ExEP received Impact, Urgency, and Trend scores of 4, 4, and 2, respectively. The highest Impact score is assigned since as a whole, starshade technology enables the reflected-light direct imaging and spectroscopy of Earth-sized planets in the habitable zone of Sun-like stars. The technologies also receive the highest Urgency score, as WFIRST, a mission currently in formulation, could benefit, should a starshade rendezvous mission be selected by NASA. The Trend score is 2, reflecting the focused technology funding that ExEP's Technology Development Activity is already providing.

D MID-IR CORONAGRAPH/TELESCOPE TECHNOLOGY GAPS

The ExEP has traditionally focused its coronagraph technology development on visible wavelengths because for a fixed telescope aperture size, the available inner working angle to study the habitable zones of nearby stars degrades linearly with wavelength. However, in the mid-infrared where a planet could be detected in thermal emission rather than in reflected starlight, the starlight suppression requirement is less stringent. The Origins Space Telescope (OST)¹⁰⁶ is a NASA-chartered large mission concept study focused on far- and mid- infrared science, formulating its mission in parallel with those of HabEX and LUVOIR. The OST team has developed two exoplanet-related science cases with technology gaps and candidate technologies appropriate for tracking and potential development by the ExEP. The first is an ultra-stable mid-infrared detector needed to take a factor ten step beyond JWST's detection capabilities in transit spectroscopy and study the atmospheres of rocky Earth-sized planets orbiting M dwarf stars (see Section E.5.1). The second is a mid-infrared coronagraph capable of directly imaging and spectrally characterizing cool giant exoplanets.

Additionally, planets in the habitable zone of the nearby Alpha Centauri system could be directly imaged with 10 m-class telescopes on the mid-infrared.¹⁰⁷ This will be attempted from the ground using the VLT,¹⁰⁸ but is potentially a science goal for a future mid-infrared space mission.

The mid-infrared direct imaging technology gaps and the technologies required to close them are shown in Figure 21. These are parallel to those for visible/near-infrared direct imaging and are contrast (Section D.1), angular resolution (Section D.2), and detection sensitivity (Section D.3). The gaps are in yellow font and the technologies that address these gaps are shown in blue.

The 2017 Technology Plan Appendix included a mid-IR spectral coronagraph technology (CG-11), a single instrument-level technology. In 2018, the OST STDT team, with the help of the ExEP, broke apart the technology gap to sub-system level technologies that need to be matured, each of which was accepted to the prioritized ExEP Technology List. Consequently, the instrument-level technology CG-11 was replaced on the Program's list.

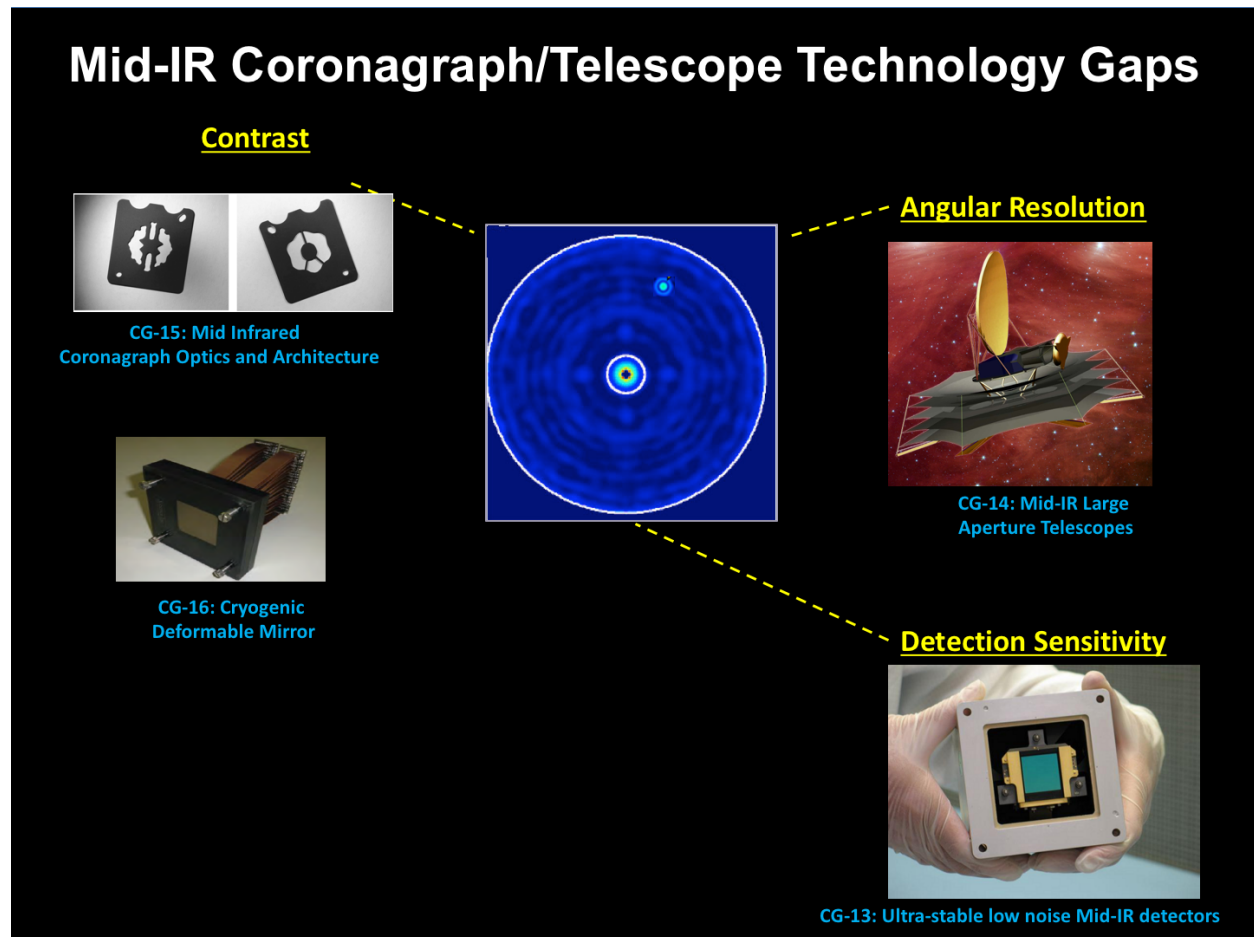


Figure 21: The ExEP mid-infrared coronagraphy technology gaps.

D.1 Contrast

A coronagraph for use on a mission observing in the mid-infrared can build on technologies originally developed for the Japan Aerospace Exploration Agency's (JAXA's) Space Infrared Telescope for Cosmology and Astrophysics (SPICA).¹⁰⁹ These technologies require specific optimization for the mid-infrared: key optics must operate at cryogenic temperatures in order to minimize thermal background noise, for example a deformable mirror capable of actuation at 5 K. On the other hand, detecting planets in thermal emission rather than in reflected light mitigates the required contrast that a coronagraph must achieve in the mid infrared. Potentially, this allows for some loosening of wavefront and telescope stability requirements as compared to visible/near infrared coronagraphy (for example fast LOWFS/C may not be needed).

D.1.1 CG-15: Mid-infrared Coronagraph Optics and Architecture

CG-15: Mid-infrared Coronagraph Optics and Architecture

Description: Coronagraph optics and architecture that suppress diffracted starlight by a factor of $< 10^{-6}$ over a broad mid-IR band (7-30 microns)

SOA: The current state of the art for mid-infrared coronagraphs are the three four-quadrant phase masks of JWST-MIRI. These provide narrow-band imaging with contrasts up to 10^{-4} in three narrow bands from 10.65-15.5 micron with inner working angles of 0.33-0.49". The MIRI coronagraphs do not offer spectral dispersion.

Needed capability: A spectro-imaging instrument with an inner working angle of 0.1" at 10 μm . This is likely less than $2 \lambda/D$ for the available aperture. The best IWA is needed to detect a 300 K Neptune-sized planet at 10 pc at a 1-2 AU separation, and the contrast should be 10^{-6} to detect Saturn at 10 pc (~ 1 microJy @ 24 micron, $3 \lambda/D$ for 16 m aperture) with $R \sim 10$. The maximum spectral dispersion should be sufficient to resolve the 15 micron CO_2 band ($R \sim 500$).

Supported Missions or Mission Concepts: Origins Space Telescope

The coronagraph architecture requires compatibility with obscured/segmented telescopes (see Sect. B.1 for a discussion of coronagraph technology maturation in the V/NIR). The PIAACMC architecture represents a useful way to reach high contrast at a narrower inner working angle in the mid-infrared, but other architectures are also applicable to this longer wavelength band. Some development in coronagraph optics and architecture technology will overlap with development in the visible band and near infrared, but there are specific optimizations that are needed for the mid-infrared band. In particular, the coronagraph instrument may need to operate entirely at cryogenic temperatures to reduce background noise.

Current State-of-the-Art:

The state-of-the-art in mid-infrared coronagraphy are the four-quadrant phase masks on JWST-MIRI (Mid-InfraRed Instrument) which are predicted to achieve contrasts to 10^{-4} at 10.65 to 15.5 μm wavelengths with inner working angles of 0.33 - 0.49" in wide bands (i.e. no spectral dispersion).¹¹⁰ To achieve its exoplanet imaging science goals, the OST STDT preliminarily estimates that it will need a coronagraph that achieves a contrast 10^{-6} with inner working angle of 0.1" at 10 μm . The maximum spectral dispersion must be sufficient to resolve the 15 μm CO_2 band, implying $R \sim 500$. The OST science case and reference design for mid-infrared direct imaging is still in development. A high contrast (i.e. using active wavefront control) mid-infrared coronagraph has not yet been demonstrated.

Progress Over the Last Year:

The OST STDT continued to work on establishing and prioritizing their science goals from which the technology requirements will be derived. To our knowledge, no technology advancements, however, have been conducted over the last year.

Next Steps:

JWST is scheduled for launch in 2019, and will represent for the first time a systems validation of space-based mid-IR coronagraphy, though it will not include active wavefront control. Gaining experience in operation of the coronagraphic modes in MIRI are likely to provide lessons for future coronagraph design in this wavelength band.

The OST STDT will finalize their reference design and instrument needs from which the technology needs will be identified. Assuming direct imaging of exoplanets at mid-infrared

wavelengths will be prioritized, performance of a coronagraph must be demonstrated in a lab environment.

Occluding and apodizing mask designs for the mid-IR can also benefit from parallel efforts at shorter wavelengths, for example using results of the SCDA study (see Sect. B.1.2). If PIAA architecture is needed to minimize the inner working angle, this technology will be advanced by the award of a TDEM16 (PI Belikov, NASA/Ames) to specific, though with no specific focus on mid-infrared optimization.

Prioritization:

This technology received Impact, Urgency, and Trend scores of 2, 3, and 3, respectively. This technology is aimed at studying cool giant planets and is not a step towards the 2010 Decadal Survey goals of characterizing exo-Earths in the Habitable Zone of Sun-like stars, and thus receives an Impact score of 2. This technology is needed by OST, and progress prior to the 2020 Decadal Survey could influence its recommendations, thus an Urgency of 3. The Trend is also set at 3: while there is some preliminary work underway at JAXA the timetable for demonstrating the needed capabilities is not clear.

D.1.2 CG-16: Cryogenic Deformable Mirror

CG-16: Cryogenic Deformable Mirror

Description: Flight-qualified deformable mirrors operable at cryogenic temperatures, and their drive electronics.

SOA: Lab: 19-actuator DMs at 40 K to < 1 micron rms (Trines et al 2016)

Needed capability: Requirements on actuator stroke, stroke resolution, heat dissipation, and actuator count are TBD but must be operable at cryogenic temperatures.

Supported Missions or Mission Concepts: Origins Space Telescope

To correct for wavefront errors, particular due to wavefront errors from the primary and secondary mirror, adaptive optics, i.e. deformable mirrors (DM), are needed. For operation in the mid-IR, the DM must be operable at cryogenic temperatures. Requirements need to be set for actuator stroke length and resolution, actuator density, heat dissipation, and will be set by coronagraph and telescope reference designs that are still in progress.

In addition, systems level studies of a mid-IR coronagraph/telescope system may conclude that wavefront control to achieve 10^{-6} contrast can be performed using a deformable secondary mirror of the telescope, in which case, an instrument-level cryogenic deformable mirror may be unnecessary.

Current State-of-the-Art:

Prototype MEMS DMs were developed for the SPICA coronagraph, have been demonstrated for functionality at 95 K, and thermally-cycled.¹¹¹

Progress Over the Last Year:

The OST STDT continued to work on establishing and prioritizing their science goals from which the technology requirements will be derived. To our knowledge, no technology advancements, however, have been conducted over the last year.

Next Steps:

The requirements of this particular technology must be developed more thoroughly. The necessary stroke length for operations in the 7-30 μm wavelength range must be verified. Heat dissipation requirements must be established and demonstrated. The actuator density and actuator count must be determined based on science objectives. Finally, a full cryogenic coronagraph must be demonstrated in a lab environment.

Prioritization:

This technology received Impact, Urgency, and Trend scores of 2, 3, and 3, respectively. This technology is needed for a mid-infrared coronagraph for studying cool giant planets and is not a step towards the 2010 Decadal Survey goals of characterizing exo-Earths in the Habitable Zone of Sun-like stars, and thus receives an Impact score of 2. This technology is needed by OST, and progress prior to the 2020 Decadal Survey could influence its recommendations, thus an Urgency of 3. The Trend is also set at 3: while there is some preliminary work underway at JAXA and elsewhere, the timetable for demonstrating the needed capabilities is not clear.

D.2 Angular Resolution

D.2.1 CG-14: Mid-IR Large Aperture Telescopes

CG-14: Mid-IR Large Aperture Telescopes

Description: Cryogenic (4K), large-aperture (> 9m) telescopes to achieve high angular resolution needed to direct-image cool exoplanets in wide orbits (> 5 AU)

SOA: JWST Be mirror segments may meet requirements now, so TRL 5 with an extremely expensive technology; TRL 3 exists for other materials like SiC. Cryogenic low-dissipation actuators exist at TRL 3-5.

Needed capability: Develop a feasible and affordable approach to producing a 10-m-class telescope with sufficiently high specific stiffness, strength, and low areal density to be launched; while maintaining compatibility with cryogenic cooling and FIR surface quality/figure of $\sim 1\mu\text{m}$ rms. Material property measurements at cryogenic temperatures for structures and optics such as damping, emissivity, thermal conductivity, etc.

Supported Missions or Mission Concepts: Origins Space Telescope

A future large aperture infrared space telescope in the 10-m class must have sufficiently high specific stiffness, strength, and low areal density to be launched, while maintaining compatibility with cryogenic cooling (to as low as 4K). The necessary surface quality optimized for the mid-infrared is relatively modest compared to UV/V/NIR telescopes and may be of order 1 μm rms. A telescope of that size will be segmented, folded for launch, and autonomously deployed. JWST is a 6.5 m segmented telescope that is passively cooled for operations in the mid-infrared and has advanced deployment technology.

Current State-of-the-Art:

JWST Beryllium mirror segments will operate at 40 K and may meet requirements now; Spitzer's Beryllium mirror operated at 5.5 K with 67-nm rms surface figure. SiC or Aluminum may be a lower cost alternative.

Progress Over the Last Year:

The OST design team considered alternatives for a segmented mirror design, and will present these in their interim report in 2018.

Next Steps:

OST's reference designs and mirror material studies will provide an assessment of the maturity of mid- and far-IR telescope components. For example, for some solutions, cryogenic low dissipation surface figure actuators, if available, may save expensive cryo-figuring and allow use of cheaper materials.

Prioritization:

This technology received Impact, Urgency, and Trend scores of 2, 3, and 3, respectively. This is an enabling technology for a single dish space telescope's ability to directly image cool giant planets and is not a step towards the 2010 Decadal Survey goals of characterizing exo-Earths in the Habitable Zone of Sun-like stars, which at infrared. This technology thus receives an Impact score of 2. This technology is needed by OST, and progress prior to the 2020 Decadal Survey could influence its recommendations, thus an Urgency of 3. The Trend is also set at 3: while there is some preliminary work underway as part of the OST study and potentially in response to the call for industry-led studies (See Sect. B.2), the timetable for demonstrating the needed capabilities is not clear.

D.3 Detection Sensitivity

D.3.1 CG-13: Low-noise Mid-IR detectors

CG-13: Low noise Mid-IR detectors

Description: Low noise and detectors for the mid-infrared band (7 - 20 microns) enabling exoplanet direct imaging.

SOA: JWST/MIRI

Needed capability: noise requirements TBD, likely to be 10 x better than JWST/MIRI

Supported Missions or Mission Concepts: Origins Space Telescope

A mid-infrared coronagraph operating in the 7-30 μm band requires low noise detectors in order to have acceptable signal to noise on an exoplanet while performing spectroscopy at a resolution of 100-500. The exact needed noise performance must be studied in more detail; it is possible that the state-of-the-art (e.g. JWST/MIRI) is acceptable.

Wavefront sensing for a mid-infrared coronagraph could be performed using an architecture similar to that of a UV/V/NIR coronagraph (WFIRST, HabEx, LUVOIR; see Sect. B.2.1), and thus require ultra-low noise visible detectors such as those being matured by WFIRST (See Sect. B.4.1).

Current State-of-the-Art:

JWST's MIRI uses arsenic-doped silicon impurity band conduction (IBC) detector arrays,¹¹² which have demonstrated read noise of 14 e⁻ (in Fowler sampling mode) and 0.2 e⁻/s dark current. These are similar technology to that previously flown on Spitzer's Infrared Array Camera.

Progress Over the Last Year:

The OST STDT and design team, and the MISC instrument team considered the read noise needs for coronagraphy in the mid-infrared; more information will be forthcoming in the OST interim report expected in 2018.

Next Steps:

Requirements must be developed for mid-infrared coronagraphy to determine whether the IBC detectors are sufficient as measured on the ground in MIRI testing and on orbit with Spitzer/IRAC. JWST is expected to establish the on-orbit state of the art for mid-IR detectors after its 2019 launch. Alternative doping for IBC detectors (such as Phosphorous) may be considered as a less-costly alternative to arsenic doping for future missions.

Prioritization:

This technology received Impact, Urgency, and Trend scores of 2, 3, and 4, respectively. This technology involves improved noise performance of mid-infrared detectors, needed for a mid-infrared coronagraph to studying cool giant planets and is not a step towards the 2010 Decadal Survey goals of characterizing exo-Earths in the Habitable Zone of Sun-like stars. Thus the technology receives an Impact score of 2. This technology is potentially needed by OST, and progress prior to the 2020 Decadal Survey could influence its recommendations, thus an Urgency of 3. The Trend is also set at 4, as there seems to be little funded activity towards improvement beyond JWST's MIRI instrument.

E OTHER TECHNOLOGY GAPS

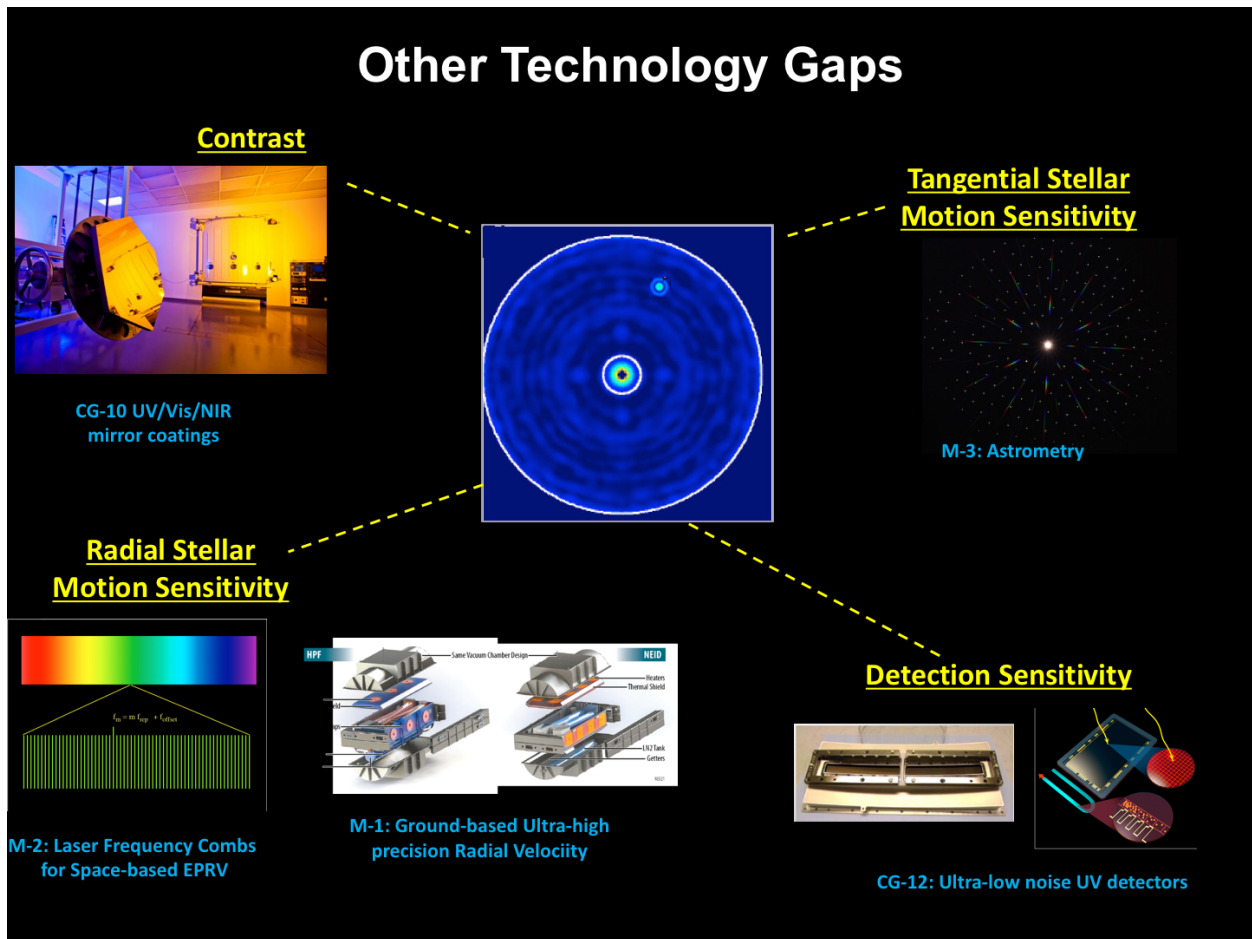


Figure 22: Other technology gaps.

E.1 Contrast

E.1.1 CG-10: UV/V/NIR mirror coatings

CG-10: UV/V/NIR mirror coatings

Description: Mirror coatings that enable high reflectivity to wavelengths as short as 90 nm

SOA: Al coating with combination of MgF2, LiF, and/or AlF3 overcoat: 90-120 nm: < 50% reflectivity 120-300 nm: 85% reflectivity 300 nm-2 μm: > 90% reflectivity Polarization differences between orthogonal polarization states, uniformity, and durability of coatings on large optics is unknown. Flight: HST uses MgF2; 85% reflectivity $\lambda > 120$ nm; 20% reflectivity $\lambda < 120$ nm

Needed capability: A mirror coating that achieves 90-120 nm: > 70% reflectivity; 120-300 nm: > 90% reflectivity; 300 nm-2 μm: > 90% reflectivity; Polarization phase and amplitude difference < 1% between orthogonal polarization states.

Supported Missions or Mission Concepts: LUVOIR, HabEx

The measurement of broad atmospheric features in the ultraviolet band can enhance the direct detection and characterization of exoplanets. For example, at wavelengths shortward of 300 nm, the reflectivity of planets with O₃ in their atmosphere (such as in an Earth-like planet) is very low, while a different reflectivity cutoff shortward of 220 nm occurs for planets with SO₄-

rich atmospheres (such as a Venus-like planet).¹¹³ While a future space observatory (such as HabEx or LUVOIR) could be driven to a wavelength cutoff less than 100 nm by general astrophysics science goals, wavelengths less than 200 nm are not likely to benefit exoplanet science directly. However, a space mission that requires both high throughput at wavelengths < 120 nm and wavefront uniformity for coronagraphy must develop appropriate mirror coatings. Coatings are needed to protect aluminum optics, which are reflective to a wide band of light, including at $\lambda < 120$ nm, from oxidation. Non-uniformities in these coatings, which may also change with time, can induce cross-polarized wavefront errors, frustrating standard wavefront control with a DM. Hence, achieving 10^{-10} contrast in a visible/near-IR coronagraph is likely to require coatings to be uniform to the 0.5% level. The ExEP is therefore interested in technology development particularly in the area of coating uniformity.

Current State-of-the-Art:

The state-of-the art in space UV mirror coatings is HST and the Galaxy Evolution Explorer, which used aluminum optics coated with a thin layer of MgF_2 . The reflectivity was > 85% for $\lambda > 120$ nm but dropped to 20% at shorter wavelengths. Hennessy et al (2016)¹¹⁴ report 2 nm rms coating uniformity for multi-layer coatings on small samples. Quijada et al. (2017)¹¹⁵ report hot coating processes, under development at GSFC and capable of extremely thin dielectric deposition on aluminum down to 3 nm thickness, allowing for high reflectivity below 100 nm while maintaining broadband performance into the near-infrared. Uniformity for larger mirrors depends strongly on the specific coating process. As one example, JWST showed better than 0.5% uniformity in near-infrared reflectance and < 10 nm peak-to-valley thickness variation in its 18 Au-coated segments.^{116,117}

Progress Over the Last Year:

Both HabEx and LUVOIR have investigated coatings and are leaning towards Aluminum with LiF, with a thin capping layer of MgF_2 or AlF_3 and have studied uniformity requirements. Balasubramanian et al. (2017)¹¹⁸ presented a summary of the field and also showed that the protective overcoat must maintain a thickness variation better than 2 nm peak-to-valley.

Next Steps:

While attaining the required coating performance has been shown to be feasible, the Al+LiF+ MgF_2 must be shown to scale beyond the coupon level. Space telescopes tend to have a fast f/# due to tight launch fairing constraints, which in turn induces additional polarization aberration from steep incidence angle rays which are difficult to compensate with a deformable mirror. A tuned mirror coating could potentially mitigate this systems-level polarization effect, though this has not yet been demonstrated.¹¹⁹

The Breckinridge TDEM15 effort seeks to characterize measure the polarization birefringence of a 3.8 m mirror designed for ground-based use at 500 nm, and while the results may not be traceable to future coating processes for space telescopes, the information will be valuable. Contamination by particulate accumulation during the ground testing and integration can also be an issue at the several percent level. For example, HST's primary mirror had a 10%

degradation in reflectivity due to pre-launch contamination.¹²⁰ Hence, handling protocols must be further refined for future space telescopes.

Prioritization:

This technology received Impact, Urgency, and Trend scores of 3, 3, and 2, respectively. Coating uniformity technology is enabling for the ability to detect and characterize exo-Earths, and thus the impact is 3. The Urgency is also 3, as both HabEx and LUVOIR need to advance this technology and thus advancement in this area can potentially influence the 2020 Decadal Survey. The Trend score is 2, as several awards in the TCOR element of SAT have advanced this technology to nearly the needed level, and look promising.

E.2 Detection Sensitivity

E.2.1 CG-12: Ultra-low noise UV detectors

CG-12: Ultra-low noise UV detectors

Description: Low-noise ultraviolet (200-400 nm) detectors to characterize exoplanets with an integral field spectrograph.

SOA: Lab: Micro-channel Plates (MCP): 0 read noise, 200–300 nm, spurious count rate 0.05 - 0.5 counts/cm²/s; QE 20-45%; resolution element size 20 μ m. EMCCD: 0 read noise, dark current > 0.005 e⁻/res/hr; QE 30-50%; resol. el. size 20 μ m Flight: HST HRC: In relevant UV band (250 nm): QE 33%, read noise 4.7 e⁻, dark current 5.8×10⁻³, 1024×1024

Needed capability: Read Noise: 0 e⁻; Dark Current: 0 e⁻/resolution/s; Spurious Count Rate: < 0.05 counts/cm²/s; QE: 75% ; Resolution size \leq 10 μ m; Tolerant to space radiation environment over mission lifetime.

Supported Missions or Mission Concepts: LUVOIR, HabEx

The measurement of broad atmospheric features in the ultraviolet band can enhance the direct detection and characterization of exoplanets. For example, at wavelengths shortward of 300 nm, the reflectivity of planets with O₃ in their atmosphere (as in an Earth-like planet) is very low, while a different reflectivity cutoff shortward of 220 nm occurs for planets with SO₄-rich atmospheres (such as a Venus-like planet).¹²¹

The HabEx and LUVOIR STDTs will determine the detailed requirements for UV detectors for exoplanet science applications during their ongoing studies; the needs listed in **Table 3** represent requirements linked to general astrophysics applications of UV detectors, and include desired sensitivity to wavelengths shorter than 100 nm.

Current State-of-the-Art:

Wavelengths shorter than 200 nm are not likely to benefit exoplanet science greatly. In the 200-400 nm band, there are several candidate technologies whose state-of-the-art is close to the needs for imaging spectral characterization of exoplanets, including EMCCD detectors and microchannel plates (MCP): see Bolcar et al. (2016)¹²² for a summary and Siegmund et al. (2017)¹²³ for an assessment of the applicability to HabEx and LUVOIR. For all of these candidate technologies, noise levels are adequate, but improvement is needed in quantum efficiency and detector lifetimes. Cryogenic MKID and TES detectors can also potentially operate in this band (Section B.4.2).

Progress Over the Last Year:

The coronagraph instrument on LUVOIR (ECLIPS) has baselined delta-doped EMCCD detectors for its UV (200-400 nm) channel.¹²⁴ These detectors meet all sensitivity requirements, though lifetime in the L2 radiation environment is not known.

Next Steps:

To further mature near-UV detectors for future exoplanet missions, radiation hardening may be needed. Radiation testing of delta-doped EMCCD devices will be performed at JPL as part of a SAT/COR effort (PI Nikzad).

Prioritization:

This technology received Impact, Urgency, and Trend scores of 2, 3, and 2, respectively. The ability to perform spectroscopy and imaging of exoplanets in the UV is considered to be an enhancing technology. The Cosmic Origins program of NASA APD has historically invested in this detector technology and a number of active SAT awards are advancing the technology (hence a Trend score of 2).

E.3 Radial Stellar Motion Sensitivity (for planetary mass measurement)

Precision radial velocity (RV) techniques measure the Doppler shift in stellar absorption lines as orbiting planets cause a gravitational recoil in the star. RV is a historically important technique for discovering exoplanets, and recently was used to discover a planet orbiting our closest neighboring star, Proxima Centauri.¹²⁵

RV is one technique for obtaining a planetary mass measurement. It is needed to interpret spectral biosignature detections by inferring a planet's density and atmospheric scale height. RV could support a future strategic exoplanet space mission in two ways: first, ground-based RV instruments could support a space mission by detecting and characterizing the masses and orbits of direct imaging targets; and second, a dedicated RV instrument could be included on a space telescope to accomplish these ends.

Both paths will require new technologies. The reflex motion (radial velocity semi-amplitude) of a Solar-mass star due to an orbiting Earth-mass planet at 1 AU is 9 cm/s. Detection of the Doppler shift of spectral lines to this precision requires exquisite control of instrumental precision and long term accuracy as well as mitigation of "stellar jitter" and of the deleterious effects of telluric atmospheric residuals on the time scales of years, or nearly an order of magnitude improvement in the current-state-of-the-art.¹²⁶

Achieving this improvement requires investment in theoretical studies of stellar stability, as well as practical issues in instrumentation, including the multi-year stability of spectrograph pressure, temperature and optical-mechanical structure and wavelength calibration using gas lamps, Fabry-Perot Etalons or Laser Frequency combs.¹²⁷

E.3.1 M-2: Laser Frequency Combs for Space-based EPRV

M-2: Laser Frequency Combs for Space-based EPRV

Description: Laser Frequency Combs (LFCs) are precise calibration sources for extreme-precision radial velocity measurement.

SOA: Lab: Electro-optic-modulation frequency combs demonstrated on ground-based observatories with needed mode spacing, need miniaturization and power reduction. Non-NASA work is advancing miniaturization.

Flight: Fiber laser-based optical frequency combs demonstrated on sounding rocket (TEXUS 51 4/15 and TEXUS 53 1/16) w/ ~ few hundred MHz mode spacing. System mass is > 10 kg.

Needed capability: Space-based Laser Frequency Combs to calibrate high resolution, fiber-fed spectrographs for radial velocity precision better than 10 cm/s. Desired parameters are: mode spacing of 5-10 GHz, bandwidth span 380 nm to 2400 nm, Allen deviation < 10-10, Low SWaP.

Supported Missions or Mission Concepts: LUVUOIR, HabEx

Additional sensitivity may be gained by including an RV instrument on a space telescope. A major systematic error faced by ground-based RV measurements is microtelluric absorption lines from the Earth's atmosphere. RV measurements in space would also open near-IR wavelengths to sensitive measurement which might help in reducing the effects of stellar noise. An essential component for obtaining extreme precision, both on ground-based and space-based spectrometers are Laser Frequency Combs (LFCs). LFCs provide an extremely stable and accurate comb of visible and near-infrared lines, creating an ideal calibration source for a high resolution, fiber-fed spectrographs for radial velocity measurements. The key parameters for LFCs for space operation require mode spacings of 5-10 GHz, an overall bandwidth spanning 380 nm to 2400 nm, as well as appropriate packaging for a space mission.

Current State-of-the-Art:

Electro-optic-modulation (EOM) frequency combs have been demonstrated on ground-based observatories with the needed mode spacing, though with size and power needs that are not yet appropriate for a space instrument. Non-NASA work is advancing miniaturization. Fiber laser-based optical frequency combs have been demonstrated on sounding rockets (TEXUS 51 4/15 and TEXUS 53 1/16) though without the required mode spacing.

Progress Over the Last Year:

An Astrophysics Probe study (PI Peter Plavchan) was funded by the NASA Astrophysics Directorate in 2017 to study the improvement in measurement errors that could be obtained from observing from space, across a broad wavelength band unaffected by residual atmospheric effects.

Next Steps:

The Probe study will complete in 2018 and is expected to define technology needs for a space based RV instrument, including the specifications of a LFC for calibration. High spectral resolution, fiber-fed, ground-based spectrographs aiming for an ultimate sensitivity of 10 cm/s will be on line in the next several years.^{128,129} Experience from these projects relating to instrument stability, mitigation of stellar jitter and atmospheric residuals, and long-term calibration, including the use of LFCs, will be directly applicable to assessing the need for and the technical readiness of space-based RV instrumentation.

Prioritization:

This technology received Impact, Urgency, and Trend scores of 3, 3, and 2, respectively. The mass measurement is a highly desired enhancing measurement, and thus an impact 3. The Urgency is 3 because the maturity of astrometry technology could potentially influence the 2020 Decadal Survey, as mission concepts like LUVOIR and HabEx, and the EarthFinder Probe concept study can use precision astrometry as a technique to measure masses of exoplanets. The Trend is 2 because it is possible that the RV calibration technology will be developed to the required needs by the ground-based community, which is actively developing laser frequency combs.

E.3.2 M-1: Extreme Precision Ground-based Radial Velocity**M-1: Extreme Precision Ground-based Radial Velocity**

Description: Ground-based radial velocity instrumentation capable of measuring the mass of candidate exo-Earths in the habitable zone and to maximize efficiency of space telescope surveys.

SOA: Single measurement precision: 80 cm/s HARPS instrument; NN-EXPLORE's NEID (WYNN observatory) in development: goal 27 cm/s

Needed capability: Signal from exo-Earths is 10 cm/s; Need to reduce systematic errors to 1 cm/s on multi-year timescales; statistical uncertainties of 1 cm/s on monthly timescales for late F, G, and early K stars

Supported Missions or Mission Concepts: LUVOIR, HabEx

Ground-based RV measurements provide two important enhancements to a space mission's ability to directly-image and characterize exoplanets. First, dedicated ground-based RV surveys in the Northern and Southern hemispheres could improve the science return of a direct imaging space mission. By pre-selecting stars with known planets, and using RV-measured planet orbits to schedule observations, the yield of a space mission would be improved. Second, precision RV measurements combined with imaging data can unambiguously determine planetary mass which is necessary for assessing potential habitability.^{130,131}

To measure the mass of Earth-mass planets orbiting Sun-like stars, a long term accuracy of 1 cm/s over the relevant orbital time scales is needed.¹³² Achieving this goal requires investment in theoretical studies of stellar stability, as well as in instrumentation, including wavelength calibration and in the stability of spectrograph pressure, temperature and optical-mechanical structure on one-year time scales. The development of the NEID instrument for the WIYN telescope under the ExEP's NN-EXPLORE program will take an important step in this direction, with a goal of 27 cm/s precision.¹³³

Current State-of-the-Art:

The state-of-the art single measurement precision is currently 80 cm/s¹³⁴, expected to be advanced to 20-30 cm/s by NN-EXPLORE's NEID instrument¹³⁵ for the WIYN telescope, and the iLocator¹³⁶ instrument for the LBT, both planned for first light in 2018-2019.

Progress Over the Last Year:

The NEID project has started its instrument build over the last year aiming towards an early 2019 deployment to the telescope, and has achieved a laboratory demonstration of better than 1 mK thermal stability at room temperature.

Next Steps:

A number of RV instruments, including NEID, are expected to deploy to ground-based telescopes in the coming few years, several aiming for 10 cm/s precision. Limiting factors are likely to be better understood as experience is gained in using these instruments for science observations. Further theoretical understanding of stellar noise and telluric atmospheric effects, as well as additional improvement in instrumental stability will be needed beyond the current generation of RV spectrometers.

Prioritization:

This technology received Impact, Urgency, and Trend scores of 2, 3, and 3, respectively. Despite the important benefits offered by ground-based precision RV technology, its enhancing nature (rather than mission-enabling) resulted in it being ranked lower than the starlight suppression needs for the ExEP. The Trend score of 3 reflects the unknown path to overcome astrophysical limits from the ground-based RV measurements.

E.4 Tangential Stellar Motion Sensitivity (for planetary mass measurement)

E.4.1 M-3: Astrometry

M-3: Astrometry

Description: Measure the mass and orbital parameters of Earth-like planets by performing astrometry of FGK stars to the sub-micro-arcsecond level.

SOA: Flight: GAIA typical uncertainty in astrometry for DR1 catalog is 300 microarcseconds; goal for V band magnitude 7-12 stars is 10 microarcseconds

Needed capability: 0.1 microarcsecond uncertainty enables survey of nearby FGK stars. Astrophysical limits (such as variable stellar surface structure) need to be well-understood. Telescope wavefront error stability and detector thermal and mechanical stability must enable sub-microarcsecond astrometry measurements.

Supported Missions or Mission Concepts: LUV01R, HabEx

Precision astrometry determines the Keplerian orbital parameters of an exoplanet, enhancing the direct imaging and characterization of exoplanets by (1) increasing science yield of follow-up coronagraph observations, and (2) determining the mass of a detected exoplanet without the $\sin(i)$ system inclination uncertainty intrinsic to radial velocity measurements. Masses are necessary to assess habitability by distinguishing Earth-like planets around Sun-like stars from small Neptunes or water worlds, and by helping to constrain the atmospheric scale height, which is crucial to understanding the atmosphere. The precision must be improved to 0.3 microarcseconds in a single measurement in order to enable detection of Earth analogs at 10 pc distance,¹³⁷ which is two orders of magnitude beyond the current state-of-the-art.

Current State-of-the-Art:

The current state of the art is the GAIA mission, preliminarily estimated to achieve 34 microarcsecond measurement error, but ultimately could achieve 10 microarcseconds on bright targets after all systematics are calibrated. GAIA is expected to be sensitive mainly to Jupiter-

mass exoplanets.¹³⁸ In addition, astrometry accuracy of 25 microarcseconds has been achieved with HST.¹³⁹

Progress over the Last Year:

An astrometry TDEM led by Eduardo Bendek (NASA-ARC) completed in 2017¹⁴⁰ achieving all of its planned milestones. The team completed a laboratory demonstration of the use of a diffractive pupil to achieve 10 microarcsecond astrometric precision (when installed on a 2.4 m telescope) while showing compatibility of a diffractive pupil with direct imaging using a PIAA coronagraph.¹⁴¹ This established an important step towards the eventual sub-microarcsecond sensitivity goal. The diffractive pupil concept consists of dots etched on a primary mirror yielding diffraction spikes in the focal plane that can be used for precise wavefront error correction for astrometry.

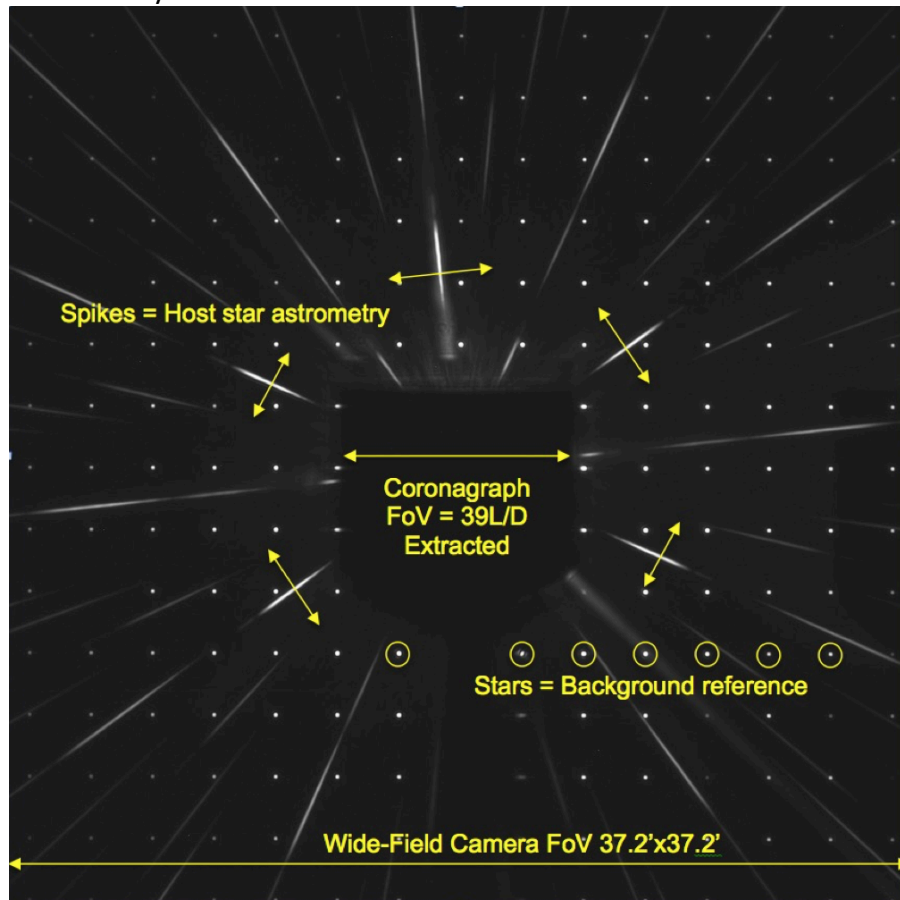


Figure 23: Demonstration of astrometry using a diffractive pupil (from Bendek TDEM 13 final report). The diffractive spikes are due to the patterns on the pupil.

Next Steps:

GAIA's Data Release 2 is expected in 2018, including many astrometric exoplanet detections. In the long run, GAIA is expected to detect thousands of Jupiter-mass planets in orbits between 0.5 and 5 AU of their host stars¹⁴² which will revolutionize the understanding of exoplanetary systems. In addition, a detailed assessment of GAIA's systematic errors and on-orbit stability,

including thermal relaxation effects and micrometeoroid impacts, will be critical for designing future missions.

Given the importance of mass measurements for understanding the potential habitability of exo-Earths, the LUVOIR and HabEx STDTs are expected to explore astrometry. Both missions require extreme telescope wavefront error stability for coronagraph performance, which may help astrometric measurements. The DP concept may provide an astrometric solution for these large mission concepts.

Prioritization:

This technology received Impact, Urgency, and Trend scores of 3, 3, and 3, respectively. The mass measurement is a highly desired enhancing measurement, and thus an impact 3. The Urgency is 3 because the maturity of astrometry technology could potentially influence the 2020 Decadal Survey, as mission concepts like LUVOIR and HabEx potentially can use precision astrometry as a technique to measure masses of exoplanets. The Trend is 3 because the path is unclear to the goal of achieving better astrometry than GAIA. Current investigations in space-based astrometry are confined to the HabEx and LUVOIR STDTs.

E.5 Mid-IR Transit and Secondary Eclipse Spectroscopy

Transit spectroscopy has proven to be an essential tool for characterizing the atmospheres of exoplanets. Like photometric transits, transit spectroscopy looks at the decrease in brightness of a host star as a planet passes through our line of sight to the star. By observing the transit in multiple wavelengths, spectroscopic absorption features in the atmosphere of the transiting planet can be measured. Similarly, secondary eclipse spectroscopy measures the spectra of light emitted from transiting planets by comparing signals during and outside of secondary eclipse, when the host star completely occults the planet. These techniques have been used to study the atmospheres of giant planets with HST and Spitzer data.

The mid-infrared wavelength band is rich with spectral features from trace gas constituents and potential biomarkers such as methane, carbon dioxide, ozone, nitrates, sulfates, and others. From its cooled and stable platform at Sun-Earth L2, JWST will be able to carry out transit spectroscopy of many planetary systems. In 2017, A Cycle-1 Early Release Science proposal was selected, entitled “The Transiting Exoplanet Community Early Release Science Program” (PI N. Batalha)¹⁴³, with plans to observe a number of transiting systems with all of JWSTs instruments. JWST will make even deeper inroads into studying the bulk atmospheres of planets via secondary eclipse spectroscopy. This is because JWST will be the first observatory capable of sensitive and high precision mid-IR spectroscopy, and this will be exploited by several Cycle 1 GTO programs that focus on this technique. These and other Cycle 1 programs will reveal much information about exoplanet atmospheres as well as demonstrate JWST’s early performance on transiting planet systems.

The key performance metric for these observations is the stability of the instrument response during the transit, secondary eclipse, or planetary orbit phase curve (typically on the time scale of hours to days). JWST MIRI will use the same detectors¹⁴⁴ as Spitzer/IRAC which has been able to achieve around 60 ppm precision on time scales of several hours, including the

phenomological calibration of on-orbit drifts. Systematic errors for transit observations expected with JWST based on previous are described in Beichman et al (2014).¹⁴⁵ Beyond JWST, further improvement in the stability of transit and secondary eclipse spectroscopy can enable further characterization of exoplanets. One goal to search for habitable worlds is through the study of the atmospheres of rocky Earth-sized planets orbiting M dwarf stars. The shallower transit depth and secondary eclipse signals of small planets require improvements in the detector system stability to ensure that systematic errors are kept to a level that does not impede measurement of a planet's spectral features. The study of the atmospheres of potentially habitable planets orbiting M-dwarf stars is a key science goal for the OST mission concept. OST has specified a needed improvement to ~ 5 ppm stability over 5 hr in mid-IR detectors. This performance is a factor 10 beyond the state-of-the-art, and may likely require new technology.

E.5.1 M-4: Ultra-Stable Mid-Infrared Detectors

M-4: Ultra-Stable Mid-Infrared Detectors

Description: Ultrastable detectors for the mid-infrared band (7 - 20 microns) enabling transit spectroscopy of rocky exoplanets in the Habitable Zone of M-dwarfs.

SOA: Lab: JWST/MIRI is expected to achieve 10-100 nm transit stability. Flight: Spitzer IRAC Si:As detector data have demonstrated about 60 ppm precision in transit observations of several hours

Needed capability: < 5 ppm stability for 5 hours

Supported Missions or Mission Concepts: Origins Space Telescope

Once on orbit, the MIRI detectors are expected to establish the state-of-the-art for transit spectroscopy in the mid-IR band. MIRI uses the same arsenic-doped silicon impurity band conductor (IBC) detector technology as Spitzer/IRAC and a hybridized readout¹⁴⁶ that improves their stability.

Current State-of-the-Art:

Spitzer IRAC Si:As detectors have demonstrated about 60 ppm precision in transit observations of several hours. JWST/MIRI is expected to achieve similar or slightly better stability. Limiting factors in stability are currently not identified.

Progress Over the Last Year:

A study of fundamental limits due to stellar activity¹⁴⁷ showed that the current generation of infrared transit spectroscopy measurements from space, including those from JWST, will not be limited by stellar activity.

Next Steps:

After the launch of JWST in 2019, MIRI is expected to show some improvement of the state-of-the-art for stability beyond that achieved by Spitzer/IRAC. In particular, additional work in on orbit calibration of transit spectroscopy observations will show how much instability can be corrected in the presence of drifts in the instrument and in the astrophysical sources. For future missions targeting several parts per million stability, such as OST, a detailed study of sources of instability in mid-IR detector systems will be needed to determine where technology

investments will be most effective. This should be done in concert with modeling on-orbit calibration, which will mitigate the detector requirements to some level. The intrinsic stability of the mid-IR detector system may be driven by fundamental detector materials properties, cryogenic detector readout circuitry, or other instabilities in the system. Additionally, alternative doping for IBC detectors (such as phosphorous) may be considered as a less costly alternative to arsenic doping for mid-IR detectors.

Astrophysical limits should be examined further to show that they will not be limitations for transit measurements at sensitivity levels beyond those achievable by JWST.

Prioritization:

This technology received Impact, Urgency, and Trend scores of 3, 3, and 4, respectively. The ability to use transit spectroscopy to measure biosignatures in the mid-infrared is a highly desired enhancing measurement for an exo-Earth mission (it can probe Earth-sized planets in the habitable zones of M-dwarfs only, rather than Sun-like stars) and thus receives Impact 3. The Urgency is 3 because the maturity of ultra-stable mid-infrared detectors could potentially influence the 2020 Decadal Survey, as they are used to perform one of the central science goals of the Origins Space Telescope mission concept. The Trend is 4 because the path to the goal of achieving better stability than JWST is not known and no efforts are heading in that direction.

F TECHNOLOGY WATCH LIST

While not meeting the selection criteria to be included on the prioritized Technology List, two of the technologies submitted by the community were determined to still be potentially beneficial to exoplanet science. These technologies will be revisited annually for possible prioritization and are listed in Table 5.

Table 5: ExEP Technology Watch List

| Gap Title |
|----------------------|
| Advanced Cryocoolers |
| Sub-Kelvin Coolers |

F.1 Advanced Cryocoolers

Some classes of energy-resolving near-infrared and visible detectors for exoplanet characterization (such as KIDs and TES microcalorimeters; see Sect. B.4.2) require cooling to temperatures < 1 K. To reach these temperatures, sub-Kelvin coolers must be pre-cooled by an advanced cryocooler. Below 25 K, passive cooling in space is not practical and compact cryocoolers are necessary for pre-cooling a sub-Kelvin cooler. Custom solutions have been successful in space for mm-wave space missions such as Planck, but additional development is required in heat lift, lower mass, lower volume, and lifetime. Sorption coolers and mechanical Joule-Thomson, pulse tube, and Stirling coolers are possible solutions, but vibration isolation must be at a level compatible with the sub-nanometer wavefront stability needed for coronagraphy. See Rauscher et al (2016)¹⁴⁸ for a discussion of technology suitable for cryogenic detectors.

F.2 Sub-Kelvin Coolers

To cool an energy-resolving exoplanet detector system below 1 K starting from a stage pre-cooled by an advanced cryocooler, a sub-Kelvin cooler must be used. While sub-Kelvin coolers have been successfully flown on Herschel and Planck, cooler technology with the necessary heat lift have not advanced beyond TRL 3. Existing candidates include ^3He - ^4He dilution refrigerators, ^3He sorption coolers, and adiabatic demagnetization refrigerators. The compatibility of these coolers with sub-nanometer wavefront stability required for a coronagraph is currently unknown.

G PRIORITIZATION

The technologies to close the technology gaps were initially prioritized by the ExEP technology team (the Program and Deputy Chief Technologists and the Program and Deputy Chief Scientists), peer-reviewed by technologists from the other NASA APD program offices (PCOS and COR) and reviewed by the Exo-TAC. The three prioritization criteria scores for each technology are shown along with the relative weighting of each used to determine the total score. Definitions of the criteria and their relative values are described in Section A.3.

| ID | Technology Title | Impact | Urgency | Trend | Total |
|-------|---|--------|---------|-------|-------|
| | weight: | 10 | 10 | 5 | Score |
| CG-2 | Coronagraph Architecture | 4 | 4 | 2 | 90 |
| S-2 | Starlight Suppression and Model Validation | 4 | 4 | 2 | 90 |
| S-1 | Controlling Scattered Sunlight | 4 | 4 | 2 | 90 |
| S-3 | Lateral Formation Sensing | 4 | 4 | 2 | 90 |
| S-5 | Petal Positioning Accuracy and Opaque Structure | 4 | 4 | 2 | 90 |
| S-4 | Petal Shape and Stability | 4 | 4 | 2 | 90 |
| CG-3 | Deformable Mirrors | 4 | 4 | 2 | 90 |
| CG-1 | Large Aperture Primary Mirrors | 4 | 3 | 3 | 85 |
| CG-6 | Mirror Segment Phasing | 4 | 3 | 3 | 85 |
| CG-7 | Telescope Vibration Sense/Control or Reduction | 4 | 3 | 3 | 85 |
| CG-9 | Ultra-Low Noise Near-Infrared Detectors | 4 | 3 | 3 | 85 |
| CG-5 | Wavefront Sensing and Control | 4 | 3 | 2 | 80 |
| CG-8 | Ultra-Low Noise Visible Detectors | 4 | 3 | 2 | 80 |
| M-4 | Ultra-Stable Mid-IR detector | 3 | 3 | 4 | 80 |
| M-3 | Astrometry | 3 | 3 | 3 | 75 |
| CG-4 | Data Post-Processing Algorithms and Techniques | 4 | 2 | 2 | 70 |
| CG-10 | Mirror Coatings for UV/NIR/Vis | 3 | 3 | 2 | 70 |
| M-2 | Space-based Laser Frequency Combs | 3 | 3 | 2 | 70 |
| CG-13 | Ultra Low-noise Mid-IR detectors | 2 | 3 | 4 | 70 |
| M-1 | Extreme Precision Ground-based Radial Velocity | 2 | 3 | 3 | 65 |
| CG-14 | Mid-IR Large Aperture Telescopes | 2 | 3 | 3 | 65 |
| CG-15 | Mid-IR Coronagraph Optics and Architecture | 2 | 3 | 3 | 65 |
| CG-16 | Cryogenic Deformable mirror | 2 | 3 | 3 | 65 |
| CG-12 | Ultra-Low Noise UV Detectors | 2 | 3 | 2 | 60 |

H CONCLUSION

The 2010 Astrophysics Decadal Survey recommended the creation of a technology development program for a potential future exoplanet mission to mature starlight-suppression technology for the detection of spectra of Earth-like exoplanets. The ExEP supports a community-based process to help NASA identify the needed technologies to achieve this goal and to mature the selected concepts to inform the 2020 Decadal Survey committee. This Appendix outlines technology development plans and activities that will lead toward that goal.

A new ExEP Technology Plan Appendix will be released each year to update the progress made in each technology area and compare it to the performance need for future exoplanet missions.

I DOCUMENT CHANGE LOG

This section contains a log of changes to the 2018 ExEP Technology Plan Appendix.

| Date | Version | Author | Description |
|------|---------|--------|-------------|
| | | | |

J ACRONYMS

| | |
|---------|---|
| ACAD | Adaptive Correction of Aperture Discontinuities |
| AIP | Astrophysics Implementation Plan |
| AFTA | Astrophysics Focused Telescope Assets |
| AMTD | Advanced Mirror Technology Development |
| APLC | Apodized Pupil Lyot Coronagraph |
| APRA | Astrophysics Research and Analysis |
| ATLAST | Advanced Technology Large Aperture Space Telescope |
| BMC | Boston Micromachines Corporation |
| CIC | Clock-Induced Charge |
| CTE | Coefficient of Thermal Expansion |
| DM | Deformable Mirror |
| DRM | Design Reference Mission |
| EMCCD | Electron Multiplying Charge Couple Device |
| ExEP | Exoplanet Exploration Program |
| ExoPAG | Exoplanet Program Analysis Group |
| HabEx | Habitable Exoplanet Imaging Mission |
| HCIT | High Contrast Imaging Testbed |
| HDST | High Definition Space Telescope |
| HiCAT | High Contrast Imager for Complex Aperture Telescopes |
| HRC | High-Resolution Channel |
| HST | Hubble Space Telescope |
| IWA | Inner Working Angle |
| JWST | James Webb Space Telescope |
| LOWFS/C | Low-Order Wavefront Sensor and Controller |
| LTF | Low-temperature Fusion |
| LTS | Low-temperature Slumping |
| LUVOIR | Large Ultra-Violet Optical Infrared |
| MCP | Micro Channel Plate |
| MEMS | Micro Electro Mechanical Systems |
| MKID | Microwave Kinetic Inductance Detectors |
| NG-VNC | Next Generation Visible Nulling Coronagraph |
| NICMOS | Near-Infrared Camera and Multi-Object Spectrometer |
| NWNH | New Worlds, New Horizons (2010 Astronomy and Astrophysics Decadal Survey) |
| PIAACMC | Phase-Induced Amplitude Apodization Complex Mask Coronagraph |
| PMN | Lead Magnesium Niobate |
| PSF | Point Spread Function |
| QE | Quantum Efficiency |
| ROSES | Research Opportunities in Space and Earth Sciences |
| SBIR | Small Business Innovation Research |
| SIM | Space Interferometry Mission |
| SLS | Space Launch System |
| SOA | State of Art |

| | |
|--------|---|
| SP | Shaped Pupil |
| SPLC | Shaped Pupil Lyot Coronagraph |
| STScI | Space Telescope Science Institute |
| TCOP | Technology Development for the Cosmic Origins Program |
| TDEM | Technology Development for Exoplanet Missions |
| ULE | Ultra-Low Expansion |
| VNC | Visible Nulling Coronagraph |
| WFC | Wavefront Control |
| WFIRST | Wide-Field Infrared Survey Telescope |
| WFSC | Wavefront Sensing and Control |

K REFERENCES

- ¹ 2014 NASA Strategic Plan, http://www.nasa.gov/sites/default/files/files/FY2014_NASA_SP_508c.pdf.
- ² NASA 2014 Science Plan, http://science.nasa.gov/media/medialibrary/2014/05/02/2014_Science_Plan-0501_tagged.pdf.
- ³ 2014 update to the Astrophysics Implementation Plan, http://science.nasa.gov/media/medialibrary/2015/01/16/ImpPlan_Rev2_15Apr2013_LL_150107TAGGED.pdf
- ⁴ National Research Council. *New Worlds, New Horizons in Astronomy and Astrophysics*. Washington, DC: The National Academies Press, 2010, <http://science.nasa.gov/astrophysics/special-events/astro2010-astronomy-and-astrophysics-decadal-survey/>
- ⁵ Brendan P. Crill, Nicholas Siegler, "Space technology for directly imaging and characterizing exo-Earths," Proc. SPIE 10398, UV/Optical/IR Space Telescopes and Instruments: Innovative Technologies and Concepts VIII, 103980H (5 September 2017); doi: 10.1117/12.2275697
- ⁶ National Research Council. *Review of Progress Toward the Decadal Survey Vision in New Worlds, New Horizons in Astronomy and Astrophysics*. Washington, DC: The National Academies Press, 2016, <https://www.nap.edu/catalog/23560/new-worlds-new-horizons-a-midterm-assessment>
- ⁷ 2014 update to the Astrophysics Implementation Plan, http://science.nasa.gov/media/medialibrary/2015/01/16/ImpPlan_Rev2_15Apr2013_LL_150107TAGGED.pdf
- ⁸ Exo-C and Exo-S Final Reports (2015); <https://exoplanets.nasa.gov/exep/studies/probe-scale-stdt/>
- ⁹ WFIRST Home Page: <http://wfirst.gsfc.nasa.gov/index.html>
- ¹⁰ LUVUOIR Science & Technology Definition Team LUVUOIR Study Office & Members of the LUVUOIR Technology Working Group. *LUVUOIR Decadal Mission Concept Study "O1" Deliverable: Technology Gap Assessment for the 2016 Program Office Technology Cycle*, 2016. http://asd.gsfc.nasa.gov/luvoir/docs/tech/2016-05-31-LUVUOIR-O1-Deliverable_rev3.0.pdf
- ¹¹ TDEM past awards: <https://exoplanets.nasa.gov/exep/technology/TDEM-awards/>
- ¹² NSPIRES APRA past awards: <https://nspires.nasaprs.com/external/solicitations/solicitations.do?method=closedPastIni&stack=push>
- ¹³ ExEP Technology Website; <http://exoplanets.nasa.gov/technology/>.
- ¹⁴ Lawson, P. R., Belikov, R., Cash, W., et al. 2013, "Survey of experimental results in high-contrast imaging for future exoplanet missions," Proc. SPIE 8864, 88641F, <http://spiedigitallibrary.org/proceeding.aspx?articleid=1744192&resultClick=1>.

- ¹⁵ Moody, D. C., Gordon, B. L., & Trauger, J. T. 2008, "Design and demonstration of hybrid Lyot coronagraph masks for improved spectral bandwidth and throughput," Proc. SPIE 7010, 70103P, <http://spiedigitallibrary.org/proceeding.aspx?articleid=787868&resultClick=1>
- ¹⁶ Trauger, J., Moody, D., Gordon, B., Krist, J., Mawet, D. 2011, "A hybrid Lyot Coronagraph for the direct imaging and spectroscopy of exoplanet systems," Proc. SPIE 8151, 81510G, <http://spiedigitallibrary.org/proceeding.aspx?articleid=1342401&resultClick=1>.
- ¹⁷ Trauger, J. et al, TDEM-09 Final Report: http://exoplanets.nasa.gov/files/exep/Lyot_TDEM_Report_121215_signed.pdf
- ¹⁸ Exo-C Final Report (2015); <https://exoplanets.nasa.gov/exep/studies/probe-scale-stdt/>
- ¹⁹ Eric Cady, Kunjithapatham Balasubramanian, Jessica Gersh-Range, Jeremy Kasdin, Brian Kern, Raymond Lam, Camilo Mejia Prada, Dwight Moody, Keith Patterson, Ilya Poberezhskiy, A. J. Eldorado Riggs, Byoung-Joon Seo, Fang Shi, Hong Tang, John Trauger, Hanying Zhou, Neil Zimmerman, "Shaped pupil coronagraphy for WFIRST: high-contrast broadband testbed demonstration," Proc. SPIE 10400, Techniques and Instrumentation for Detection of Exoplanets VIII, 104000E (1 September 2017);
- ²⁰ Byoung-Joon Seo, Eric Cady, Brian Gordon, Brian Kern, Raymond Lam, David Marx, Dwight Moody, Richard Muller, Keith Patterson, Ilya Poberezhskiy, Camilo Mejia Prada, Erkin Sidick, Fang Shi, John Trauger, Daniel Wilson, "Hybrid Lyot coronagraph for WFIRST: high-contrast broadband testbed demonstration," Proc. SPIE 10400, Techniques and Instrumentation for Detection of Exoplanets VIII, 104000F (1 September 2017);
- ²¹ Prabal Saxena, Maxime J. Rizzo, Camilo Mejia Prada, Jorge Llop Sayson, Qian Gong, Eric J. Cady, Avi M. Mandell, Tyler D. Groff, Michael W. McElwain, "Commissioning and performance results of the WFIRST/PISCES integral field spectrograph," Proc. SPIE 10400, Techniques and Instrumentation for Detection of Exoplanets VIII, 104001P (1 September 2017);
- ²² <https://exoplanets.nasa.gov/exep/technology/TDEM-awards/>
- ²³ Breckinridge, J. and Chipman, R. TDEM-15 Abstract: https://exoplanets.nasa.gov/system/internal_resources/details/original/355_Abstract_TDEM15_.pdf
- ²⁴ Breckinridge, J., W. Lam, and R. Chipman, 2015, "Polarization Aberrations in Astronomical Telescopes: The Point Spread Function". Publications of the Astronomical Society of the Pacific, 127: 445-468. <http://dx.doi.org/10.1086/681280>
- ²⁵ Krist, J., B. Nemati, and B. Mennesson, 2016, "Numerical modeling of the proposed WFIRST-AFTA coronagraphs and their predicted performances," J. Astron. Telesc. Instrum. Syst. 2016; 2 (1): 011003, <http://astronomicaltelescopes.spiedigitallibrary.org/article.aspx?articleid=2468019>.
- ²⁶ Pueyo, L, and Norman, C. 2013, "High-contrast Imaging with an Arbitrary Aperture: Active Compensation of Aperture Discontinuities ", ApJ 769, 102, <http://adsabs.harvard.edu/cgi-bin/nph->

[data_query?bibcode=2013ApJ...769..102P&db_key=AST&link_type=ABSTRACT&high=5697e4cafa22878](https://ui.adsabs.harvard.edu/abs/2013ApJ...769..102P&db_key=AST&link_type=ABSTRACT&high=5697e4cafa22878)

- ²⁷ John Trauger; Dwight Moody; John Krist; Brian Gordon, *J. Astron. Telesc. Instrum. Syst.* 2016; 2(1):011013. doi: 10.1117/1.JATIS.2.1.011013
- ²⁸ Clampin, M., et al, 2013, TDEM-9 Technology Milestone #1 Final Report, "Visible Nulling Coronagraph Technology Maturation: High Contrast Imaging and Characterization of Exoplanets", Jet Propulsion Laboratory Doc. D-68671, http://exoplanets.nasa.gov/technology/Clampin_Report_FINAL.pdf
- ²⁹ Cook, T., Cahoy, K., Chakrabarti, S., Douglas, E., Finn, S. C., Kuchner, M. J., et al. (2015). Planetary Imaging Concept Testbed Using a Recoverable Experiment–Coronagraph (PICTURE C). *Journal of Astronomical Telescopes, Instruments, and Systems*, 1(4), 044001. <http://doi.org/10.1117/1.JATIS.1.4.044001>
- ³⁰ <http://hicibas.copl.ulaval.ca/>
- ³¹ Douglas, E. S., Allan, G., Barnes, D., Figura, J. S., Haughwout, C. A., Gubner, J. N., et al. (2017). Design of the deformable mirror demonstration CubeSat (DeMi). In S. Shaklan (Ed.), *Techniques and Instrumentation for Detection of Exoplanets VIII* (Vol. 10400, p. 1040013). International Society for Optics and Photonics. <http://doi.org/10.1117/12.2274430>
- ³² Soummer, R., et al., 2014, "Five Debris Disks Newly Revealed in Scattered Light from the Hubble Space Telescope NICMOS Archive," *The Astrophysical Journal Letters* 786 (23S), http://adsabs.harvard.edu/cgi-bin/nph-data_query?bibcode=2014ApJ...786L..23S&db_key=AST&link_type=ABSTRACT&high=5697e4cafa04593
- ³³ Menesson, D., 2015, "AFTA coronagraph performance feedback from post-processing studies to overall design," *Proc. SPIE* 9605, <http://spiedigitallibrary.org/proceeding.aspx?articleid=2443259&resultClick=1>
- ³⁴ Ygouf, M., et al., 2015, "Data processing and algorithm development for the WFIRST-AFTA coronagraph: reduction of noise free simulated images, analysis and spectrum extraction with reference star differential imaging" *Proc. SPIE* 9605 9605 0S, <http://spiedigitallibrary.org/proceeding.aspx?articleid=2443266&resultClick=1>
- ³⁵ Paul A. Lightsey, J. Scott Knight, Lee D. Feinberg, Matthew R. Bolcar, Stuart B. Shaklan, "First-order error budgeting for LUVOIR mission," *Proc. SPIE* 10398, *UV/Optical/IR Space Telescopes and Instruments: Innovative Technologies and Concepts VIII*, 103980C (5 September 2017);
- ³⁶ J. Brent Knight, H. Philip Stahl, Andy Singleton, Ron Hunt, Melissa Therrell, Kate Caldwell, Jay Garcia, Mike Baysinger, "Dynamic/jitter assessment of multiple potential HabEx structural designs," *Proc. SPIE* 10374, *Optical Modeling and Performance Predictions IX*, 1037402 (6 September 2017);
- ³⁷ Lee Feinberg, Matthew Bolcar, Scott Knight, David Redding, "Ultra-stable segmented telescope sensing and control architecture," *Proc. SPIE* 10398, *UV/Optical/IR Space*

- Telescopes and Instruments: Innovative Technologies and Concepts VIII, 103980E (5 September 2017);
- ³⁸ Sang C. Park, Michael J. Eisenhower, Marcel Bluth, Matthew R. Bolcar, Lee D. Feinberg, J. Scott Knight, David C. Redding, "LUVOIR backplane thermal architecture development through the composite CTE sensitivity study," Proc. SPIE 10398, UV/Optical/IR Space Telescopes and Instruments: Innovative Technologies and Concepts VIII, 103980D (5 September 2017);
- ³⁹ <https://nspires.nasaprs.com/external/viewrepositorydocument/cmdocumentid=602546/solicitationId=%7B7537A31C-AA12-E8D0-F3CF-2BD999B21B0A%7D/viewSolicitationDocument=1/D.15%20SLSTD%20Amend%2050.pdf>
- ⁴⁰ Fang Shi, Eric Cady, Byoung-Joon Seo, Xin An, Kunjithapatham Balasubramanian, Brian Kern, Raymond Lam, David Marx, Dwight Moody, Camilo Mejia Prada, Keith Patterson, Ilya Poberezhskiy, Joel Shields, Erkin Sidick, Hong Tang, John Trauger, Tuan Truong, Victor White, Daniel Wilson, Hanying Zhou, "Dynamic testbed demonstration of WFIRST coronagraph low order wavefront sensing and control (LOWFS/C)," Proc. SPIE 10400, Techniques and Instrumentation for Detection of Exoplanets VIII, 104000D (1 September 2017);
- ⁴¹ Belikov, R., Bendek, E., Pluzhnik, E., Sirbu, D., Thomas, S.J., 2016, "High contrast imaging in multi-star systems: technology development and first lab results," Proc SPIE 9904. <http://proceedings.spiedigitallibrary.org/proceeding.aspx?articleid=2541995>
- ⁴² E. Douglas, A. Carlton, J. Clark, O. Guyon, J. Lumbres, J. Males, W. Marlow, & K. Cahoy "Laser Guide Star for Large Segmented Aperture Space Telescopes, Part I: Implications for Observatory Stability." In-prep.
- ⁴³ Lee Feinberg, Matthew Bolcar, Scott Knight, David Redding, "Ultra-stable segmented telescope sensing and control architecture," Proc. SPIE 10398, UV/Optical/IR Space Telescopes and Instruments: Innovative Technologies and Concepts VIII, 103980E (5 September 2017);
- ⁴⁴ Albanese, M., et al. 2006, "Verification of the James Webb Space Telescope coarse phase sensor using the Keck Telescope," Proc. SPIE 6265 05, <http://spiedigitallibrary.org/proceeding.aspx?articleid=1326681&resultClick=1>
- ⁴⁵ Lee Feinberg, Matthew Bolcar, Scott Knight, David Redding, "Ultra-stable segmented telescope sensing and control architecture," Proc. SPIE 10398, UV/Optical/IR Space Telescopes and Instruments: Innovative Technologies and Concepts VIII, 103980E (5 September 2017);
- ⁴⁶ Bijan Nemati, Mark T. Stahl, H. Philip Stahl, Stuart B. Shaklan, "The effects of space telescope primary mirror segment errors on coronagraph instrument performance," Proc. SPIE 10398, UV/Optical/IR Space Telescopes and Instruments: Innovative Technologies and Concepts VIII, 103980G (5 September 2017);
- ⁴⁷ Joel A. Nissen, Alireza Azizi, Feng Zhao, Shannon Kian G. Zareh, Shanti R. Rao, Jeffrey B. Jewell, Dustin Moore, "Laser metrology for ultra-stable space-based coronagraphs," Proc.

- SPIE 10398, UV/Optical/IR Space Telescopes and Instruments: Innovative Technologies and Concepts VIII, 103980I (5 September 2017); doi: 10.1117/12.2274704
- ⁴⁸ Stahl, H. P., Postman, M., Smith, W. S. 2013, "Engineering specifications for large aperture UVO space telescopes derived from science requirements," Proc. SPIE 8860, <http://spiedigitallibrary.org/proceeding.aspx?articleid=1762023&resultClick=1>
- ⁴⁹ Stahl, M. T., Shaklan, S. B., Stahl, H. P. 2015, "Preliminary Analysis of effect of random segment errors on coronagraph performance," Proc SPIE 9605 OP, <http://spiedigitallibrary.org/proceeding.aspx?articleid=2446862&resultClick=1>
- ⁵⁰ Stahl, H. P., Postman, M., Smith, W. S. 2013, "Engineering specifications for large aperture UVO space telescopes derived from science requirements," Proc. SPIE 8860 06, <http://spiedigitallibrary.org/proceeding.aspx?articleid=1762023&resultClick=1>
- ⁵¹ Feinberg, L.D., et al. 2009, "Large segmented UV-optical space telescope using a Hybrid Sensor Active Control (HSAC) architecture," Proc. SPIE 7436 08, <http://spiedigitallibrary.org/proceeding.aspx?articleid=785987&resultClick=1>
- ⁵² Gonzales, M. A., et al., "Unprecedented Vibration isolation Demonstration using the Disturbance Free Payload Concept," AIAA 2004-5247, (2004), <http://arc.aiaa.org/doi/pdf/10.2514/6.2004-5247>
- ⁵³ Larry D. Dewell, Kiarash Tajdaran, Raymond M. Bell, Kuo-Chia Liu, Matthew R. Bolcar, Lia W. Sacks, Julie A. Crooke, Carl Blaurock, "Dynamic stability with the disturbance-free payload architecture as applied to the Large UV/Optical/Infrared (LUVOIR) Mission," Proc. SPIE 10398, UV/Optical/IR Space Telescopes and Instruments: Innovative Technologies and Concepts VIII, 103980B (5 September 2017).
- ⁵⁴ Chris Stark et al. 2015, "Lower Limits on Aperture Size for an ExoEarth Detecting Coronagraphic Mission", ApJ 808 149S, <http://adsabs.harvard.edu/abs/2015ApJ...808..149S>
- ⁵⁵ Rafanelli, G. L., Cosner, C. M., Spencer, S. B., Wolfe, D., Newman, A., Polidan, R., & Chakrabarti, S. (2017). Revolutionary astrophysics using an incoherent synthetic optical aperture. In *UV/Optical/IR Space Telescopes and Instruments: Innovative Technologies and Concepts VIII* (Vol. 10398, p. 103980P). International Society for Optics and Photonics. <http://doi.org/10.1117/12.2272782>
- ⁵⁶ H. Philip Stahl, "Habitable exoplanet imager optical telescope concept design," Proc. SPIE 10398, UV/Optical/IR Space Telescopes and Instruments: Innovative Technologies and Concepts VIII, 1039806 (5 September 2017);
- ⁵⁷ J. Brent Knight, H. Philip Stahl, Andy Singleton, Ron Hunt, Melissa Therrell, Kate Caldwell, Jay Garcia, Mike Baysinger, "Dynamic/jitter assessment of multiple potential HabEx structural designs," Proc. SPIE 10374, Optical Modeling and Performance Predictions IX, 1037402 (6 September 2017);
- ⁵⁸ Stahl, H. P., Postman, M., Smith, W. S. 2013, "Engineering specifications for large aperture UVO space telescopes derived from science requirements," Proc. SPIE 8860 06, <http://spiedigitallibrary.org/proceeding.aspx?articleid=1762023&resultClick=1>

- ⁵⁹ Davis, J. M., Stahl, P. H., Arnold, W. R., & Smith, W. S. (2017). HabEx primary mirror trade studies. In D. M. Stubbs & A. E. Hatheway (Eds.), *Optomechanical Engineering 2017* (Vol. 10371, p. 103710B). International Society for Optics and Photonics.
<http://doi.org/10.1117/12.2274476>
- ⁶⁰ Brooks, T. E. (2017). Predictive thermal control applied to HabEx. In *UV/Optical/IR Space Telescopes and Instruments: Innovative Technologies and Concepts VIII* (Vol. 10398, p. 1039814). International Society for Optics and Photonics.
<http://doi.org/10.1117/12.2274338>
- ⁶¹ Postman, M., et al., 2009, "Advanced Technology Large-Aperture Space Telescope (ATLAST): A Technology Roadmap for the Next Decade,"
http://www.stsci.edu/institute/atlast/documents/ATLAST_NASA_ASMCS_Public_Report.pdf
- ⁶² Dalcanton, J. and Seager, S., et al. [From Cosmic Birth to Living Earths], Association for Universities for Research in Astronomy, Washington, DC, (2015).
- ⁶³ <https://ntrs.nasa.gov/archive/nasa/casi.ntrs.nasa.gov/20160013273.pdf>
- ⁶⁴ Eisenhower, M. J., Cohen, L. M., Feinberg, L. D., Matthews, G. W., Nissen, J. A., Park, S. C., & Peabody, H. L. (2015). ATLAST ULE mirror segment performance analytical predictions based on thermally induced distortions. In H. A. MacEwen & J. B. Breckinridge (Eds.), *UV/Optical/IR Space Telescopes and Instruments: Innovative Technologies and Concepts VII* (Vol. 9602, p. 96020A). International Society for Optics and Photonics.
<http://doi.org/10.1117/12.2188008>
- ⁶⁵ Roming et al. 2005, "The SWIFT Ultra-violet and Optical Telescope", *Space Science Reviews* (2005) 120: 95–142, <https://link.springer.com/content/pdf/10.1007/s11214-005-5095-4.pdf>
- ⁶⁶ Tiffenberg et al. 2017, "Single-Electron and Single-Photon Sensitivity with a Silicon Skipper CCD" *Phys. Rev. Lett* 199, 131082,
<https://journals.aps.org/prl/abstract/10.1103/PhysRevLett.119.131802>
- ⁶⁷ E. Fossum, "The Quanta Image Sensor (QIS): Concepts and Challenges," in *Imaging and Applied Optics*, OSA Technical Digest (CD) (Optical Society of America, 2011), paper JTUE1.
- ⁶⁸ S. M. Baggett, J. Anderson, M. Sosey, C. Gosmeyer, M. Bourque, V. Bajaj, H. Khandrika, C. Martlin, "HST/WFC3: understanding and mitigating radiation damage effects in the CCD detectors," *Proc. SPIE 9904, Space Telescopes and Instrumentation 2016: Optical, Infrared, and Millimeter Wave*, 99045D (29 July 2016);
- ⁶⁹ Private communications with Bernie Rauscher (December 2015)
- ⁷⁰ Rauscher, B. et al. 2015, "ATLAST detector needs for direct spectroscopic biosignature characterization in the visible and near-IR", *SPIE 9602, 96020D*,
<http://spiedigitallibrary.org/proceeding.aspx?articleid=2444184&resultClick=1>
- ⁷¹ Atkinson, D., Hall, D., Baranec, C., Baker, I., Jacobson, S., and Riddle, R., 2014, "Observatory deployment and characterization of SAPHIRA HgCdTe APD arrays," *SPIE 9154, 915419*,
<http://spiedigitallibrary.org/proceeding.aspx?articleid=1891378&resultClick=1>

- ⁷² Mazin, B. A., et al., "A superconducting focal plane array for ultraviolet, optical, and near-infrared astrophysics," *Opt. Express* 20, 1503-1511 (2012), <http://arxiv.org/pdf/1112.0004v1.pdf>
- ⁷³ Allman, M. S., Verma, V. B., Stevens, M., Gerrits, T., Horansky, R. D., Lita, A. E., et al. (2015). A near-infrared 64-pixel superconducting nanowire single photon detector array with integrated multiplexed readout. *Applied Physics Letters*, 106(19), 192601. <http://doi.org/10.1063/1.4921318>
- ⁷⁴ Rauscher, B., et al., 2015, "ATLAST detector needs for direct spectroscopic biosignature characterization in the visible and near-IR", SPIE 9602, 96020D, <http://spiedigitallibrary.org/proceeding.aspx?articleid=2444184&resultClick=1>
- ⁷⁵ Rauscher, B. et al. 2015, "ATLAST detector needs for direct spectroscopic biosignature characterization in the visible and near-IR", SPIE 9602, 96020D, <http://spiedigitallibrary.org/proceeding.aspx?articleid=2444184&resultClick=1>
- ⁷⁶ Private communications with Bernie Rauscher (December 2015)
- ⁷⁷ Shaklan, S. B., Noecker, M. C., Glassman, T., et al. 2010, "Error budgeting and tolerancing of starshades for exoplanet detection," *Proc. SPIE* 7731, 77312G, <http://spiedigitallibrary.org/proceeding.aspx?articleid=749972&resultClick=1>
- ⁷⁸ Shaklan, S. B., Marchen, L., Lisman, P. D., et al. 2011, "A starshade petal error budget for exo-earth detection and characterization," *Proc. SPIE* 8151, 815113, <http://spiedigitallibrary.org/proceeding.aspx?articleid=1268343&resultClick=1>
- ⁷⁹ Exo-S Final Report, <https://exoplanets.nasa.gov/exep/studies/probe-scale-stdt/>
- ⁸⁰ Manan Arya, David Webb, James McGown, P. Douglas Lisman, Stuart Shaklan, S. Case Bradford, John Steeves, Evan Hilgemann, Brian Trease, Mark Thomson, Steve Warwick, Gregg Freebury, Jamie Gull, "Starshade mechanical design for the Habitable Exoplanet imaging mission concept (HabEx)," *Proc. SPIE* 10400, Techniques and Instrumentation for Detection of Exoplanets VIII, 104001C (12 September 2017);
- ⁸¹ Martin, S. R., Shaklan, S. B., Crawford, S. L., et al. 2013, "Starshade optical edge modelling, requirements, and laboratory tests," *Proc. SPIE* 8864, 88641A, <http://spiedigitallibrary.org/proceeding.aspx?articleid=1744188&resultClick=1>
- ⁸² Casement et al., TDEM-12 Whitepaper "Starshade Stray Light Mitigation through Edge Scatter Modeling and Sharp-Edge Materials Development"; http://exoplanets.nasa.gov/technology/casement_whitepaper.pdf
- ⁸³ Steeves, J.S., Martin, S. R., et. al. 2016, "Precision optical edges for a starshade external occulter", *Proc. SPIE* 9912, 99122O, <http://proceedings.spiedigitallibrary.org/proceeding.aspx?articleid=2538386>
- ⁸⁴ Schindhelm, E., Shipley, A., Oakley, P., et al. 2007, "Laboratory studies of petal-shaped occulter" *Proc. SPIE* 6693, 669305, <http://spiedigitallibrary.org/proceeding.aspx?articleid=817922&resultClick=1>

- ⁸⁵ Leviton, D. B., Cash, W. C., Gleason, B., et al. 2007, "White-light demonstration of one hundred parts per billion irradiance suppression in air by new starshade occulters." Proc. SPIE 6687 66871B,
<http://spiedigitallibrary.org/proceeding.aspx?articleid=817377&resultClick=1>
- ⁸⁶ Lo, A. S., Glassman, T., Dailey, D., Sterk, K., Green, J., Cash, W., Soummer, R. 2010, "New Worlds Probe," Proc. SPIE 7731, 77312E,
<http://spiedigitallibrary.org/proceeding.aspx?articleid=749969&resultClick=1>
- ⁸⁷ Samuele, R., Varshneya, R., Johnson, T. P., et al. 2010, "Progress at the starshade testbed at Northrop Grumman Aerospace Systems: comparisons with computer simulations," Proc. SPIE 7731, 773151,
<http://spiedigitallibrary.org/proceeding.aspx?articleid=750104&resultClick=1>
- ⁸⁸ Cady, E. et al. 2010, "Broadband suppression and occulter position sensing at the Princeton occulter testbed." Proc. SPIE 7731, 77312F,
<http://spiedigitallibrary.org/proceeding.aspx?articleid=749970&resultClick=1>
- ⁸⁹ Sirbu, D., Kasdin, N. J., Vanderbei, R. J., 2013, "Progress on optical verification for occulter-based high contrast imaging," Proc. SPIE 8864, 886419,
<http://spiedigitallibrary.org/proceeding.aspx?articleid=1744187&resultClick=1>
- ⁹⁰ Glassman, T. et al., TDEM-12 Final Report, "Demonstration of Starshade Starlight-Suppression Performance in the Field";
http://exoplanets.nasa.gov/files/exep/GlassmanTDEM2012_FinalReport.pdf
- ⁹¹ Yunjong Kim, Anthony Harness, Dan Sirbu, Mengya Hu, Mike Galvin, N. Jeremy Kasdin, Robert J. Vanderbei, Stuart B. Shaklan, "Optical demonstration of a starshade at flight Fresnel numbers ," Proc. SPIE 10400, Techniques and Instrumentation for Detection of Exoplanets VIII, 104001A (1 September 2017);
- ⁹² Anthony Harness, Stuart Shaklan, Philip Dumont, Yunjong Kim, N. Jeremy Kasdin, "Modeling and performance predictions for the Princeton Starshade Testbed," Proc. SPIE 10400, Techniques and Instrumentation for Detection of Exoplanets VIII, 1040019 (1 September 2017);
- ⁹³ Yunjong Kim, Anthony Harness, Dan Sirbu, Mengya Hu, Mike Galvin, N. Jeremy Kasdin, Robert J. Vanderbei, Stuart B. Shaklan, "Optical demonstration of a starshade at flight Fresnel numbers ," Proc. SPIE 10400, Techniques and Instrumentation for Detection of Exoplanets VIII, 104001A (1 September 2017);
- ⁹⁴ Anthony Harness, Stuart Shaklan, Philip Dumont, Yunjong Kim, N. Jeremy Kasdin, "Modeling and performance predictions for the Princeton Starshade Testbed," Proc. SPIE 10400, Techniques and Instrumentation for Detection of Exoplanets VIII, 1040019 (1 September 2017);
- ⁹⁵ Seager, S., et al., 2015, "Exo-S: starshade probe-class exoplanet direct imaging mission concept, Final Report," https://exoplanets.nasa.gov/exep/stdt/Exo-S_Starshade_Probe_Class_Final_Report_150312_URS250118.pdf

- ⁹⁶ Cash, W., Kendrick, S., Noecker, et al., 2009, "The New Worlds Observer: the astrophysics strategic mission concept study," Proc. SPIE 7436, <http://spiedigitallibrary.org/proceeding.aspx?articleid=785984&resultClick=1>
- ⁹⁷ N.J. Kasdin et al., 2009, "Occulter design for THEIA," Proc. SPIE 7440, <http://proceedings.spiedigitallibrary.org/proceeding.aspx?articleid=786370>
- ⁹⁸ D.P.Scharf,S.R.Martin,C.C.Liebe,Z.H.Rahman,C.R.Seubert,M.C.Noecker,andG.H.Purcell,"Pre- cision formation flying at megameter separations for exoplanet characterization," Acta Astronautica 123, pp. 420–434, June 2016.
- ⁹⁹ Exo-S Final Report, <https://exoplanets.nasa.gov/exep/studies/probe-scale-stdt/>
- ¹⁰⁰ Michael Bottom, Stefan Martin, Carl Seubert, Eric Cady, Shannon Kian Zareh, Stuart Shaklan, "Precise starshade stationkeeping and pointing with a Zernike wavefront sensor," Proc. SPIE 10400, Techniques and Instrumentation for Detection of Exoplanets VIII, 104001B (1 September 2017);
- ¹⁰¹ *ibid*
- ¹⁰² Exo-S Final Report, <https://exoplanets.nasa.gov/exep/studies/probe-scale-stdt/>
- ¹⁰³ Cash, W., Kendrick, S., Noecker, et al., 2009, "The New Worlds Observer: the astrophysics strategic mission concept study," Proc. SPIE 7436. <http://spiedigitallibrary.org/proceeding.aspx?articleid=785984&resultClick=1>
- ¹⁰⁴ Stuart B. Shaklan, Luis Marchen, Eric Cady, "Shape accuracy requirements on starshades for large and small apertures," Proc. SPIE 10400, Techniques and Instrumentation for Detection of Exoplanets VIII, 104001T (1 September 2017); doi: 10.1117/12.2273436
- ¹⁰⁵ Manan Arya, David Webb, James McGown, P. Douglas Lisman, Stuart Shaklan, S. Case Bradford, John Steeves, Evan Hilgemann, Brian Trease, Mark Thomson, Steve Warwick, Gregg Freebury, Jamie Gull, "Starshade mechanical design for the Habitable Exoplanet imaging mission concept (HabEx)," Proc. SPIE 10400, Techniques and Instrumentation for Detection of Exoplanets VIII, 104001C (12 September 2017);
- ¹⁰⁶ <http://asd.gsfc.nasa.gov/firs/>
- ¹⁰⁷ Males, J. R., Close, L. M., Guyon, O., Morzinski, K., Puglisi, A., Hinz, P., et al. (2014). Direct imaging of exoplanets in the habitable zone with adaptive optics. In E. Marchetti, L. M. Close, & J.-P. Véran (Eds.), *Adaptive Optics Systems IV* (Vol. 9148, p. 914820). International Society for Optics and Photonics. <http://doi.org/10.1117/12.2057135>
- ¹⁰⁸ ESO news release 9 January 2017 "ESO Signs Agreement with Breakthrough Initiatives" <https://www.eso.org/public/usa/news/eso1702/>
- ¹⁰⁹ Enya, K., Abe, L., Haze, K., Tanaka, S., Nakagawa, T., Kataza, H., et al. (2008). Mid-infrared coronagraph for SPICA. In J. M. Oschmann Jr, M. W. M. de Graauw, & H. A. MacEwen (Eds.), *Space Telescopes and Instrumentation 2008: Optical, Infrared, and Millimeter* (Vol. 7010, p. 70102Z). International Society for Optics and Photonics. <http://doi.org/10.1117/12.788509>
- ¹¹⁰ Boccaletti, A., et al., 2015, "The Mid-Infrared Instrument for the James Webb Space Telescope, V: Predicted Performance of the MIRI Coronagraphs," Publications of the

Astronomical Society of the Pacific Vol 127, 953,
<http://iopscience.iop.org/article/10.1086/682256>

- ¹¹¹ Enya, K., Abe, L., Haze, K., Tanaka, S., Nakagawa, T., Kataza, H., et al. (2008). Mid-infrared coronagraph for SPICA. In J. M. Oschmann Jr, M. W. M. de Graauw, & H. A. MacEwen (Eds.), *Space Telescopes and Instrumentation 2008: Optical, Infrared, and Millimeter* (Vol. 7010, p. 70102Z). International Society for Optics and Photonics. <http://doi.org/10.1117/12.788509>
- ¹¹² Rieke, G. H., Ressler, M. E., Morrison, J. E., Bergeron, L., Bouchet, P., García-Marín, M., et al. (2015). The Mid-Infrared Instrument for the James Webb Space Telescope, VII: The MIRI Detectors. *Publications of the Astronomical Society of the Pacific*, 127(953), 665–674. <http://doi.org/10.1086/682257>
- ¹¹³ Robinson, T., et al., 2014, “Detection of Ocean Glint and Ozone Absorption using LCROSS Earth Observations”, *ApJ* 787: 171. <http://dx.doi.org/10.1088/0004-637X/787/2/171>
- ¹¹⁴ Hennessy, J., et al., 2016, “Performance and prospects of far ultraviolet aluminum mirrors protected by atomic layer deposition” *J. Astron. Telesc. Instrum. Syst.* 2(4), 041206 (Jun 07, 2016). doi:10.1117/1.JATIS.2.4.041206
<http://astronomicaltelescopes.spiedigitallibrary.org/article.aspx?articleid=2528070>
- ¹¹⁵ Quijada, M. A., Del Hoyo, J., Boris, D. R., & Walton, S. G. (2017). Improved mirror coatings for use in the Lyman Ultraviolet to enhance astronomical instrument capabilities. In H. A. MacEwen & J. B. Breckinridge (Eds.), *UV/Optical/IR Space Telescopes and Instruments: Innovative Technologies and Concepts VIII* (Vol. 10398, p. 103980Z). International Society for Optics and Photonics. <http://doi.org/10.1117/12.2274790>
- ¹¹⁶ Lightsey, P. A., Atkinson, C. B., Clampin, M. C., & Feinberg, L. D. (2012). James Webb Space Telescope: large deployable cryogenic telescope in space. *Optical Engineering*, 51(1), 011003. <http://doi.org/10.1117/1.OE.51.1.011003>
- ¹¹⁷ Lightsey, P. A., Gallagher, B. B., Nickles, N., & Copp, T. (2012). Optical transmission for the James Webb Space Telescope. In M. C. Clampin, G. G. Fazio, H. A. MacEwen, & J. M. Oschmann (Eds.), *Space Telescopes and Instrumentation 2012: Optical, Infrared, and Millimeter Wave* (Vol. 8442, p. 84423A). International Society for Optics and Photonics. <http://doi.org/10.1117/12.924841>
- ¹¹⁸ Balasubramanian, K., Hennessy, J., Raouf, N., Nikzad, S., Del Hoyo, J., & Quijada, M. (2017). Mirror coatings for large aperture UV optical infrared telescope optics. In H. A. MacEwen & J. B. Breckinridge (Eds.), *UV/Optical/IR Space Telescopes and Instruments: Innovative Technologies and Concepts VIII* (Vol. 10398, p. 103980X). International Society for Optics and Photonics. <http://doi.org/10.1117/12.2274794>
- ¹¹⁹ Balasubramanian, K., Shaklan, S., Give'on, A., Cady, E., & Marchen, L. (2011). Deep UV to NIR space telescopes and exoplanet coronagraphs: a trade study on throughput, polarization, mirror coating options and requirements. In S. Shaklan (Ed.), (Vol. 8151, pp. 81511G–14). Presented at the SPIE Optical Engineering + Applications, SPIE. <http://doi.org/10.1117/12.902440>

- ¹²⁰ Hubble Space Telescope Optical Telescope Assembly Handbook version 1.0 May 1990, NASA-CR-189.751, Space Telescope Science Institute (1990)
- ¹²¹ Robinson, T., et al., 2014, "Detection of Ocean Glint and Ozone Absorption using LCROSS Earth Observations", *ApJ* 787: 171. <http://dx.doi.org/10.1088/0004-637X/787/2/171>
- ¹²² Bolcar, M., et al., 2016, "Technology Gap Assessment for a Future Large-aperture Ultraviolet-Optical-Infrared Space Telescope," *J. Astron. Telesc. Instrum. Syst.* 2(4), 041209. doi:10.1117/1.JATIS.2.4.041209
<http://astronomicaltelescopes.spiedigitallibrary.org/article.aspx>
- ¹²³ O. H. W. Siegmund, C. Ertley, J. V. Vallerga, E. R. Schindhelm, A. Harwit, B. T. Fleming, K. C. France, J. C. Green, S. R. McCandliss, W. M. Harris, "Microchannel plate detector technology potential for LUVOIR and HabEx," *Proc. SPIE 10397, UV, X-Ray, and Gamma-Ray Space Instrumentation for Astronomy XX*, 1039711 (29 August 2017); doi: 10.1117/12.2274281
- ¹²⁴ Pueyo, L., Zimmerman, N., Bolcar, M., Groff, T., Stark, C., Ruane, G., et al. (2017). The LUVOIR architecture "A" coronagraph instrument. In H. A. MacEwen & J. B. Breckinridge (Eds.), *UV/Optical/IR Space Telescopes and Instruments: Innovative Technologies and Concepts VIII* (Vol. 10398, p. 103980F). International Society for Optics and Photonics.
<http://doi.org/10.1117/12.2274654>
- ¹²⁵ Anglada-Escudé, G., Amado, P. J., Barnes, J., Berdiñas, Z. M., Butler, R. P., Coleman, G. A. L., et al. (2016). A terrestrial planet candidate in a temperate orbit around Proxima Centauri. *Nature*, 536(7617), 437–440. <http://doi.org/10.1038/nature19106>
- ¹²⁶ Fischer, D. A., Anglada-Escudé, G., Arriagada, P., Baluev, R. V., Bean, J. L., Bouchy, F., et al. (2016). State of the Field: Extreme Precision Radial Velocities*. *Publications of the Astronomical Society of the Pacific*, 128(964), 066001. <http://doi.org/10.1088/1538-3873/128/964/066001>
- ¹²⁷ Plavchan, P., et al., 2015, "Radial Velocity Prospects Current and Future: A White Paper Report prepared by the Study Analysis Group 8 for the Exoplanet Program Analysis Group (ExoPAG)" <https://arxiv.org/abs/1503.01770>
- ¹²⁸ Schwab, C., et al, 2016, "Design of NEID, an extreme precision Doppler spectrograph for WIYN", *Proc. SPIE 9908, Ground-based and Airborne Instrumentation for Astronomy VI*, 99087H (August 9, 2016); doi:10.1117/12.2234411 <http://proceedings.spiedigitallibrary.org/proceeding.aspx?articleid=2544294>
- ¹²⁹ Crepp, J, et al, 2016, "iLocater: A Diffraction-limited Doppler Spectrometer for the Large Binocular Telescope", *Proc. SPIE 9908, Ground-based and Airborne Instrumentation for Astronomy VI*, 990819 (4 August 2016); doi:10.1117/12.2233135, <http://proceedings.spiedigitallibrary.org/proceeding.aspx?articleid=2543021>
- ¹³⁰ Plavchan, P., et al., 2015, "Radial Velocity Prospects Current and Future: A White Paper Report prepared by the Study Analysis Group 8 for the Exoplanet Program Analysis Group (ExoPAG)" <https://arxiv.org/abs/1503.01770>
- ¹³¹ Fischer, D. A., Anglada-Escudé, G., Arriagada, P., Baluev, R. V., Bean, J. L., Bouchy, F., et al. (2016). State of the Field: Extreme Precision Radial Velocities*. *Publications of the Astronomical Society of the Pacific*, 128(964), 066001. <http://doi.org/10.1088/1538-3873/128/964/066001>

- ¹³² Plavchan, P., et al., 2015, “Radial Velocity Prospects Current and Future: A White Paper Report prepared by the Study Analysis Group 8 for the Exoplanet Program Analysis Group (ExoPAG)” <https://arxiv.org/abs/1503.01770>
- ¹³³ Halverson, S., Terrien, R., Mahadevan, S., Roy, A., Bender, C., Stefánsson, G. K., et al. (2016). A comprehensive radial velocity error budget for next generation Doppler spectrometers. In C. J. Evans, L. Simard, & H. Takami (Eds.), *Ground-based and Airborne Instrumentation for Astronomy VI* (Vol. 9908, p. 99086P). International Society for Optics and Photonics. <http://doi.org/10.1117/12.2232761>
- ¹³⁴ Plavchan, P., et al., 2015, “Radial Velocity Prospects Current and Future: A White Paper Report prepared by the Study Analysis Group 8 for the Exoplanet Program Analysis Group (ExoPAG)” <https://arxiv.org/abs/1503.01770>
- ¹³⁵ Schwab, C., et al, 2016, “Design of NEID, an extreme precision Doppler spectrograph for WIYN”, Proc. SPIE 9908, Ground-based and Airborne Instrumentation for Astronomy VI, 99087H (August 9, 2016); doi:10.1117/12.2234411
<http://proceedings.spiedigitallibrary.org/proceeding.aspx?articleid=2544294>
- ¹³⁶ Crepp, J, et al, 2016, “iLocater: A Diffraction-limited Doppler Spectrometer for the Large Binocular Telescope”, Proc. SPIE 9908, Ground-based and Airborne Instrumentation for Astronomy VI, 990819 (4 August 2016); doi:10.1117/12.2233135,
<http://proceedings.spiedigitallibrary.org/proceeding.aspx?articleid=2543021>
- ¹³⁷ Catanzarite, J, et al., 2006, “Astrometric Detection of Terrestrial Planets in the Habitable Zone of Nearby Stars with SIM PlanetQuest” PASP 118, 847
<http://iopscience.iop.org/article/10.1086/504442>
- ¹³⁸ Perryman, M., et al., 2014, “Astrometric Exoplanet Detection with GAIA”, ApJ 797, 14,
<http://iopscience.iop.org/article/10.1088/0004-637X/797/1/14/meta>
- ¹³⁹ Riess, A. G., Casertano, S., Anderson, J., MacKenty, J., Filippenko, A., “Parallax beyond a kiloparsec from spatially scanning the wide field camera 3 on the Hubble space telescope,” ApJ, 785, 2, 2014
- ¹⁴⁰ Bendek, E. A., Belikov, R., Pluzhnik, E., Guyon, O., Milster, T., Johnson, L., et al. (2017). Results of the astrometry and direct imaging testbed for exoplanet detection. In S. Shaklan (Ed.), *Techniques and Instrumentation for Detection of Exoplanets VIII* (Vol. 10400, p. 104001G). International Society for Optics and Photonics. <http://doi.org/10.1117/12.2274729>
- ¹⁴¹ Bendek, E., et al., TDEM-13 Final Report: “Enhanced Direct Imaging Exoplanet Detection with Astrometry Mass Determination,” <http://exoplanets.nasa.gov/technology>
- ¹⁴² Sozzetti, A. (2017). Gaia and exoplanets: a revolution in the making. In S. Shaklan (Ed.), *Techniques and Instrumentation for Detection of Exoplanets VIII* (Vol. 10400, p. 104001E). International Society for Optics and Photonics. <http://doi.org/10.1117/12.2276987>
- ¹⁴³ Stevenson, K. B., Lewis, N. K., Bean, J. L., Beichman, C., Fraine, J., Kilpatrick, B. M., et al. (2016). Transiting Exoplanet Studies and Community Targets for JWST’s Early Release

- Science Program. *Publications of the Astronomical Society of the Pacific*, 128(967), 094401. <http://doi.org/10.1088/1538-3873/128/967/094401>
- ¹⁴⁴ Rieke, G. H., Ressler, M. E., Morrison, J. E., Bergeron, L., Bouchet, P., García-Marín, M., et al. (2015). The Mid-Infrared Instrument for the James Webb Space Telescope, VII: The MIRI Detectors. *Publications of the Astronomical Society of the Pacific*, 127(953), 665–674. <http://doi.org/10.1086/682257>
- ¹⁴⁵ Beichman, C., Benneke, B., Knutson, H., Smith, R., Lagage, P.-O., Dressing, C., et al. (2014). Observations of Transiting Exoplanets with the James Webb Space Telescope (JWST). *Publications of the Astronomical Society of the Pacific*, 126(946), 1134–1173. <http://doi.org/10.1086/679566>
- ¹⁴⁶ Lum, N. A., Asbrock, J. F., White, R., Kelchner, R. E., Lum, L., Le T Pham, et al. (1993). Low-noise, low-temperature 256 x 256 Si:As IBC staring FPA. In A. M. Fowler (Ed.), *Infrared Detectors and Instrumentation* (Vol. 1946, pp. 100–110). International Society for Optics and Photonics. <http://doi.org/10.1117/12.158664>
- ¹⁴⁷ Zellem, R. T., Swain, M. R., Roudier, G., Shkolnik, E. L., Creech-Eakman, M. J., Ciardi, D. R., et al. (2017). Forecasting the Impact of Stellar Activity on Transiting Exoplanet Spectra. *The Astrophysical Journal*, 844(1), 27. <http://doi.org/10.3847/1538-4357/aa79f5>
- ¹⁴⁸ Rauscher, B, et al., 2016, “Detectors and cooling technology for direct spectroscopic biosignature characterization” *J. Astron. Telesc. Instrum. Syst.* 2(4), <http://astronomicaltelescopes.spiedigitallibrary.org/article.aspx?articleid=2545567>